FINITE ELEMENT MODELING OF STATIC INDENTATION DAMAGE IN LAMINATED COMPOSITES

BY

HAN SOO JUNG

A DISSERTATION PRESENTED TO THE GRADUATE SCHOOL
OF THE UNIVERSITY OF FLORIDA IN PARTIAL FULFILLMENT
OF THE REQUIREMENTS FOR THE DEGREE OF
DOCTOR OF PHILOSOPHY

UNIVERSITY OF FLORIDA

1991

DEDICATION

This thesis is dedicated to my father-in-law, Dong Seung Kim, who could not wait to see this thesis. He passed away in August 1989.

Also this thesis is dedicated to my younger brother-in-law, strong and courageous seafarer, Captain Ja Sup Kim, who must have perished with his crew sometime during September 1990 on his last voyage from Chile.

ACKNOWLEDGEMENTS

First of all, acknowledgement must go to the professors of my supervisory committee. Without the care and guidance of Dr. Bhavani V. Sankar, chairman of the committee, this work could not have been possible. Dr. Lawrence E. Malvern, who also was a member of the supervisory committee for my master program, encouraged me to continue my graduate study to the doctoral program. Dr. C. T. Sun introduced me to composite materials, about which I had no experience before. Dr. Ibrahim Ebcioglu taught me about plate theories. His encouragement always helped me when I was dispirited. Dr. John J. Mecholsky has widened my vision about composite materials. His many suggestions greatly helped this research. I also heartily appreciate the financial assistance I received during the doctoral program.

My special appreciation extends to Dr. C. A. Ross and Dr. J. E. Milton at the Graduate Center of the University of Florida at the Eglin Air Force Base in Fort Walton Beach, Florida. Both professors were members of my supervisory committee for the master's degree. Without their help, I could not have begun my graduate education. So many fond memories are there with them.

I would like to express my appreciation for the financial support of the United States Air Force for my master's program. I appreciate Dr. David Ebeoglu, Mr. Robert J. Arnold and Dr. David J. Butler of the Armament Division, Eglin AFB, Florida. Dr. Ebeouglu was always there whenever I need help. Mr. Arnold was very kind to me and to my family. The advice and cheerfulness of Dr. Butler helped me all the time.

I sincerely appreciate the Agency for Defense Development where I devoted fourteen years of my young life. I extend special thanks to Dr. J. H. Hong, Dr. Y. K. Yoon, Dr. Y. H. Kang, Dr. K. S. Chon, Dr. S. H. Do and many other bosses and colleagues: I wish I could name them all.

Finally, I am very grateful to my wife Ki Young and two children, En Jae and En Kyum, who must hold the traveling mileage records in their schools, for their endurance and support. And special appreciations must go to my parents, brothers and sisters for their prayers and encouragement.

TABLE OF CONTENTS

LIST OF TABLES

LIST OF FIGURES

Abstract of Dissertation Presented to the Graduate School of the University of Florida in Partial Fulfillment of the Requirements for the Degree of Doctor of Philosophy

FINITE ELEMENT MODELING OF STATIC INDENTATION DAMAGE IN LAMINATED COMPOSITES

BY

HAN SOO JUNG

AUGUST 1991

Chairman : Bhavani V. Sankar
Major Department: Aerospace Engineering,
Mechanics and Engineering Science

The objective of this research is to study progressive failure of circular laminated brittle matrix composite plates due to static indentation loading using finite elements. The plates are assumed to be simply supported along the edge, and are indented by a rigid indenter with a hemispherical nose. A quasi-isotropic homogenization process is used to make the problem axisymmetric. Four noded, isoparametric, quadrilateral, axisymmetric solid elements are used to model the plate. A new algorithm is used to analyze the progressive contact between the indenter and the plate. Hashin's failure criteria are modified so that they can be applied to axisymmetric, transversely isotropic laminates. Stiffness matrices of failed elements are modified suitably. New slip surface is introduced when delamination occurs. Very stiff

springs are attached to nodes on delamination surfaces to prevent interpenetration of the nodes. The results from incremental damage analysis agree well with experimental results. This program can be applied to analyze impact problems involving large masses impacting at very low velocities.

CHAPTER 1

INTRODUCTION

1.1 Introduction

Currently composite materials are used in primary structures of aircraft, particularly aircraft wings and frames, because significant weight savings can be achieved due to their high strength to weight ratio. Also, composite materials can easily be tailored to obtain desired properties in different directions. For example, more 0^0 layers can be used for longitudinal loads, 90^0 layers for transverse loads and $\pm$ 45^0 layers for shear loads. Also, there are other advantages such as resistance to damage by fatigue loading, immunity to corrosion, ease of processing, and low coefficient of thermal expansion. Structural forms that are otherwise inconvenient or impossible to manufacture, e.g., more complex airfoils or helicopter blades, can be easily fabricated. Hence, the utilization of composite materials in aerospace and transportation industries is continuously increasing [1,2].

However, it is well known that brittle matrix composites such as graphite epoxy are very susceptible to low velocity impact, which may be caused by dropping tools, runway debris, hailstones, bird strikes and ground service vehicles hitting

aircraft structures. High and medium levels of impact energy cause surface damage that is relatively easily detected, and therefore, repairs may be undertaken. However, low velocity impacts which are at quite low energy levels can seriously damage laminated composite structures internally so that frequently it is very hard to detect damage through visual inspections. The damage can be detected only by using nondestructive inspection (NDI) techniques. For example, low velocity impact to an aluminum plate may cause denting damage and the structure does not lose very much strength. However, inside of an impacted composite plate there may be fiber breakage, matrix cracks, and delaminations, while the impacted surface may not show any damage. Commonly it is termed as "Barely Visible Impact Damage" or BVID [2]. After impact, composite materials lose considerable strength because of internal damage and delaminations. [2-7]

It becomes very important to understand the response of composites to the impact of rigid objects and to predict damage in order to make composite materials more reliable. The study of the effect of BVID on static and fatigue strengths of graphite/epoxy panels shows that impact degradation is of more concern in compression loading than in tension because of delaminations which occur during impact. Importance of the impact study is emphasized by the fact that upper surfaces of the aircraft are more likely to receive impacts from tool

drops than lower surfaces, and upper surfaces operate in a compression-dominated load regime [2].

Because of the extremely complicated nature of impact on the composite materials, empirical methods have been widely employed. Generally, empirical methods have several distinct limitations. First, it is very expensive and also time consuming to conduct testing and to process the data. Second, it is practically difficult to test all the combinations of material properties, boundary conditions of the composite structures, and impactor velocities and weight variations. This problem can be critical, if the composite material is in a developing stage, and only limited quantities are available. Third, it is very difficult to comprehend all the stress and strain distributions, and damage progression inside composites by empirical methods. And also there are difficulties in matching results from specimens to the real structures. [6,7]

Therefore, numerous analytical methods have been developed to overcome the shortcomings of empirical methods. However, so far, because of the extremely complicated nature of impact problem, there are no complete three-dimensional models available which can simulate the entire impact process and predict damage progression. There is an urgent need to develop a three dimensional progressive finite element program which calculates contact forces, contact displacements, stresses and strains inside the composite plate. During the contact process, the finite element program must be able to

check all the failure criteria for fiber breakage, matrix cracking and delamination. If failure occurs, then the program could modify the stiffness matrix to account for failures .

Fortunately, low velocity impact due to large masses can be treated as a static indentation problem, because the impact duration is much longer than the time required by the propagating waves to travel from the impact site to the supports or free edges, and the test results show good agreement with this assumption. Strictly speaking, the terminology of low velocity impact is not clearly defined. Rather low impact velocity is generally defined as the impact velocity which is low enough to justify a static analysis of the response of the structure, especially in the vicinity of impact [3,4,8,9]. This velocity depends upon the mass, shape and the material property of the impactor and also upon the impacted structure boundary conditions and its natural frequencies. Generally it ranges 1-3 meter/second with impactor mass less than 10 kg [10].

The advantage of static analysis is that the time variable is eliminated. Hence, we can closely look into progressive damage mechanisms with a small amount of computational resources. If time effects are considered, it will be a formidable task to obtain all the meaningful stress and strain distributions inside the plate and to map the damage pattern and its progression because of computational time and storage limitations of the computer system. If

coarser elements are employed, it will be very hard to obtain accurate data because meaningful data must be obtained in the small confined area under the indenter.

The experimentally determined contact laws account for local damage in an empirical manner, and hence cannot be used to study the local damage. A fully three dimensional formulation is required to study the progressive damage.

In the present study a finite element program performs an incremental analysis of the contact problem, and assesses the damage due to indentation.

1.2 Experimental Background

In this section some results from an experimental study [11] are presented to bring out the importance and necessity of the finite element modeling of the damage process due to static indentation.

Test specimens were made of Hercules carbon prepreg tape AS4/3501-6, which is an amine-cured epoxy resin reinforced with unidirectional carbon fibers. All specimens were cut from a 30.48 cm (12 inch) by 30.48 cm, $[0^0, +45^0, -45^0, 90^0]_{8S}$ composite plate lay-up. In order to obtain the specimens with the quality suggested by the manufacturer, the curing instructions was carefully followed as in Ref. [12]. An autoclave (Baron Model BAC-24) was used to fabricate all the specimens of composite laminates used in this study. Detailed

procedure of fabrication can be found in Ref. [11]. Material property of the 0^0 lamina can be found in Table 2.1.

Figure 1.1 shows the pendulum impact test facility in which all impact tests were conducted. The pendulum includes the support strings connecting the tup to the laboratory ceiling, and the tup, which is a combination of weights, a load cell, and an indenter with one inch diameter hemispherical head. The total mass of the tup is 13.84 kg. Static indentation tests were done in a standard MTS material testing machine.

The composite laminate was placed on a circular steel ring of 5.08 cm (2 inch) diameter to simulate a circular plate with simply supported boundary condition. The test configuration is shown in Figure 1.2.

The test results of contact force vs. center deflection of the circular composite plate for the static indentation and impact tests are shown in Figure 1.3. This graph suggests that static indentation tests can simulate low velocity impact tests. Also it suggests that indenting process is highly nonlinear due to internal damages. A sudden drop of the contact force is a unique feature of indentation of composite plates. Figure 1.4 shows the picture of the C-scan of the impacted plate. The circular damage pattern justifies the axisymmetric formulation used in the present study. Figure 1.5 shows the picture of the photo-micrograph of the polished

cross section of the indented plate. This shows matrix cracks due to shear failure and delaminations.

However, these data are not sufficient to understand the entire impact or indentation process. They do not explain how damage initiates and propagates. Also, it is very hard to quantify this damage.

1.3 Objective and Scope

The major objective of this research is to develop a finite element program which models the static response of laminated composite plates indented by a rigid spherical indenter and to predict progression of damages inside the plate. The results are applicable to low velocity impact of the composite plates.

A circular plate and a rigid hemispherical indenter were chosen in modeling because they correspond to many practical impact situations. Quadrilateral, isoparametric, axisymmetric finite elements were employed in this research. By employing axisymmetric elements, the three dimensional problem can be treated as two dimensional by eliminating dependency on θ.

In Chapter 2, the finite element formulation and the incremental displacement method are introduced. The input to the finite element program is the displacements necessary to close the gap between the indenter and candidate contact nodes of the plate. The laminated plate consists of many plies that are orthotropic and have different angles of fiber

orientation. As axisymmetric finite elements were employed in this research, there must be special considerations of the material properties and failure criteria to account for this discrepancy. The in-plane strains, ϵ_{xx}, ϵ_{yy} and γ_{xy} are continuous at the interface between two adjacent plies whereas the stresses, σ_{xx}, σ_{yy} and τ_{xy} are not. On the other hand, σ_{zz}, τ_{xz} and τ_{yz} are continuous through thickness and are better represented in a homogeneous plate model than ϵ_{zz}, γ_{xz} and γ_{yz}, which can be discontinuous through the thickness. A set of transversely isotropic elastic constants is derived for a group of plies that can be considered as a quasi-isotropic laminate.

In Chapter 3, the accuracy and efficiency of the present method were evaluated by comparing the results with some early work [10]. The contact force vs. center deflection curve of a AS4/3501-6 graphite/epoxy plate was compared with experimental results in the elastic range. Then, some widely used contact laws were compared with the present finite element results. The effect of friction was studied by assuming stick friction conditions between the indenter and the top surface of the plate.

In Chapter 4, the failure criteria are introduced. Among many interactive and independent failure modes, three-dimensional failure criteria introduced by Hashin [13,14] were employed in the present studies. These criteria have the same quadratic form as Tsai-Hill's criterion, but they can

distinguish different failure modes such as fiber breakage, matrix cracking and delamination. Since we use an axisymmetric formulation, the damage pattern is also going to be axisymmetric, which does not strictly represent the damage pattern in a composite laminate. However, experimental impact studies [15] have indicated that the actual damage pattern is like a spiralling stair case, and the projection of these delaminations can be considered as circular and hence axisymmetric. This was also confirmed by studies in the laboratory [11]. The extent of delamination, fiber breakage and matrix failure were mapped during the contact process. After failures are detected, the total stiffness matrix of the plate must be modified properly depending upon the failure modes. Matrix and fiber failure can be implemented by reducing or eliminating element stiffness matrices. Implementing delamination into the finite element program requires creation of new free surfaces, consequently new nodes. Rigid springs are inserted across the newly created free surfaces to prevent interpenetration of the nodes. Delamination can be assumed as Mode II (Shear Mode) crack propagation. Incremental damage analysis results are compared with experimental results.

A summary of conclusions and some suggestions for future research are listed in Chapter 5.

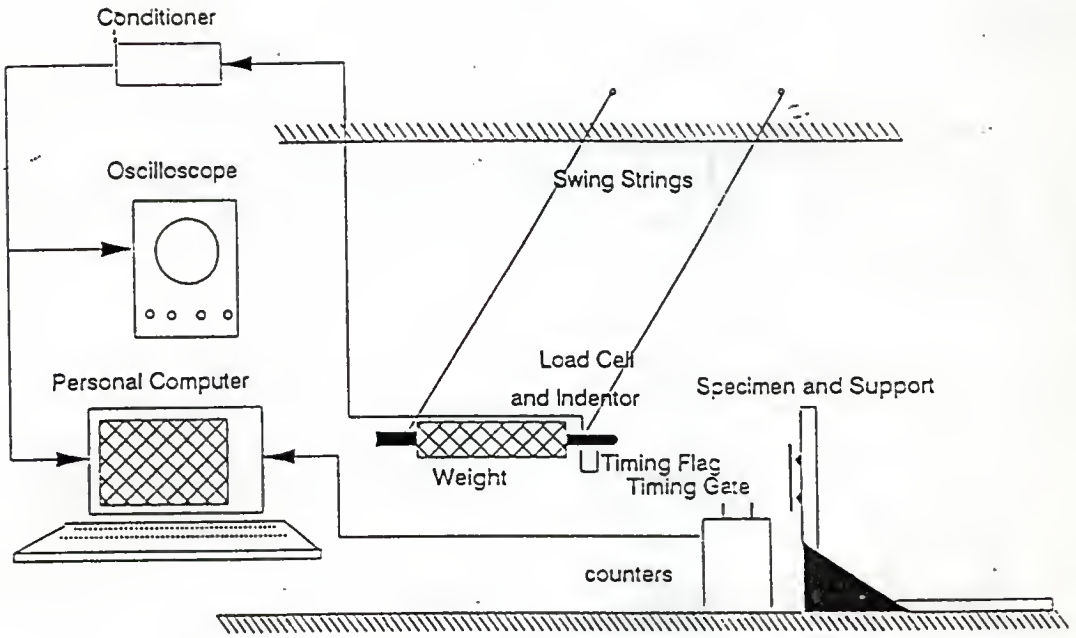

Figure 1.1 Impact test Scheme

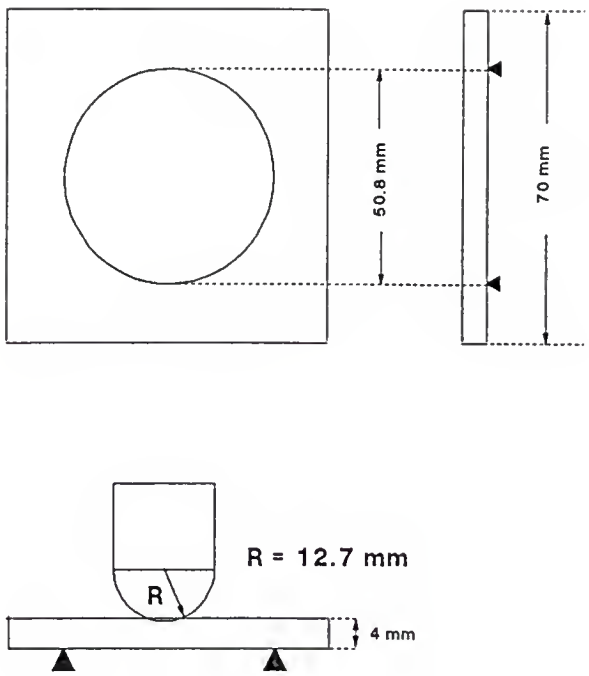

Figure 1.2 Test configuration

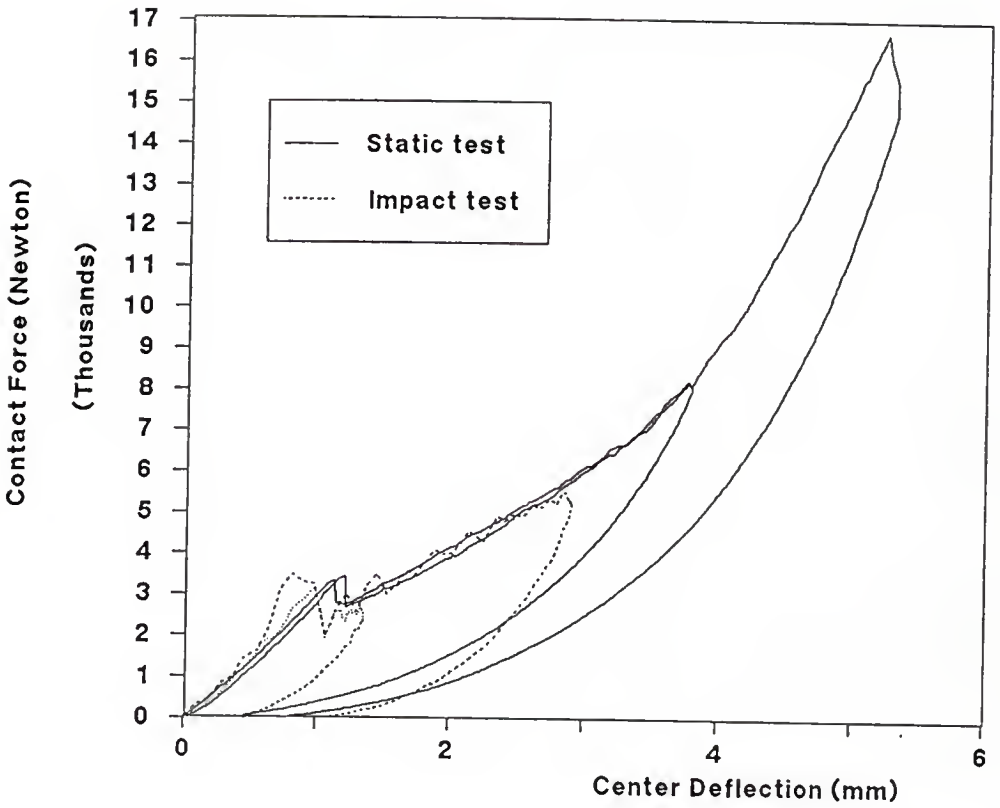

Figure 1.3 Contact Force vs. center deflection Curve

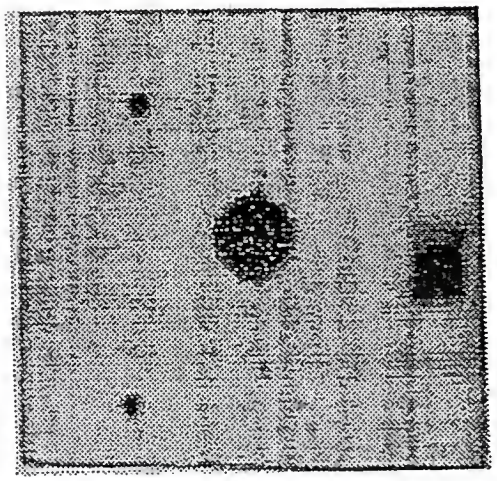

Figure 1.4 C-Scan picture of impacted composite plate

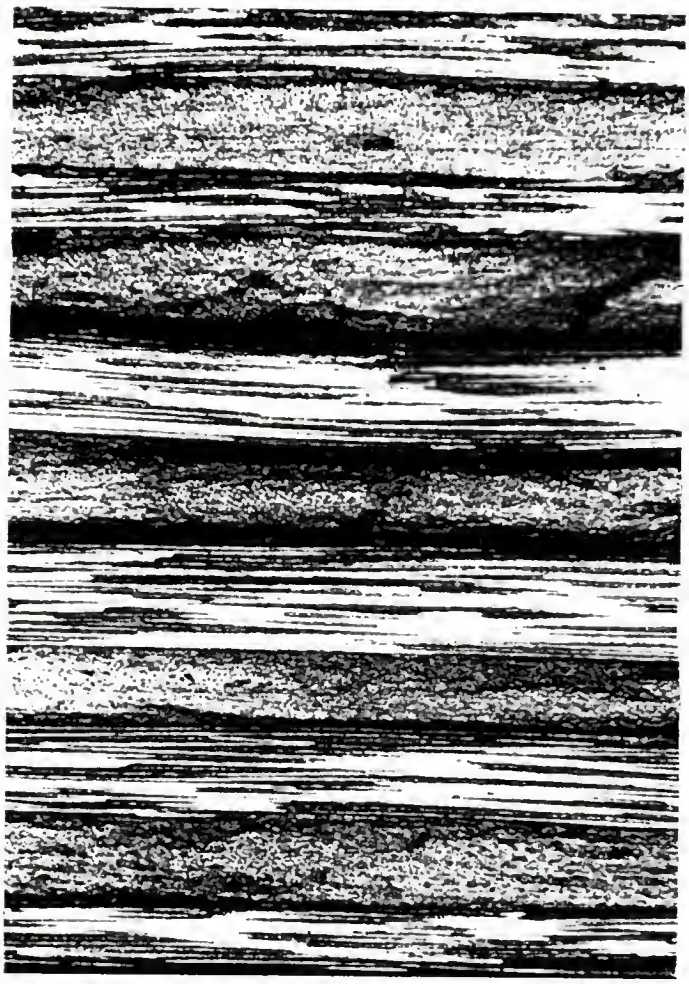

Figure 1.5 A photo-micrograph of the impacted plate

CHAPTER 2

FINITE ELEMENT PROGRAMMING OF THE CONTACT PROCESS

2.1 Introduction

The finite element method has been established as a powerful and versatile tool of analysis for contact problems involving isotropic bodies. In the present study, a method for solving the problem of indentation of composite laminates is developed.

The contact problem of quadratic surfaces of elastic bodies was first solved analytically by Hertz in 1881. Since then, numerous contact problems have been solved by formulating the problem as an integral equation. The solution is either obtained by solving the equation numerically or, for simple configurations, in closed form. The Hertzian type problem has three general assumptions. First, the contacting solids are homogeneous, isotropic and linear elastic. Second, the contact areas are essentially flat and relatively small compared to the various radii of curvature of the undeformed bodies in the vicinity of the contact interfaces. Third, the contacting solids are perfectly smooth and only normal pressures are considered [6,16].

Hertzian type solutions are not suitable for indentation of composite laminates which are inhomogeneous, anisotropic and also involve significant damages at low load levels. Further, most laminated composites in use can not be adequately represented as a half-space as in Hertzian contact problem. Because of these complexities, three dimensional analysis, especially three dimensional finite element methods, are required in the present study.

In the last two decades, many researchers thought that contact problems could be considered as a special case of constrained minimization of either total or complementary potential energy. The minimization is formulated as a mathematical programming problem, and the solutions are obtained by either using incremental linear programming, quadratic programming or conjugate (modified) gradient methods. The minimization problem can also be formulated as a variational inequality using penalty methods or Lagrange multipliers [17-21]. However, these methods have certain disadvantages such as creation of flexibility matrix, the awkwardness involved in introducing additional unknowns, such as slack variables and Lagrange parameters. Nothing can be better than direct formulation of finite element method as a simple design tool, which calculates the detailed stress field in various types of laminates for various boundary conditions accounting for the damages inside the plate. The goal is to use simple and conventional elements so that the method can be

implemented in commercial finite element programs. The novel incremental contact algorithm developed in this study is explained in Section 2.4.

2.2 Axisymmetric Formulation

The benefit of employing an axisymmetric element is that the three dimensional problem can be treated as two dimensional. Especially in the case of rigid ball indentation, where the contact surface is circular, axisymmetric formulation is a very efficient method to treat the indenting process in a computer program, because upper surface nodes of the plate come into contact successively and the contact area is readily determined. If we use three dimensional solid elements, it will be a formidable task to determine the contact nodes for the case of a spherical indenter, although the employment of three dimensional solid elements has a distinct advantage in that we can use orthotropic material properties and also the failure criteria for orthotropic laminates directly without any modifications. Complexity of the contact algorithm demands employment of axisymmetric elements, and consequently there must be some considerations to convert the material properties of a laminated plate, which are basically orthotropic, into equivalent axisymmetric properties. The circular damage distribution pattern of the C-scan pictures of the damaged plates (Figure 1.4) justifies the employment of axisymmetric elements to solve the problem.

Stress-strain relationships of the axisymmetric element are discussed extensively in Section 2.3.

In the present study u(r,z) and w(r,z) represent the radial and transverse displacements, respectively. The axisymmetric stress and strain components are

$$\{ \sigma \} = \{ \sigma_{rr} \quad \sigma_{zz} \quad \tau_{rz} \quad \sigma_{\theta\theta} \}^T \tag{2.1}$$

$$\{ \epsilon \} = \{ \epsilon_{rr} \quad \epsilon_{zz} \quad \gamma_{rz} \quad \epsilon_{\theta\theta} \}^T \tag{2.2}$$

where,

$$\epsilon_{rr} = \frac{\partial u}{\partial r}$$

$$\epsilon_{zz} = \frac{\partial w}{\partial z} \tag{2.3}$$

$$\gamma_{rz} = \frac{\partial u}{\partial z} + \frac{\partial w}{\partial r}$$

$$\epsilon_{\theta\theta} = \frac{u}{r}$$

As graphite/epoxy composite is very brittle and can be considered as elastic until failure, material non-linearities are ignored [2]. As will be seen later, the deflections considered are smaller than the plate thickness, and hence geometric non-linearities are also not considered.

2.3 Constitutive Relations for an Axisymmetric Laminated Plate

A composite laminate can be considered as having several sublaminates. If each sublaminate is quasi-isotropic, then each sublaminate can be idealized as a homogeneous transversely isotropic material. Then the composite laminate can be considered as a laminate made up of several transversely isotropic layers. Hence the axisymmetric formulation can be employed if the external loading and boundary conditions are also axisymmetric.

The stress-strain relationship in the Cartesian coordinates are

$$\{ \epsilon \} = [S] \{ \sigma \} \tag{2.4}$$

where $\{ \sigma \}$ and $\{ \epsilon \}$ are,

$$\{ \epsilon \} = \{ \epsilon_{xx} \; \epsilon_{yy} \; \gamma_{xy} \; \epsilon_{zz} \; \gamma_{zx} \; \gamma_{zy} \}^T \tag{2.5}$$

$$\{ \sigma \} = \{ \sigma_{xx} \; \sigma_{yy} \; \tau_{xy} \; \sigma_{zz} \; \tau_{zx} \; \tau_{zy} \}^T \tag{2.6}$$

For the ply which has fiber orientation angle θ from the x coordinate, lamina constitutive relations can be obtained from

$$\{ \epsilon \}_0 = [T_\epsilon]^T [S] [T_\sigma] \{ \sigma \}_\theta \tag{2.7}$$

where [S] is

$$[S] = \begin{bmatrix} \frac{1}{E_1} & -\frac{\nu_{21}}{E_2} & 0 & -\frac{\nu_{31}}{E_3} & 0 & 0 \\ -\frac{\nu_{12}}{E_1} & \frac{1}{E_2} & 0 & -\frac{\nu_{32}}{E_3} & 0 & 0 \\ 0 & 0 & \frac{1}{G_{12}} & 0 & 0 & 0 \\ -\frac{\nu_{13}}{E_1} & -\frac{\nu_{23}}{E_2} & 0 & \frac{1}{E_3} & 0 & 0 \\ 0 & 0 & 0 & 0 & \frac{1}{G_{31}} & 0 \\ 0 & 0 & 0 & 0 & 0 & \frac{1}{G_{23}} \end{bmatrix}$$

and [T_σ], [T_e] are given by,

$$[T_\sigma] = \begin{bmatrix} \cos^2\theta & \sin^2\theta & 2\cos\theta\sin\theta & 0 & 0 & 0 \\ \sin^2\theta & \cos^2\theta & -2\cos\theta\sin\theta & 0 & 0 & 0 \\ -\cos\theta\sin\theta & \cos\theta\sin\theta & \cos^2\theta-\sin^2\theta & 0 & 0 & 0 \\ 0 & 0 & 0 & 1 & 0 & 0 \\ 0 & 0 & 0 & 0 & \cos\theta & \sin\theta \\ 0 & 0 & 0 & 0 & -\sin\theta & \cos\theta \end{bmatrix}$$

$$[T_e] = \begin{bmatrix} \cos^2\theta & \sin^2\theta & \cos\theta\sin\theta & 0 & 0 & 0 \\ \sin^2\theta & \cos^2\theta & -\cos\theta\sin\theta & 0 & 0 & 0 \\ -2\cos\theta\sin\theta & 2\cos\theta\sin\theta & \cos^2\theta-\sin^2\theta & 0 & 0 & 0 \\ 0 & 0 & 0 & 1 & 0 & 0 \\ 0 & 0 & 0 & 0 & \cos\theta & \sin\theta \\ 0 & 0 & 0 & 0 & -\sin\theta & \cos\theta \end{bmatrix}$$

For the fiber orientation angle θ,

$$\{ \epsilon \}_\theta = [S]_\theta \{ \sigma \}_\theta$$

$$[S]_\theta = [T_\epsilon]_\theta^T [S] [T_\sigma]_\theta$$

Averaging $[S]_\theta$ for the number of plies from this form is not suitable because in-plane stresses such as σ_{xx}, σ_{yy} and τ_{xy} are not continuous through thickness of the element while ϵ_{xx}, ϵ_{yy} and γ_{xy} are continuous. And, also, out-of-plane stresses σ_{zz}, τ_{zx} and τ_{zy} are continuous through thickness while out-of-plane strains ϵ_{zz}, γ_{zx} and γ_{zy} are not continuous. These are well illustrated in Figure 2.1 and Figure 2.2, which Wu and Springer have obtained [23]. These figures show the continuity of the stresses and strains through the thickness of the impacted plate. The best way to average the modulus of the element can be done after denoting $[S]_\theta$ as,

$$[S]_\theta = \begin{bmatrix} p & q \\ r & s \end{bmatrix} \qquad (2.8)$$

where p, q, r and s are 3 x 3 matrices. Then the stress-strain relationship can be written as

$$\begin{Bmatrix} \sigma_{xx} \\ \sigma_{yy} \\ \tau_{xy} \\ \sigma_{zz} \\ \tau_{zx} \\ \tau_{zy} \end{Bmatrix} = \begin{bmatrix} p & q \\ r & s \end{bmatrix} \begin{Bmatrix} \epsilon_{xx} \\ \epsilon_{yy} \\ \gamma_{xy} \\ \epsilon_{zz} \\ \gamma_{zx} \\ \gamma_{zy} \end{Bmatrix} \tag{2.9}$$

The stress-strain relationship can be rearranged such that all the components of stress and strain that are continuous through the thickness are on one side and the remaining components are on the other side as shown in Figure 2.9.

$$\begin{Bmatrix} \sigma_{xx} \\ \sigma_{yy} \\ \tau_{xy} \\ \epsilon_{zz} \\ \gamma_{zx} \\ \gamma_{zy} \end{Bmatrix} = \begin{bmatrix} p^{-1} & -p^{-1}q \\ rp^{-1} & s-rp^{-1}q \end{bmatrix} \begin{Bmatrix} \epsilon_{xx} \\ \epsilon_{yy} \\ \gamma_{xy} \\ \sigma_{zz} \\ \tau_{zx} \\ \tau_{zy} \end{Bmatrix} \tag{2.10}$$

Let us denote $[\ D\ ]_{\theta i}$

$$[\ D\ ]_{\theta_i} = \begin{bmatrix} p^{-1} & -p^{-1}q \\ rp^{-1} & s-rp^{-1}q \end{bmatrix} \tag{2.11}$$

Then an average [D] matrix for a group of N plies can be obtained as,

$$[D]_{av} = \frac{1}{N}\sum_{i=1}^{N}[D]_{\theta_i} = \begin{bmatrix} P & Q \\ R & S \end{bmatrix} \tag{2.12}$$

Now the elastic matrix $[C]_{av}$ can be recovered from $[D]_{av}$. The $[C]_{av}$ can be expressed in terms of P, Q, R and S as,

$$[C]_e = \begin{bmatrix} P-QS^{-1}R & QS^{-1} \\ -S^{-1}R & S^{-1} \end{bmatrix} \tag{2.13}$$

The stress-strain relations take the form

$$\{\sigma\}_{av} = [C]_{av}\{\epsilon\}_{av}$$

For widely used cross ply or quasi-isotropic laminates, such as $[0, 90]_S$ or $[0^0, \pm 45^0, 90^0]_S$ laminates, $[C]_{av}$ becomes transversely isotropic. For axisymmetric problems, where

$$\sigma_{r\theta} = \sigma_{z\theta} = \epsilon_{r\theta} = \epsilon_{z\theta} = 0 \tag{2.14}$$

$$[C]_e = \begin{bmatrix} C_{rr} & C_{r\theta} & 0 & C_{rz} \\ C_{\theta r} & C_{\theta\theta} & 0 & C_{\theta z} \\ 0 & 0 & C_{rz} & o \\ C_{zr} & C_{z\theta} & 0 & C_{zz} \end{bmatrix} \tag{2.15}$$

Further, the present homogenization scheme yielded a symmetric stiffness matrix, i.e., $C_{ij} = C_{ji}$, and also

$$\begin{aligned} C_{rr} &= C_{\theta\theta} \\ C_{rz} &= C_{\theta z} \end{aligned} \tag{2.16}$$

Sometimes, five engineering elastic constants, such as E_r, E_z, G_{rz}, $\nu_{r\theta}$, ν_{rz} can describe the material properties of a transversely isotropic laminate plate [10]. For this case, the stress-strain relationship can be obtained as follows.

$$[C]_{av} = \begin{bmatrix} \frac{1}{E_r} & -\frac{\nu_{r\theta}}{E_r} & 0 & -\frac{\nu_{rz}}{E_r} \\ -\frac{\nu_{r\theta}}{E_r} & \frac{1}{E_r} & 0 & -\frac{\nu_{rz}}{E_r} \\ 0 & 0 & \frac{1}{G_{rz}} & 0 \\ -\frac{\nu_{rz}}{E_r} & -\frac{\nu_{rz}}{E_r} & 0 & \frac{1}{E_z} \end{bmatrix}^{-1} \tag{2.17}$$

Table 2.1 shows the material properties of the AS4/3501-6 graphite/epoxy lamina. Also, the calculated transversely isotropic element material property matrix $[C]_{av}$ for a plate, which consists of four plies in $[0^0 , \pm 45^0 , 90^0]$ orientation is given in Table 2.1. This configuration is chosen because of its wide application in aircraft structures. For example, the main wing box for a straight wing aircraft, 0^0 plies carry the spanwise direct stresses induced by wing bending like a cantilever beam bending, $\pm 45^0$ plies carry shear stresses caused by wing twisting, and finally 90^0 plies carry the chordwise direct stresses due to fore and aft bending of the aircraft wing [2].

2.4 Algorithm for the Contact Problem

Unlike conventional finite element problems, contact problems are mixed boundary value problems where nonzero displacements are specified at parts of the boundary and zero tractions are specified in the rest. Further, the displacements in the contact surface have to satisfy certain conditions specified by the geometry of the indenter. Sankar [10] used a contact algorithm in conjunction with a finite difference method. In the present study, the algorithm has been modified to suit the finite element method. Unlike the finite difference method, the finite element method has the advantage of modeling complex geometries and multi-layer media.

For the frictionless contact problem, the vertical degrees of freedom of the top surface nodes of the plate become contact candidates. In Equation (2.18), the displacements of these contact candidate degrees of freedom are notated as d_u and other displacements as d_r. The d_r degrees of freedom can be condensed to obtain a smaller stiffness matrix as shown below.

$$\begin{bmatrix} K_{uu} & K_{ur} \\ K_{ru} & K_{rr} \end{bmatrix} \begin{Bmatrix} d_u \\ d_r \end{Bmatrix} = \begin{Bmatrix} F_u \\ 0 \end{Bmatrix} \tag{2.18}$$

$$\{ d_r \} = - [K_{rr}]^{-1} [K_{ru}] \{ d_u \} \tag{2.19}$$

After condensation, the equilibrium equations take the form

$$[K_c] \{ d_u \} = \{ F_u \} \tag{2.20}$$

where

$$[K_c] = [K_{uu}] - [K_{ur}] [K_{rr}]^{-1} [K_{ru}] \tag{2.21}$$

Since we are dealing with an axisymmetric problem, the contact area is always circular. Let us assume that the contact has progressed to Node k-1 (see Figure 2.4). The

procedure for determining the incremental load required to bring the k^{th} Node into contact is as follows. Equation (2.20) can be partitioned as

$$\begin{bmatrix} K_{cc} & K_{cf} \\ K_{fc} & K_{ff} \end{bmatrix} \begin{Bmatrix} w_c \\ w_f \end{Bmatrix} = \begin{Bmatrix} F_c \\ 0 \end{Bmatrix} \tag{2.22}$$

where w_c are the z displacements of nodes within the contact region including k-1 and w_f are the remaining degrees of freedom for which the forces are zero. Let us use g_i to denote the gap between the indenter and nodes outside the contact region, i.e., $i \geq k$. The first step is to determine the incremental displacement of the indenter to close the gap g_k. We first apply a unit displacement to the indenter, i.e.,

$$w_i = 1, \; i = 1, 2, \ldots, k-1 \tag{2.23}$$

The equation (2.22) is solved for F_c and w_f. Now the new gap g'_i becomes

$$g'_i = g_i - 1 + w_i, \quad i \geq k \tag{2.24}$$

Now we can calculate the displacement δ of the indenter to make the gap g'_k identically equal to zero.

$$\delta = \frac{g_k}{(g_k - g'_k)} = \frac{g_k}{(1 - w_k)} \qquad (2.25)$$

After determining δ, the nodal force F_c can be computed. By integrating all the nodal forces, we obtain the incremental contact force, ΔP. The procedure is repeated for the next contact node k+1.

When frictional effects are included, radial forces at nodes in the contact region can not be considered as zero. The procedure has to be slightly modified, as is explained in Section 3.5.

The damage alters the stiffness matrix. We assume that the indentation process is under displacement control, and hence the w-displacements of the contact nodes are kept the same when passing from one iteration to the next. The changes in [K] cause a change in the contact load (usually reduction) for the same indentation displacement. Detailed damage analyses are presented in Chapter 4.

2.5 Axisymmetric Finite Element

In this section, the derivation of the stiffness matrix of a quadrilateral, isoparametric, axisymmetric element is given for the sake of completeness.

In isoparametric elements, the element coordinates and the element displacements are expressed with the same shape functions associated with nodal coordinates and displacements respectively as shown below.

$$
\begin{aligned}
r &= \sum_{i=1}^{n} N_i(\xi,\eta)\, r_i \\
z &= \sum_{i=1}^{n} N_i(\xi,\eta)\, z_i \\
u &= \sum_{i=1}^{n} N_i(\xi,\eta)\, u_i \\
w &= \sum_{i=1}^{n} N_i(\xi,\eta)\, w_i
\end{aligned}
\qquad (2.26)
$$

where r and z are element coordinates, ξ and η are the natural coordinates and u and w are element displacements as shown in Figure 2.5. Subscript i signifies node number. Shape function or interpolation function N_i are expressed in the natural coordinate system, which has variable ξ and η that each vary from -1 to +1 as shown in Figure 2.5. The characteristic of the shape function N_i is that its value is unity at node i and is zero at all other nodes. For the quadrilateral element, the N_i are as follows.

$$
\begin{aligned}
N_1 &= \frac{1}{4} (1 + \xi) (1 + \eta) \\
N_2 &= \frac{1}{4} (1 - \xi) (1 + \eta) \\
N_3 &= \frac{1}{4} (1 - \xi) (1 - \eta) \\
N_4 &= \frac{1}{4} (1 + \xi) (1 - \eta)
\end{aligned}
\qquad (2.27)
$$

To evaluate the stiffness matrix of the element, we need to calculate the strain-displacement transformation matrix for the small strain case as,

$$\epsilon_{rr} = \frac{\partial u}{\partial r}$$

$$\epsilon_{zz} = \frac{\partial w}{\partial z}$$

$$\gamma_{rz} = \frac{\partial u}{\partial z} + \frac{\partial w}{\partial r}$$

$$\epsilon_{\theta\theta} = \frac{u}{r}$$

As the interpolation functions, N_i, are defined in the natural coordinate system by Equation (2.27), we need the relationship between r and z derivatives and ξ and η derivatives. By using chain rules, the following expressions can be obtained.

$$\begin{Bmatrix} \frac{\partial u}{\partial r} \\ \frac{\partial u}{\partial z} \end{Bmatrix} = \begin{bmatrix} \frac{\partial r}{\partial \xi} & \frac{\partial z}{\partial \xi} \\ \frac{\partial r}{\partial \eta} & \frac{\partial z}{\partial \eta} \end{bmatrix}^{-1} \begin{Bmatrix} \frac{\partial u}{\partial \xi} \\ \frac{\partial u}{\partial \eta} \end{Bmatrix} = J^{-1} \begin{Bmatrix} \frac{\partial u}{\partial \xi} \\ \frac{\partial u}{\partial \eta} \end{Bmatrix} \tag{2.28}$$

$$\begin{Bmatrix} \frac{\partial w}{\partial r} \\ \frac{\partial w}{\partial z} \end{Bmatrix} = \begin{bmatrix} \frac{\partial r}{\partial \xi} & \frac{\partial z}{\partial \xi} \\ \frac{\partial r}{\partial \eta} & \frac{\partial z}{\partial \eta} \end{bmatrix}^{-1} \begin{Bmatrix} \frac{\partial w}{\partial \xi} \\ \frac{\partial w}{\partial \eta} \end{Bmatrix} = J^{-1} \begin{Bmatrix} \frac{\partial w}{\partial \xi} \\ \frac{\partial w}{\partial \eta} \end{Bmatrix} \tag{2.29}$$

In the above equations, J is the Jacobian operator relating the natural coordinate derivatives to the local coordinate derivatives. The inverse of Jacobian matrix must exist in order for the isoparametric element to be used. This means that there is a one-to-one correspondence between the natural and the local coordinates of the elements. In actual computations, the sign of the Jacobian determinant is monitored at the Gaussian integration points to ensure the existence of the inverse Jacobian. Generally, a zero or negative value of the Jacobian determinant indicates input data error or an overly distorted element, and the computations are terminated automatically for the purpose of node renumbering [22].

Equations (2.28) and (2.29) can be calculated as follows.

$$\begin{aligned} \frac{\partial r}{\partial \xi} &= \frac{1}{4}(1+\eta)\, r_1 - \frac{1}{4}(1+\eta)\, r_2 - \frac{1}{4}(1-\eta)\, r_3 + \frac{1}{4}(1-\eta)\, r_4 \\ \frac{\partial r}{\partial \eta} &= \frac{1}{4}(1+\xi)\, r_1 + \frac{1}{4}(1-\xi)\, r_2 - \frac{1}{4}(1-\xi)\, r_3 - \frac{1}{4}(1+\xi)\, r_4 \end{aligned} \tag{2.30}$$

$$\frac{\partial z}{\partial \xi} = \frac{1}{4}(1+\eta)\, z_1 - \frac{1}{4}(1+\eta)\, z_2 - \frac{1}{4}(1-\eta)\, z_3 + \frac{1}{4}(1-\eta)\, z_4$$

$$\frac{\partial z}{\partial \eta} = \frac{1}{4}(1+\xi)\, z_1 + \frac{1}{4}(1-\xi)\, z_2 - \frac{1}{4}(1-\xi)\, z_3 - \frac{1}{4}(1+\xi)\, z_4 \qquad (2.31)$$

$$\frac{\partial u}{\partial \xi} = \frac{1}{4}(1+\eta)\, u_1 - \frac{1}{4}(1+\eta)\, u_2 - \frac{1}{4}(1-\eta)\, u_3 + \frac{1}{4}(1-\eta)\, u_4$$

$$\frac{\partial u}{\partial \eta} = \frac{1}{4}(1+\xi)\, u_1 + \frac{1}{4}(1-\xi)\, u_2 - \frac{1}{4}(1-\xi)\, u_3 - \frac{1}{4}(1+\xi)\, u_4 \qquad (2.32)$$

$$\frac{\partial w}{\partial \xi} = \frac{1}{4}(1+\eta)\, w_1 - \frac{1}{4}(1+\eta)\, w_2 - \frac{1}{4}(1-\eta)\, w_3 + \frac{1}{4}(1-\eta)\, w_4$$

$$\frac{\partial w}{\partial \eta} = \frac{1}{4}(1+\xi)\, w_1 + \frac{1}{4}(1-\xi)\, w_2 - \frac{1}{4}(1-\xi)\, w_3 - \frac{1}{4}(1+\xi)\, w_4 \qquad (2.33)$$

Eventually, the unknown variables of the system will be the nodal displacements { U }

$$\{ U \} = \{ u_1 \; w_1 \; u_2 \; w_2 \; u_3 \; w_3 \; u_4 \; w_4 \}^T \qquad (2.34)$$

Then,

$$\begin{Bmatrix} \frac{\partial u}{\partial r} \\ \frac{\partial u}{\partial z} \end{Bmatrix} = \frac{1}{4} J^{-1} \begin{bmatrix} 1+\eta & 0 & -(1+\eta) & 0 & -(1-\eta) & 0 & 1-\eta & 0 \\ 1+\xi & 0 & 1-\xi & 0 & -(1-\xi) & 0 & -(1+\xi) & 0 \end{bmatrix} \{ U \}$$

$$\begin{Bmatrix} \frac{\partial w}{\partial r} \\ \frac{\partial w}{\partial z} \end{Bmatrix} = \frac{1}{4} J^{-1} \begin{bmatrix} 0 & 1+\eta & 0 & -(1+\eta) & 0 & -(1-\eta) & 0 & 1-\eta \\ 0 & 1+\xi & 0 & 1-\xi & 0 & -(1-\xi) & 0 & -(1+\xi) \end{bmatrix} \{ U \}$$

Strain can be expressed with nodal variables { U }, and also stress can be obtained by multiplying the strain vector by the elasticity matrix $[C]_e$.

$$\begin{aligned} \{ \epsilon \} &= [B]_e \{ U \} \\ \{ \sigma \} &= [C]_e [B]_e \{ U \} \end{aligned} \qquad (2.35)$$

In the axisymmetric case, unlike other isoparametric elements, the strain-displacement matrix $[B]_e$ has terms containing r. Thus, for two elements of identical shapes and material properties but at different r locations, the $[K]_e$ will be different. Also, a problem arises when r is zero because some terms have r in the denominator. A proper numerical scheme, such as Gaussian quadrature, can avoid this problem [24].

In the axisymmetric case, { ϵ } becomes

$$\{ \epsilon \} = \{\epsilon_{rr} \ \epsilon_{zz} \ \gamma_{rz} \ \epsilon_{\theta\theta}\}^T \tag{2.36}$$

and $[\ B\ ]_e$ becomes 4 by 8 matrix as follows.

$$\frac{1}{4}\begin{bmatrix} 1+\eta & 0 & 1+\xi & \frac{(1+\xi)(1+\eta)}{r} \\ 0 & 1+\xi & 1+\eta & 0 \\ -(1+\eta) & 0 & 1-\xi & \frac{(1-\xi)(1+\eta)}{r} \\ 0 & 1-\xi & -(1+\eta) & 0 \\ -(1-\eta) & 0 & -(1-\xi) & \frac{(1-\xi)(1+\eta)}{r} \\ 0 & -(1-\xi) & -(1-\eta) & 0 \\ 1-\eta & 0 & -(1+\xi) & \frac{(1+\xi)(1+\eta)}{r} \\ 0 & -(1+\xi) & 1-\eta & 0 \end{bmatrix}^T \tag{2.37}$$

The element stiffness matrix can be formulated by using the virtual work principle. The principle requires that for a body under equilibrium,

$$\int_{V_e} \delta\epsilon^T \sigma \, dV = \int_{V_e} \delta a^T f_B dV + \int_{S_e} \delta a^T f_S dS + \delta a^T f_N \tag{2.38}$$

where

σ ; actual stress

$\delta\epsilon$; virtual strain that corresponds to the imposed virtual displacement

δa ; virtual displacement

f_B ; actual body force

f_S ; actual surface force

f_N ; actual nodal force

for the axisymmetric element, the volume integral of any function A becomes

$$\int_{V_e} A \, dV = \int_{V_e} A \, r \, dr \, dz \, d\theta \tag{2.39}$$

Volume integration can be written in the natural coordinate system. Notice that r, which is a global coordinate, appears in the integration, which is a unique feature of the axisymmetric element.

$$\int_{V_e} A \, dV = 2\pi \iint A \, r \, \det [J] \, d\xi \, d\eta \tag{2.40}$$

If there are no body forces, or initial stresses, Equation (2.38) becomes

$$\delta a^T \int_{V_e} [\, B \,]_e^T [\, C \,]_e [\, B \,]_e \, dV \, \{ \, U \, \} = \delta a^T \, f_N \tag{2.41}$$

by applying

$$\begin{aligned} \{ \delta\epsilon \} &= [B]_e \{ \delta U \} \\ \{ \sigma \} = [C]_e \{ \epsilon \} &= [C]_e [B]_e \{ U \} \\ \{\delta a \} &= [N] \{\delta U \} \end{aligned} \tag{2.42}$$

The stiffness matrix is obtained as,

$$[K]_e = \int_{V_e} [B]_e^T [C]_e [B]_e \, dV \tag{2.43}$$

It is very easy and convenient to use Gauss-Legendre numerical quadrature integration formula to evaluate Equation (2.43). The Gauss-Legendre integration points ξ_i and η_j and corresponding weighing factor α_{ij} are found in Ref. [24]. Care must be taken to substitute r in Equations (2.37) and (2.43). From Equation (2.26), r can be obtained as

$$\begin{aligned} r = \frac{1}{4}(1+\xi_i)\ (1+\eta_j)\, r_1 + \frac{1}{4}(1-\xi_i)\,(1+\eta_j)\, r_2 \\ + \frac{1}{4}(1-\xi_i)\,(1-\eta_j)\, r_3 + \frac{1}{4}(1+\xi_i)\,(1-\eta_j)\, r_4 \end{aligned} \tag{2.44}$$

After substituting ξ_i and η_j into ξ and η at the previous equations, $[K]_e$ can be obtained numerically as

$$[K]_e = \sum_{i,j=1}^{2} [B]_{i,j}^T [C]_e [B]_{i,j} \alpha_{i,j} \det[J]_{i,j} r \tag{2.45}$$

The assembly of element stiffness matrices, applying boundary conditions and the solution of resulting linear equations follow the standard procedures that can be found in Ref. [24,25].

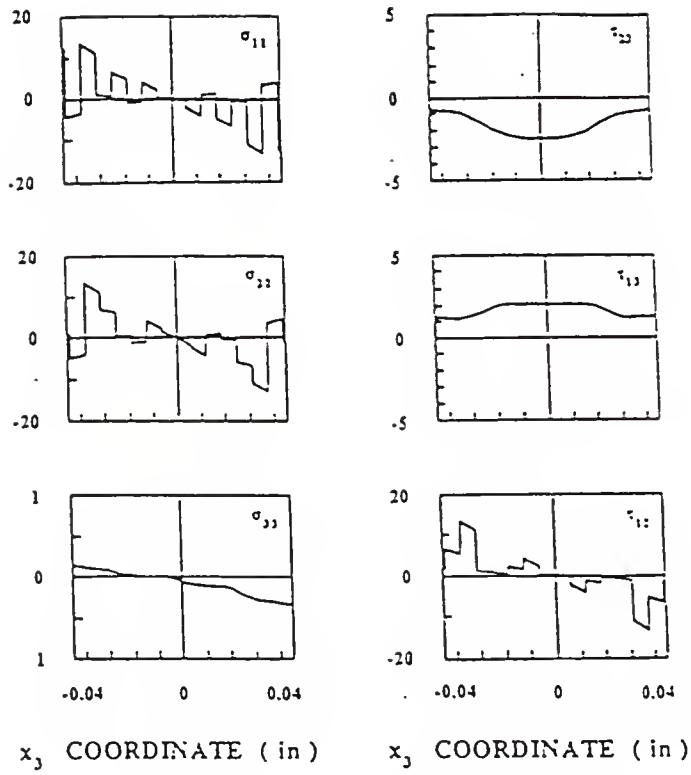

Figure 2.1 The continuity of the stresses through the thickness of the composite plate, Ref. [23]

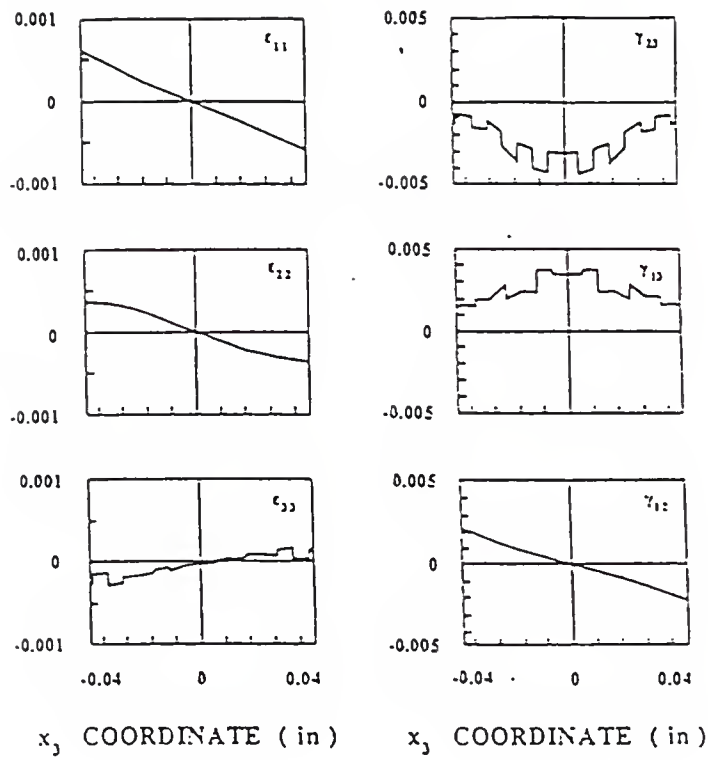

Figure 2.2 The continuity of the strains through the thickness of the composite plate, Ref. [23]

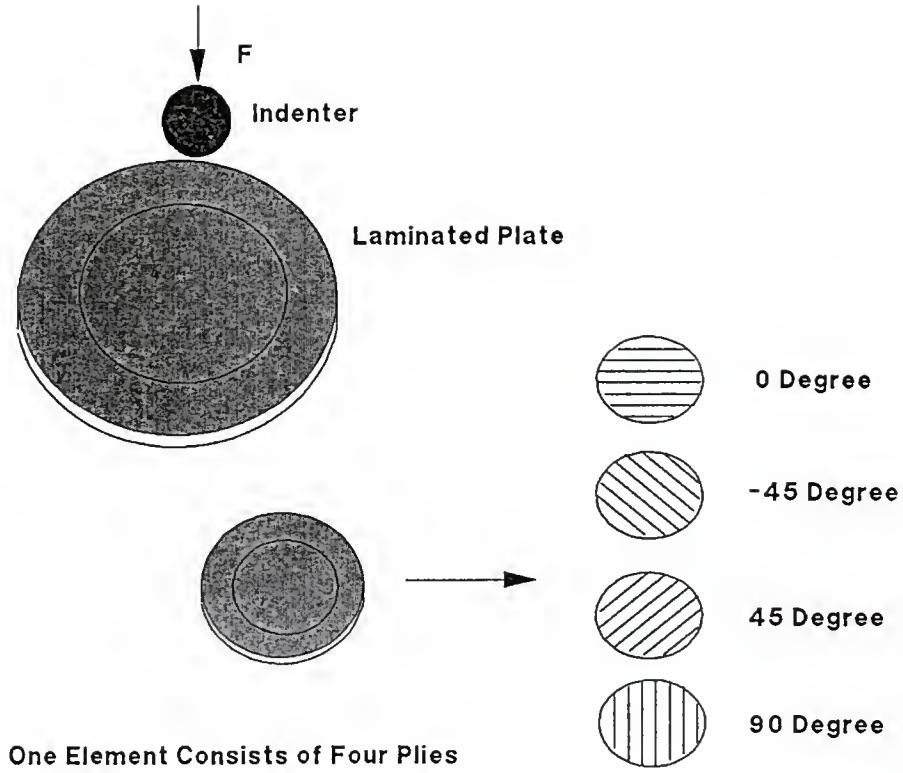

Figure 2.3 Stacking of plies to one element

Table 2.1 Material Properties of AS4/3501-6

(unit; Gpa)

E_1	144.8	$E_2=E_3$	9.7
$G_{12}=G_{13}$	6.0	G_{23}	3.6
$\nu_{12}=\nu_{13}$	0.3	ν_{23}	0.34

* Courtesy of Hercules Advanced Materials and Systems Company

Axisymmetric Element Property Matrix, $[\ C\ ]_e$

for $[\ 0^0,\ \pm 45^0,\ 90^0\ ]$

(unit ; Gpa)

$$\begin{bmatrix} 63.593 & 4.178 & 0 & 20.198 \\ 4.178 & 11.105 & 0 & 4.178 \\ 0 & 0 & 4.500 & 0 \\ 20.198 & 4.178 & 0 & 63.593 \end{bmatrix}$$

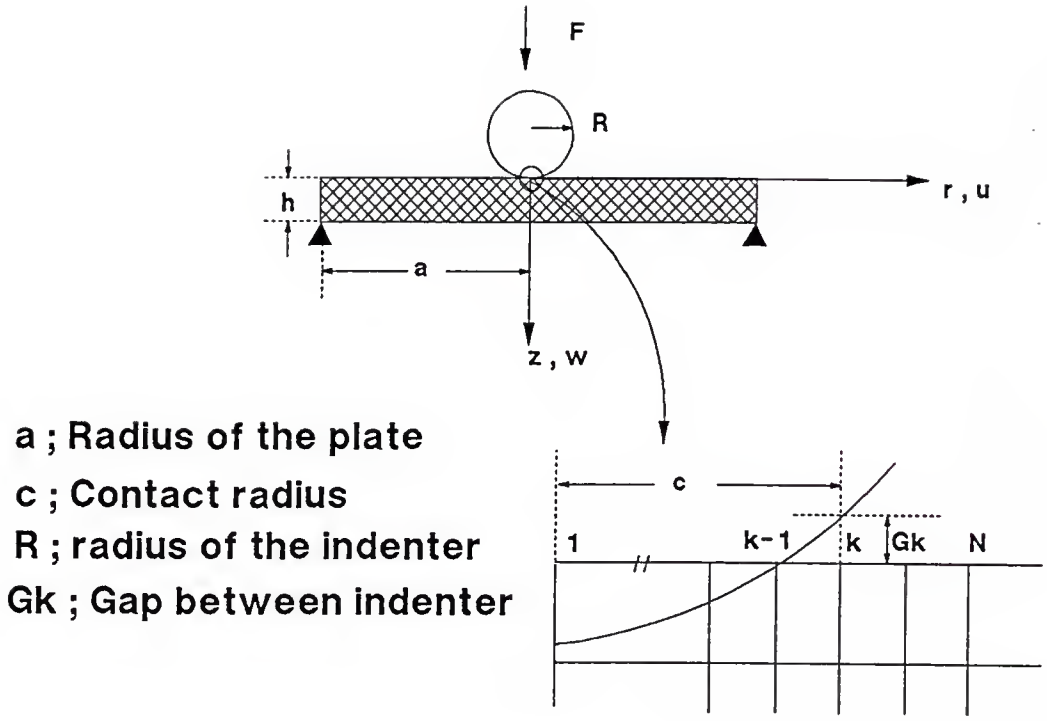

Figure 2.4 Indentation of a plate

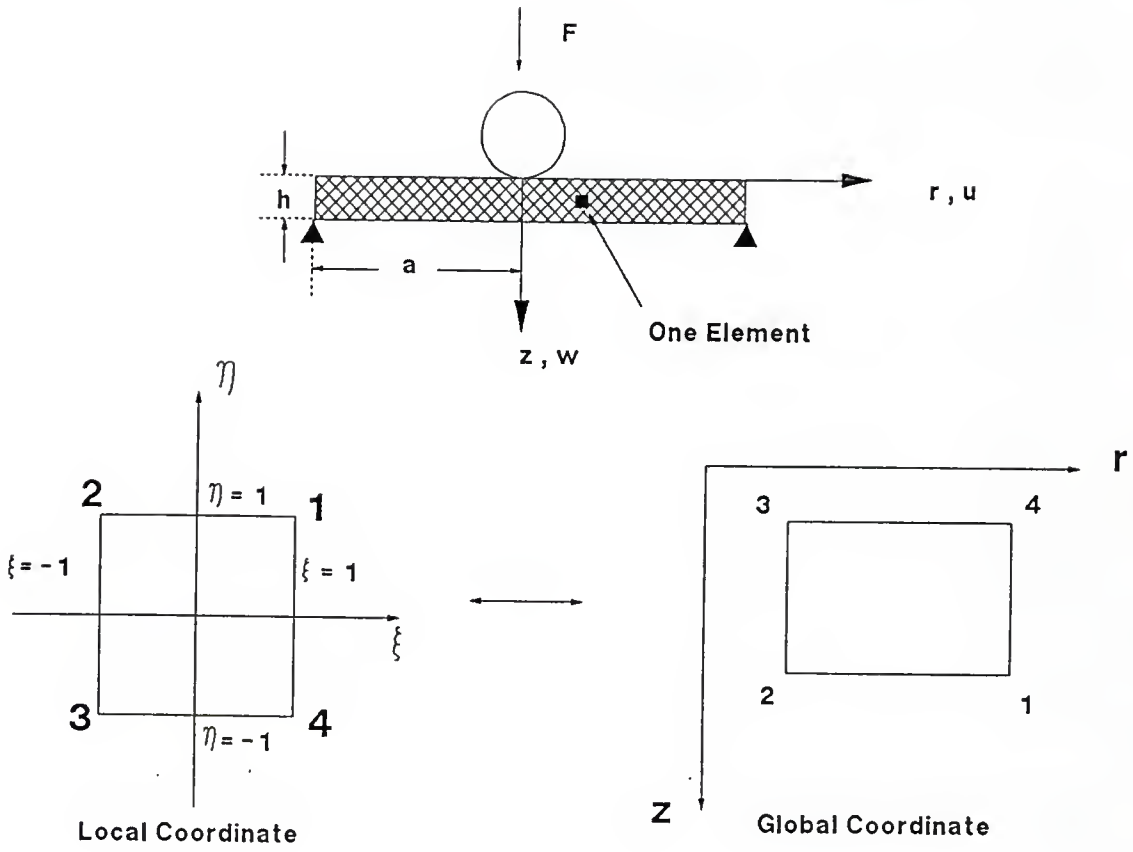

Figure 2.5 Axisymmetric Element

CHAPTER 3

RESULTS OF FINITE ELEMENT ANALYSIS

3.1 Introduction

In this chapter, the accuracy of the finite element program is evaluated by comparing with the results of Sankar [10], who employed a finite difference method to solve the equilibrium equations. The results obtained using only 384 finite elements (24 x 16) in the present study compared very well with that of Ref.[10]. In Section 3.2, available methods of increasing toughness and damage tolerance are briefly discussed. In Section 3.3, the finite element program was applied to the experimental test configuration shown in Figure 1.2 to obtain contact force vs. center deflection. Without modification of the total stiffness of the plate due to internal damages, finite element results seem to deviate from the experimental results. These deviations can be attributed to various damages as will be discussed in Chapter 4. However, in the elastic range, where damage is minimal, finite element results match the test curves well (Figure 3.6). In Section 3.4, various empirical equations including the Hertzian indentation law are briefly introduced and compared with finite element results in the elastic range. In Section 3.4.1,

the finite element program is used to study the indentation of solid cylinders and plates to compare with Hertzian indentation law. Effects of plate radius and indenter radius on indentation and deflection of the plate are studied. In Section 3.4.2, Hertzian contact pressure distribution, which is known to be elliptic, was compared with finite element results. In Section 3.4.3, the relation between contact force and contact radius was studied. It is known that in a half-space contact force varies as the cube of the contact radius. Finite element results matched very well with the available empirical equations. In Section 3.4.4, the relation between contact force and center deflection was studied. In Section 3.5, the effect of friction between indenter and plate was considered.

3.2 Evaluation of the Program

Hybridization, such as mixing the fiber types, thus utilizing the advantageous properties of one material to overcome deficiencies of another, is one method to deal with impact damages. The higher strain to failure of glass fiber or Aramid fibers (Kevlar) led to substantial increases in threshold energies for impact damage, with the energy level required to produce delamination being increased. The Aramid/graphite/epoxy hybridization is promising because Aramid material is relatively inexpensive and it increases impact resistance while graphite fibers provide compressive

strength, which Aramid fibers lack. Tests showed that doubling of residual strength after impact was possible using Aramid/graphite hybridization compared to an all graphite specimen [2].

It is well known that tough resins can significantly reduce the damage caused by impact and substantially improve the residual strength following impact. This is because the onset of delamination and the delamination growth in a composite depends on its interlaminar fracture toughness, which in turn depends on the toughness of the matrix material. Widely used epoxy resins are brittle, but crystalline thermoplastics such as PEEK (Poly-ether-ether-ketone) can be used in place of epoxy to increase toughness. Mode I fracture toughness of the graphite/epoxy ranges 80-200 J/m^2 , while the fracture toughness of graphite/PEEK is about 2500 J/m^2 [2]

Interleaving is a process in which thin layers of thermoplastics are placed in between layers of thermosetting prepreg materials to form a tough interlayer. It is useful if the failure occurs through delamination. It is not effective if the transverse shear is high and, for this case, an improvement of shear modulus of the resin is more important [2].

Through thickness reinforcements, such as a three dimensional braiding process or through-the-thickness stitching, can improve impact resistance. However, in-plane

strength will be reduced because of wavy fibers and irregular fiber orientations.

Sankar [10] performed the analysis of indentation of hybrid and interleaved plate problems by using a finite difference method starting from the axisymmetric equilibrium equations.

$$C_{11}\left(u_{,rr} + r^{-1}u_{,r} - r^{-2}u \right) + C_{44}u_{,zz} + \left(C_{13} + C_{44} \right) w_{,rz} = 0 \tag{3.1}$$

$$\left(C_{13} + C_{44} \right) \left(u_{,rz} + r^{-1}u_{,z} \right) + C_{33}w_{,zz} + C_{44}\left(w_{,rr} + r^{-1}w_{,r} \right) = 0 \tag{3.2}$$

where

$$\begin{Bmatrix} \sigma_{rr} \\ \sigma_{\theta\theta} \\ \sigma_{zz} \end{Bmatrix} = \begin{bmatrix} C_{11} & C_{12} & C_{13} \\ C_{12} & C_{11} & C_{13} \\ C_{13} & C_{13} & C_{33} \end{bmatrix} \begin{Bmatrix} \epsilon_{rr} \\ \epsilon_{\theta\theta} \\ \epsilon_{zz} \end{Bmatrix} \tag{3.3}$$

$$\tau_{rz} = C_{44}\,\gamma_{rz} \tag{3.4}$$

The results obtained by the present finite element program coincide very well with results in Ref. [10]. Figure 3.2 shows contact force vs. contact radius relationship for

the three different laminated plates. Material properties of the composite laminates are listed in Table 3.1.

Figure 3.3 shows interlaminar shear stress in the homogeneous graphite/epoxy laminate. Figure 3.4 shows interlaminar shear stress in the hybrid laminate. Employing the finite element program is very economical because only 384 (24 x 16) elements were used, and computing time was about 30 minutes in a Vax main frame computer. Although this analysis does not account for the internal damages of the plate, it provides information about the possible onset of delamination and its subsequent propagation. As delamination failure occurs where shear stress is high, shear stress distributions such as Figures 3.3 and 3.4 suggest locations where delamination failures possibly may initiate. By obtaining other strain and stress distributions inside plate, possible damage pattern, such as matrix crack and fiber breakage, and its extent can be predicted conservatively and less expensively before detailed damage analysis. Strengthening by inserting tough materials or hybrid laminates to minimize delaminations can be studied by using the finite element program.

Detail damage analyses are presented in Chapter 4.

3.3 Comparison with Test Results

The finite element program was used to analyze some of the specimens used in the indentation tests discussed in Section 1.2. The contact force vs. center deflection curve was

obtained without considering damages inside the plate and was compared with the test results in Figure 3.5. Even in the presumably elastic range, finite element results make the plate appear stiffer. However, from Hashin's failure criteria, which will be discussed in Section 4.1, the damages begin to accumulate at about 140 N contact force or 0.33 mm center deflection. Hence the actual elastic range is very small. Comparing the results only in this elastic range, results of finite element and experimental data showed fairly good agreement. A total of 512 elements (32 x 16) were employed. Fine mesh was used near the center of the plate, and coarser elements were employed outside the contact region. Actually, finite element results form an upper bound for the test results. It can be easily explained that these early deviations of the stiffness of the test results are due to the inherent imperfections in the test specimens such as voids, debonds and nonuniform fiber orientations.

3.4 Comparison of Contact Behavior

In this section, various results concerning indentation, contact pressure distribution, contact radius and center deflection obtained using the present finite element method are compared with available results.

3.4.1 Hertzian contact law

Because of the extremely difficult nature of analytical solutions of contact problem, which involves permanent deformations and damage such as matrix cracks and delamination, an experimental approach has been taken to determine the contact law of composite materials. Naturally, loading and unloading curves (contact force-indentation relation) are different because damages occur even at low load levels. This is because composite materials, unlike monolithic materials, have very low resistance to the damage due to loads transverse to the fiber direction.

For the loading curve of contact between an elastic sphere and elastic half space, the Hertzian contact law [6] is

$$F = K_c \, \alpha^{\frac{3}{2}} \tag{3.5}$$

where K_c is

$$K_C = \frac{4}{3} \sqrt{R_s} \left[\frac{(1 - \nu_s)^2}{E_s} + \frac{(1 - \nu_t)^2}{E_t} \right]^{-1} \tag{3.6}$$

Subscript s denotes the indenter and t denotes the target. In Equation (3.6), R_s, ν_s and E_s are the radius, the Poisson's ratio and the Young's modulus of the indenter, respectively. When a metal indenter like a steel ball indents a polymer

composite, the indenter can be assumed rigid because Young's modulus of steel is much higher than E_z, the modulus of elasticity of the composite in the transverse direction. For loading, Sun and Yang [6] suggested the contact force-indentation relationship in the form

$$F = \frac{4}{3} E_z \sqrt{R_s}\, \alpha^{3/2} \tag{3.7}$$

A more complex form of contact law obtained by Conway [26] for an elastic spherical impactor striking a transversely isotropic composite medium has only 3 percent difference from Equation (3.7) in the example problem to be presented in this section. In Equation (3.7), C_{44} of $[\ C\ ]_{av}$ matrix can be replaced by E_z without significant error (4 percent difference in this example problem).

The unloading formula suggested by Sun and Yang [6] was

$$F = \frac{K_c}{\alpha_{cr}} (\alpha - \alpha_0)^{2.5} \tag{3.8}$$

where

$$\alpha_0 = \alpha_m \left[1 - \left(\frac{\alpha_{cr}}{\alpha_m}\right)^{\frac{2}{5}}\right] \quad , \quad \alpha_m > \alpha_{cr}$$
$$\alpha_0 = 0 \quad , \quad \alpha_m \le \alpha_{cr} \tag{3.9}$$

In Equation (3.9), α_m is the indentation corresponding to the maximum contact force before unloading. It is assumed that the critical indentation, α_{cr}, depends only on the material properties.

Contact force vs. indentation graphs were obtained by the finite element program for the clamped solid cylinder of 20 mm radius and 20 mm thickness of a hypothetical isotropic material, and also for AS4/3501-6 composite laminate plate of 25.4 mm radius. The material properties are listed in Table 3.1. A total of 512 elements (32 x 16) were employed. Inside the contact region, fine mesh is used, while coarser mesh size is assigned outside the contact region. Each computer run took 75 minutes on the average in the Vax main frame computer. In the case of indentation of the thick cylinder, the center displacement at the top becomes indentation directly. For the plate, indentation is defined as displacement difference between top and bottom surface of the plate at the center,

$$\alpha = w(0) - w(h) \tag{3.10}$$

The results for contact force-indentation are presented in Figures 3.8 and 3.9. For the solid cylinder of isotropic material, the finite element results and Hertzian indentation law of Equation (3.6) agree very well as seen in Figure 3.8, although errors were expected because we have not solved the half space contact problem, and the indenter can not be

simulated exactly as a sphere in a finite element program. For the plate of isotropic material, contact forces predicted by the finite element model are larger than forces calculated by Hertzian contact law when the indentation is large (Figure 3.8). Sankar [27] noticed this difference in the contact coefficients of Equation (3.5) between contacts of a sphere with a half space and with a plate. He suggested that differences of the definitions of indentation between half space and plate may be the cause of the problem. The finite element contact forces of the composite plate (4 mm thickness) are shown in Figure 3.9.

To check the influence of the radius of the plate, 25.4 mm, 38.1 mm, and 50.8 mm radius plates are compared in Figures 3.10 and 3.11 (the indenter radius is 12.7 mm). Although the contact force vs. center deflection curve shows a big difference due to the bending effect of the plate (Figure 3.10), contact force vs. indentation curve does not vary so much (Figure 3.11). At small indentation, contact force seems to be independent of thickness and radius of the target.

To verify that contact force is proportional to the square root of indenter radius, two different indenter radii, 6.35 mm and 12.7 mm, were used to indent a 4 mm composite plate (Figure 3.12). The contact force curve obtained using the finite element program for the indenter radius 6.35 mm was denoted as F_1 and the curve for 12.7 mm indenter as F_2. It may

be seen that for the small indentation, the contact force is proportional to the square root of indenter radius.

3.4.2 Contact pressure distribution of the plate

The contact pressure distribution for half-space indentation is as follows [27].

$$\sigma = \frac{3\,P}{2\,\pi\,C^2}\sqrt{1-(r/C)^2} \qquad (3.11)$$

where P is contact force, and C is contact radius. Finite element results were compared with these equations in Figure 3.13. Obtaining contact stress distribution by experimental test is not easy and no data is available for the tests done as in Section 1.2. Contact pressure distribution calculated by the finite element method in the 4 mm plate (Figure 3.13) is elliptic. Contact pressure of the finite element method was computed from the average vertical stress σ_z of the elements in contact with the indenter. Although calculated contact forces were larger than predicted by the half-space formula, Equation (3.11), the contact pressure distribution is still elliptical.

3.4.3 Contact radius of the plate

In a half-space the contact force is proportional to the cube of the contact radius C. By inserting an empirically

obtained relationship between indentation and contact radius for the indenter radius as in Equation (3.12) into Hertzian contact law, Equation (3.7), we can obtain Equation (3.13) [28].

$$\alpha = \frac{C^2}{R_s} \tag{3.12}$$

$$P = \frac{4E_z}{3R_s} C^3 \tag{3.13}$$

Finite element results for a 4 mm plate are compared with the above equation in Figure 3.14. In Figure 3.15, contact force vs. contact radius curves of plates of different thicknesses are compared. As plate thickness becomes larger, more contact force is needed to maintain the same radius of contact, as expected. However, for the small contact radius, contact force can be assumed to be independent of thickness of the plate as suggested in Equation (3.13).

3.4.4 Center deflection of the plate

The center deflection δ of the impacted surface of the plate can be expressed as the sum of indentation and of displacements due to bending and shear. In the case of small deflection, membrane effects can be neglected. Indentation was

obtained from Equation (3.7). Plate bending stiffness, K_p, can be expressed as [29],

$$K_p = \frac{16\pi(1+\nu)D}{(3+\nu)a^2} \tag{3.14}$$

for the axisymmetric plate with thickness h and radius a. In Equation (3.14), D is

$$D = \frac{Eh^3}{12(1-\nu^2)} \tag{3.15}$$

where, E can be replaced by C_{11} of the matrix $[\ C\ ]_{av}$ and ν, Poisson ratio, can be replaced by ν_{12}. Shear deflection can be obtained from

$$\tau_{rz} = G\frac{\partial w}{\partial r} = \frac{P}{2\pi r h} \tag{3.16}$$

Plate shear stiffness, K_s, can be obtained as

$$K_s = \frac{2\pi G h}{[\ Ln\ a - Ln\ C\ ]} \tag{3.17}$$

and C can be obtained from Equation (3.12).

Then, the center deflection δ is expressed as

$$\delta = \left(\frac{P}{K_c} \right)^{\frac{1}{1.5}} + \frac{P}{K_p} + \frac{P}{K_s} \qquad (3.18)$$

Finite element results of a 4 mm plate are compared with Equation (3.18) in Figure 3.16. It is shown that Equation (3.18) can predict good results for the elastic response of the plate. This result suggests that center deflection is a more reliable parameter than indentation to obtain the contact force.

3.5 Friction Effect

The effect of friction is studied by assuming that the coefficient of friction is very large. There are only compressive forces between the upper surface of the plate and the indenter. Stick condition requires that there be no relative motion during a load increment between indenter and plate at the contact nodes. This condition is satisfied by constraining the radial displacements of the nodes after they come into contact with the indenter [30-31]. This can be easily implemented in the finite element program by modifying the contact algorithm which was developed in Section 2.4. Now, displacements in Equation (2.22) in Section 2.4 must include radial displacements of the upper nodes. In Equation (2.22), w_c is replaced by

$$\{ w_k \} = \{ u_1, w_1, u_2, w_2, \ldots . u_{i-1}, w_{i-1} \}^T \qquad (3.19)$$

Treating the vertical displacements in the same way as in Chapter 2.4, we now put zero for the radial displacements in Equation (3.19) during contact.

Radial force is very large compared to vertical force because of the high modulus of radial and circumferential stiffness due to the presence of fibers. Hence, matrix failure may occur virtually immediately after contact starts. Calculated contact force vs. center deflection for both frictional and frictionless contact are shown in Figure 3.17. The effect of friction is significant at higher contact forces. However, the radial stresses developed may cause failure even at smaller loads, and the result shown in Figure 3.17 may not be applicable in practical situations.

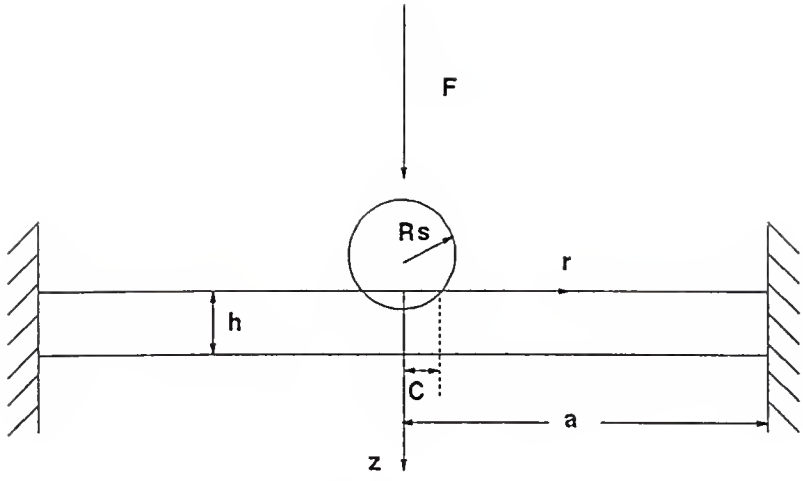

Rs ; Radius of indenter, 10 mm

h ; Thickness of plate, 2 mm

C ; Contact radius

a ; Radius of plate, 50 mm

Figure 3.1 Plate dimensions in numerical examples

Table 3.1 Material properties of the plates used in the examples [10],

(unit, GPa)

Material	E_r	E_z	G_{rz}	ν_{rz}	$\nu_{r\theta}$
1	50	7	3.8	0.285	0.265
2	20	8	3.6	0.270	0.255
3	3	3	1.1	0.350	0.350

1. Homogeneous laminate plate

   material 1, thickness 2 mm

2. Hybrid laminate plate

   material 1, thickness 0.25 mm

   material 2, thickness 0.25 mm

   material 1, thickness 1.5 mm

3. Interleaf laminate plate

   material 1, thickness 0.25 mm

   material 3, thickness 0.25 mm

   material 1, thickness 1.5 mm

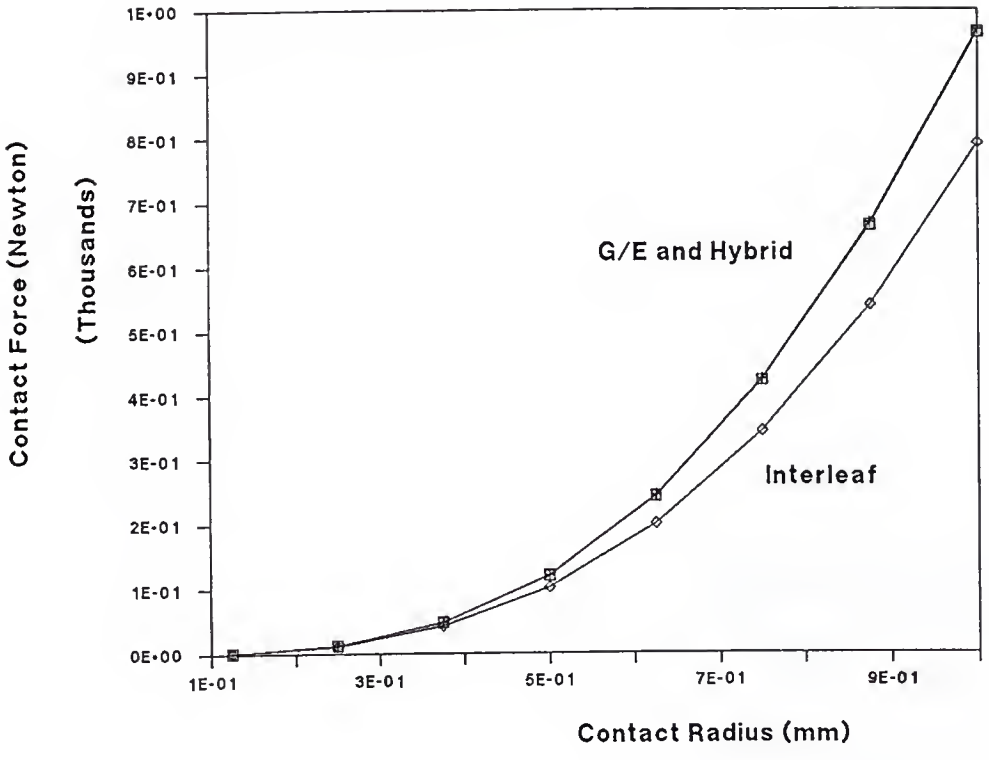

Figure 3.2 Contact force vs. contact radius relationship

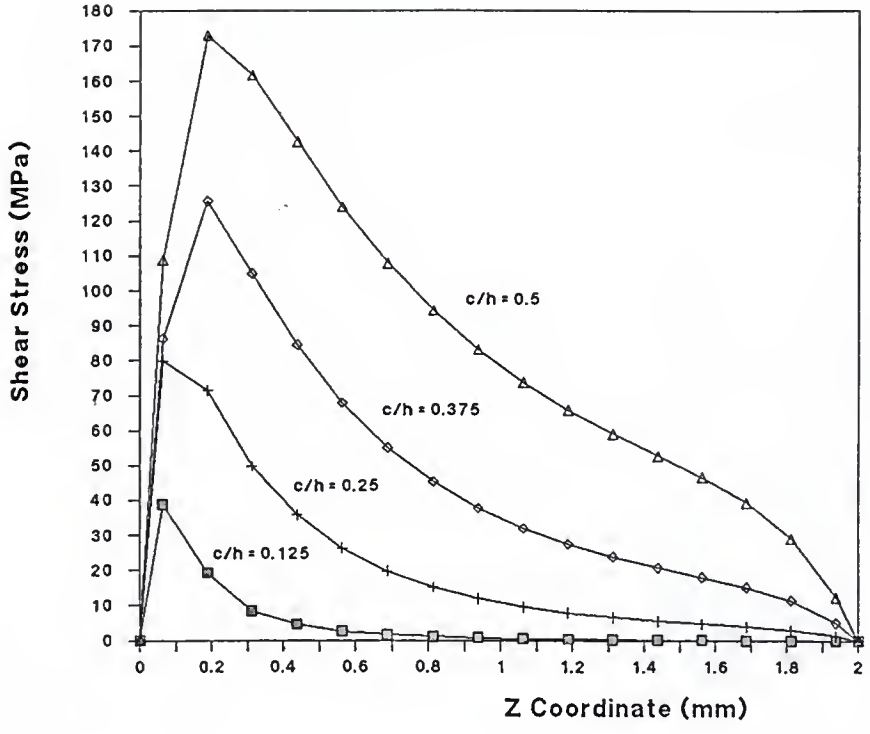

Figure 3.3 Interlaminar shear stresses in the graphite/epoxy laminates

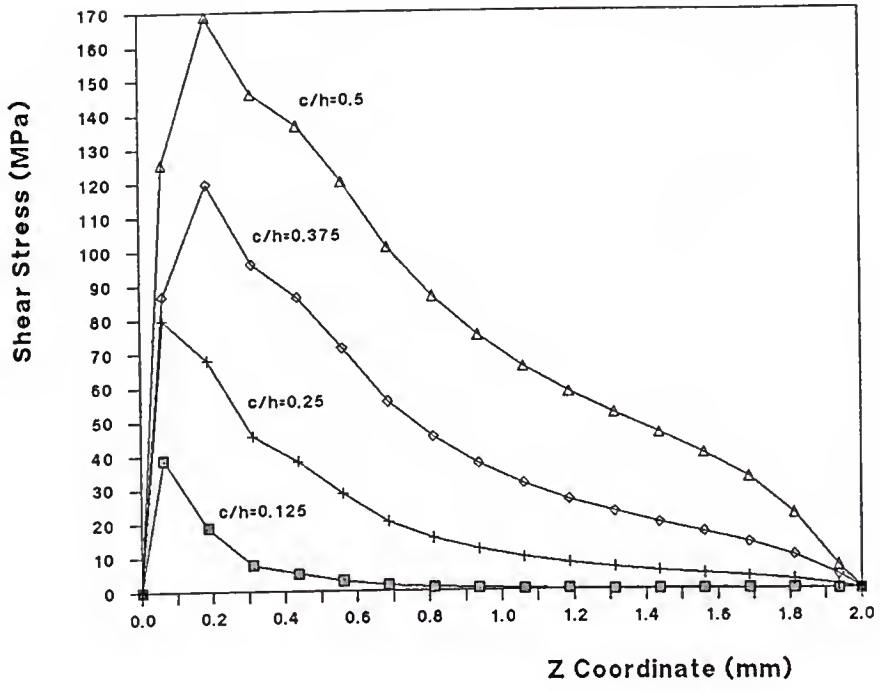

Figure 3.4 Interlaminar shear stresses in the hybrid laminates

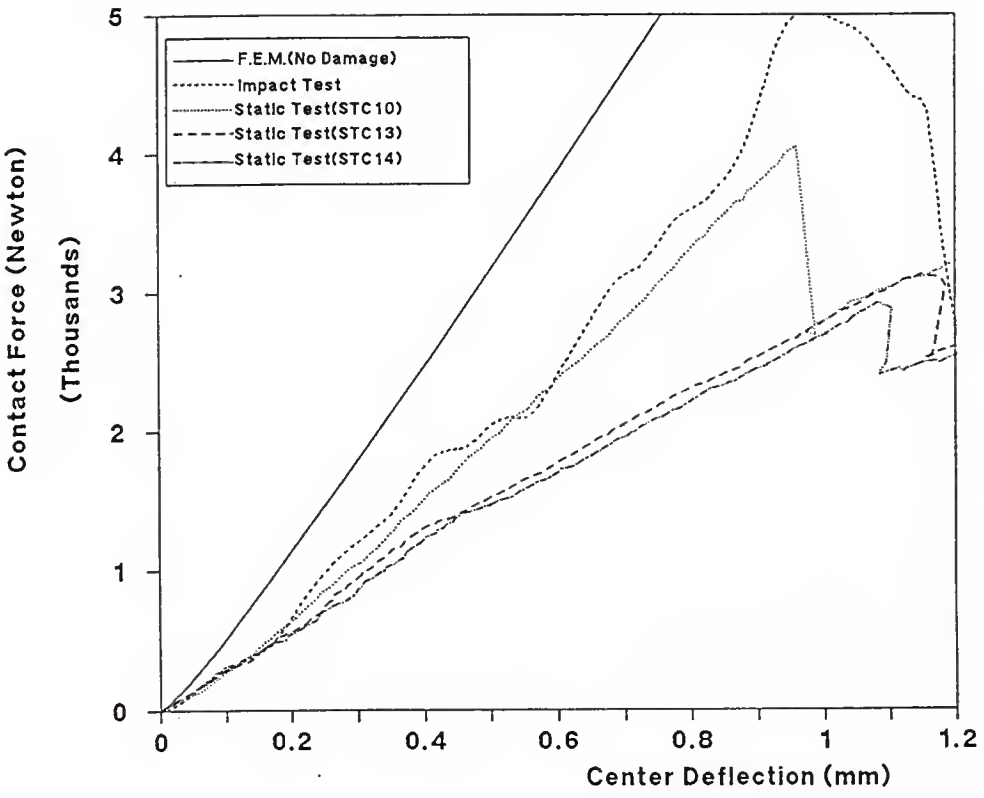

Figure 3.5 Contact force vs. center deflection curve

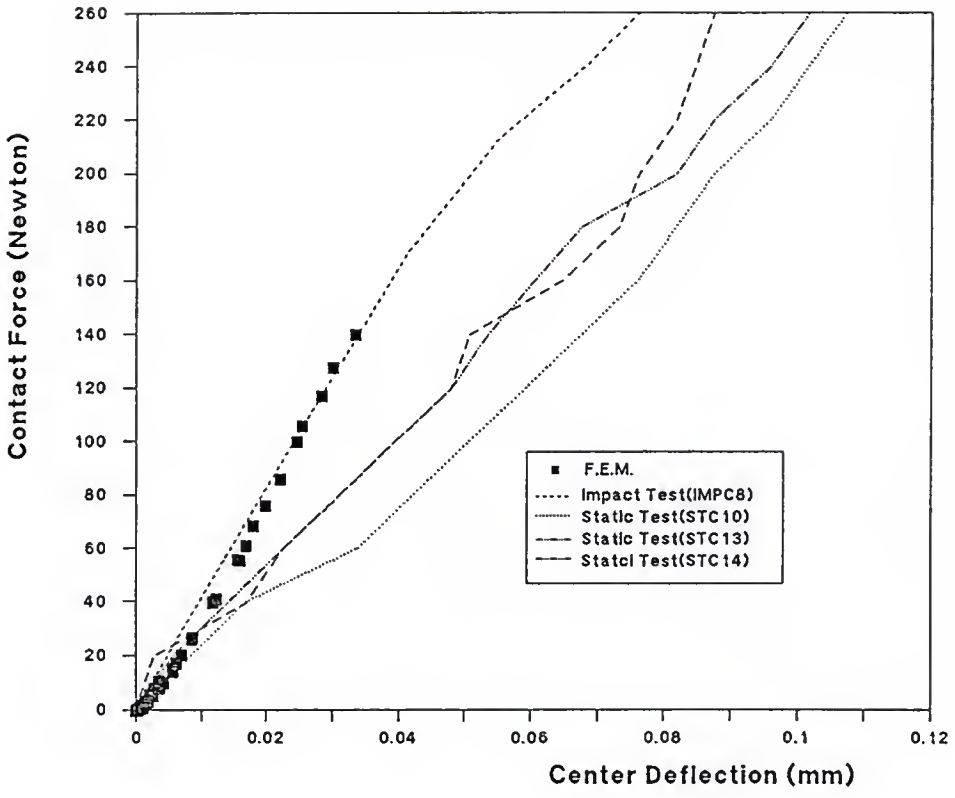

Figure 3.6 Contact force vs. center deflection curve, elastic range

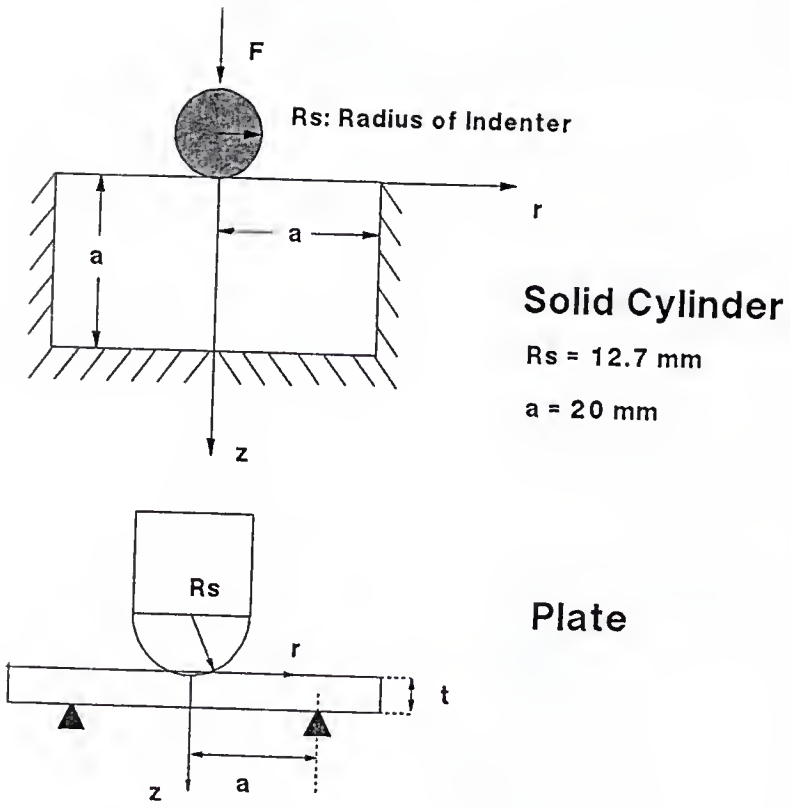

Figure 3.7 Configurations for numerical examples

Table 3.2 Material properties of the Numerical applications

Isotropic Material

E = 2.0 GPa ν = 0.25 G = 0.8 GPa

$$[C]_e = \frac{E(1-\nu)}{(1+\nu)(1-2\nu)} \begin{bmatrix} 1 & \frac{\nu}{1-\nu} & 0 & \frac{\nu}{1-\nu} \\ \frac{\nu}{1-\nu} & 1 & 0 & \frac{\nu}{1-\nu} \\ 0 & 0 & \frac{1-2\nu}{2(1-\nu)} & 0 \\ \frac{\nu}{1-\nu} & \frac{\nu}{1-\nu} & 0 & 1 \end{bmatrix}$$

$$[C]_e = \begin{bmatrix} 2.4 & 0.8 & 0 & 0.8 \\ 0.8 & 2.4 & 0 & 0.8 \\ 0 & 0 & 0.8 & 0 \\ 0.8 & 0.8 & 0 & 2.4 \end{bmatrix}$$

Composite Material

E_r = 56.427 GPa E_z = 10.688 GPa G_{rz} = 4.5 GPa ν_{rz} = 0.263

$\nu_{r\theta}$ = 0.3

$$[C]_{av} = \begin{bmatrix} 63.593 & 4.178 & 0 & 20.198 \\ 4.178 & 11.105 & 0 & 4.178 \\ 0 & 0 & 4.5 & 0 \\ 20.198 & 4.178 & 0 & 63.593 \end{bmatrix}$$

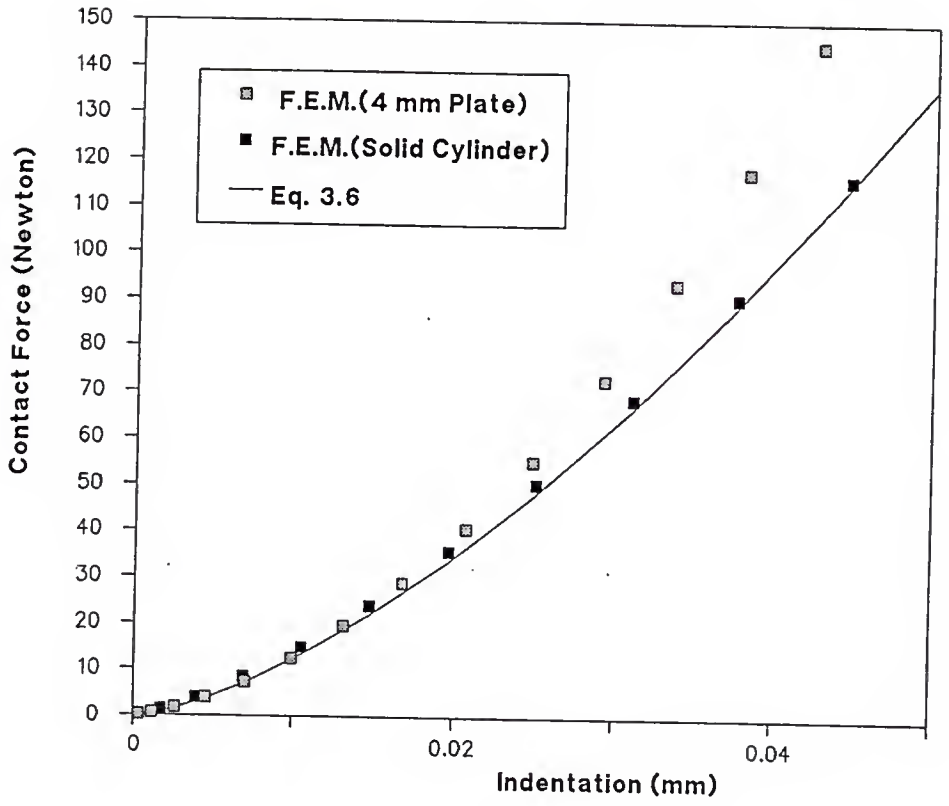

Figure 3.8. Contact force vs. indentation curve, isotropic material

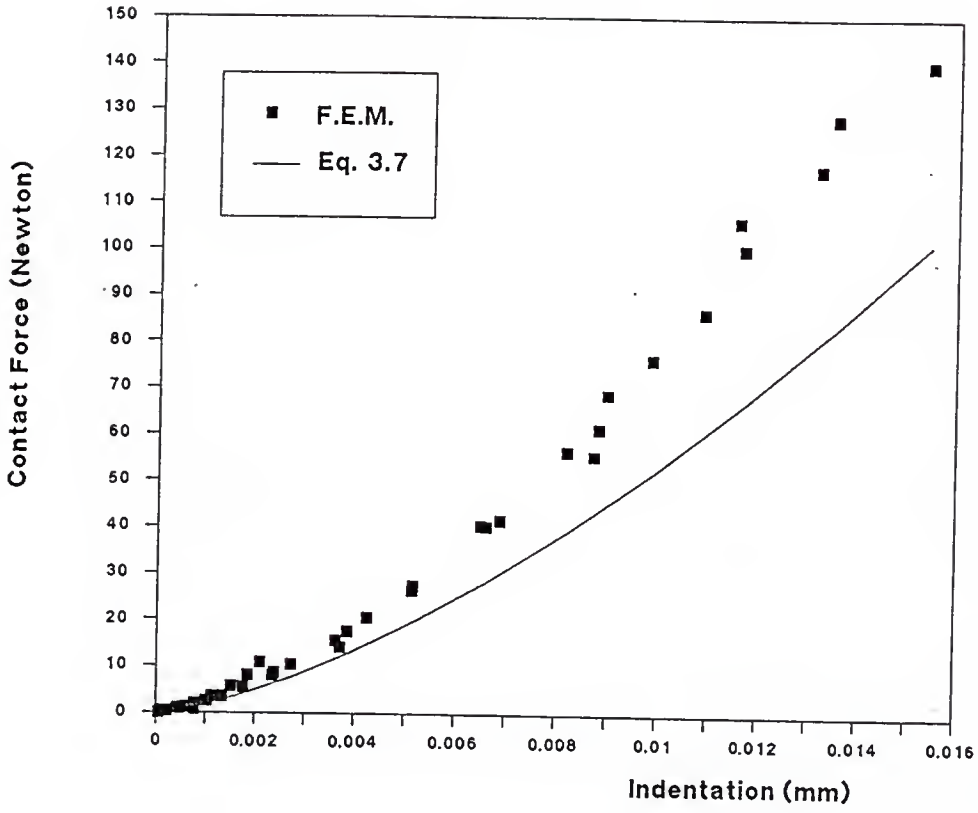

Figure 3.9. Contact force vs. indentation curve, composite plate (4 mm thickness)

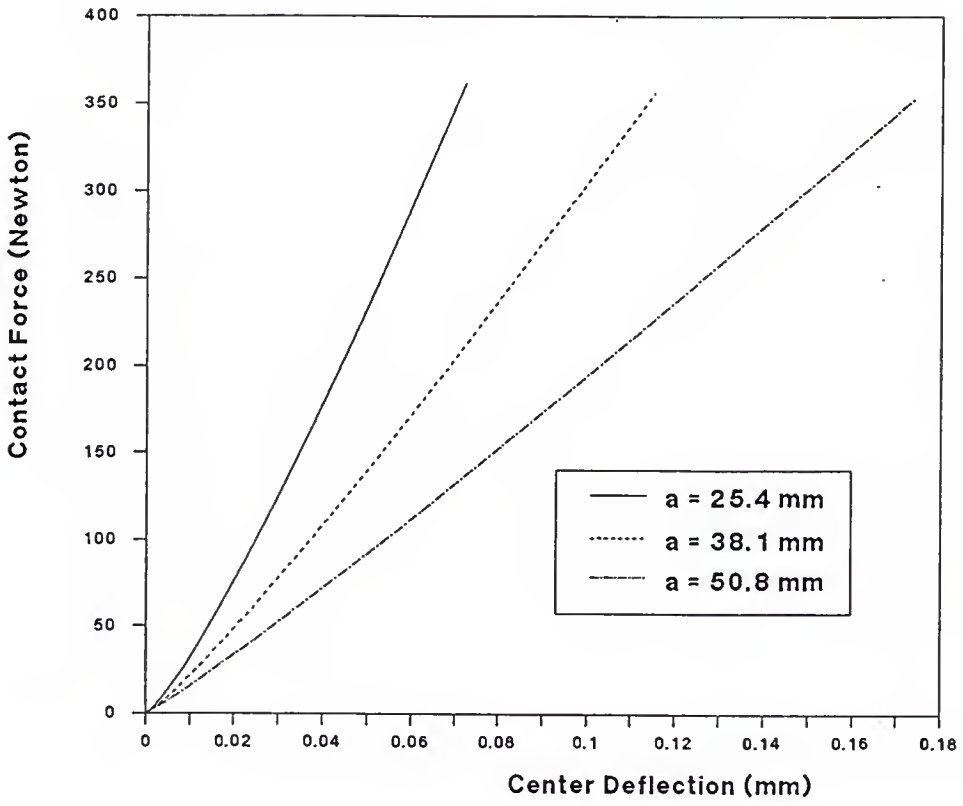

Figure 3.10. Effect of plate radius on contact force vs. center deflection curve

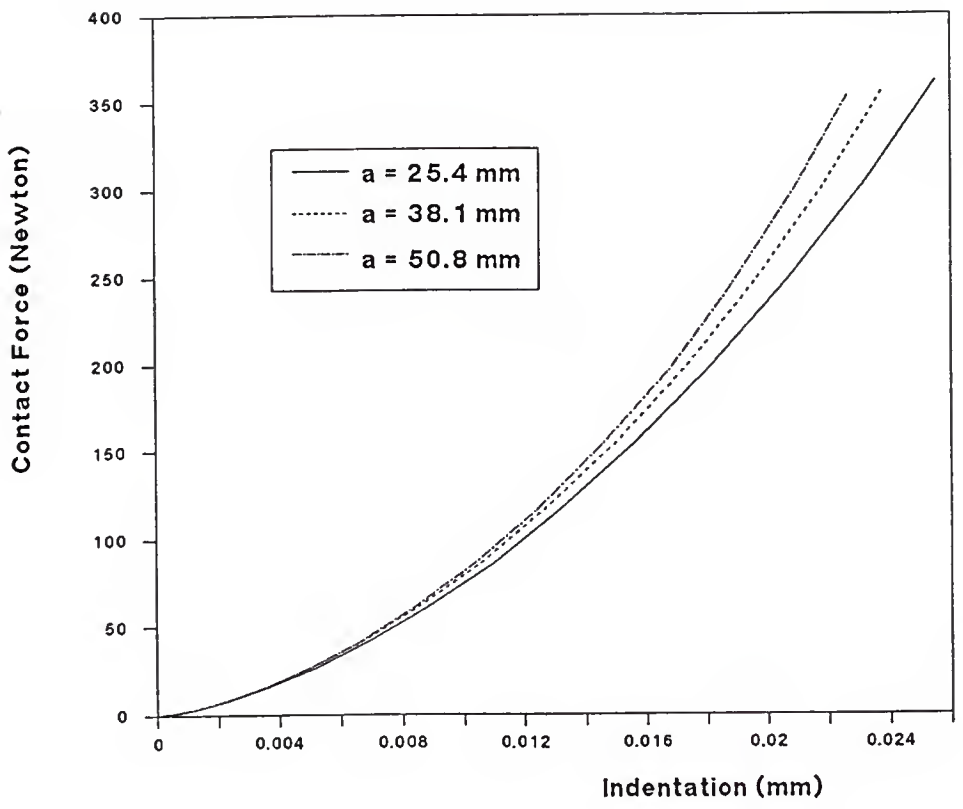

Figure 3.11. Effect of plate radius on contact force vs. indentation curve

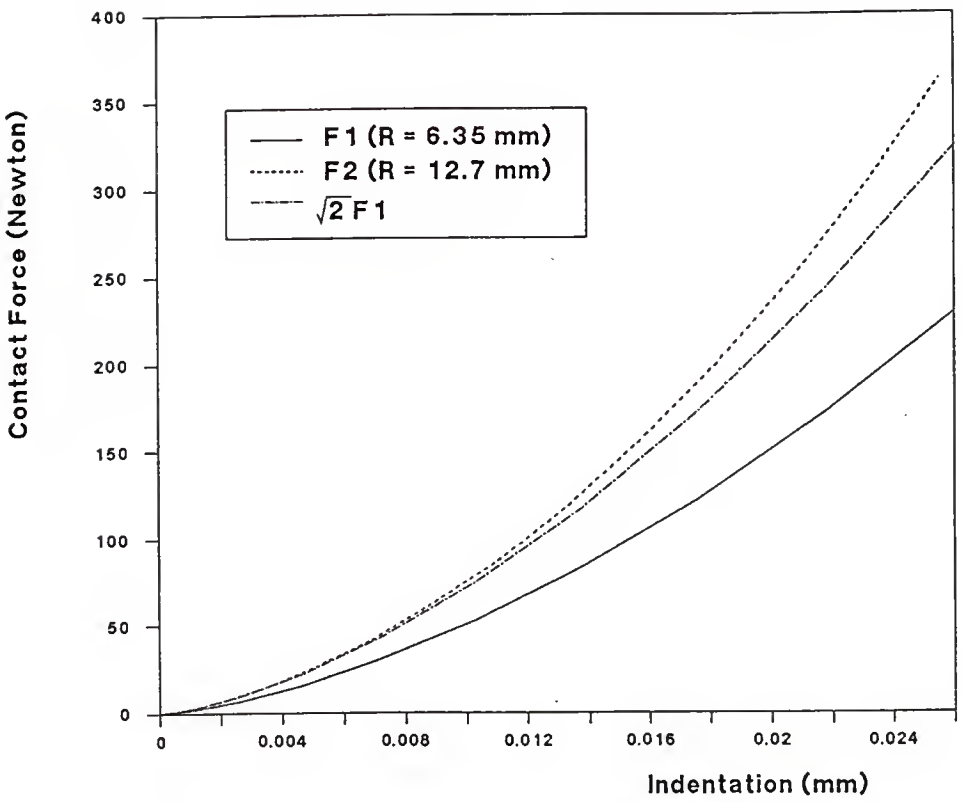

Figure 3.12. Effect of indenter radius on contact force vs. indentation curve

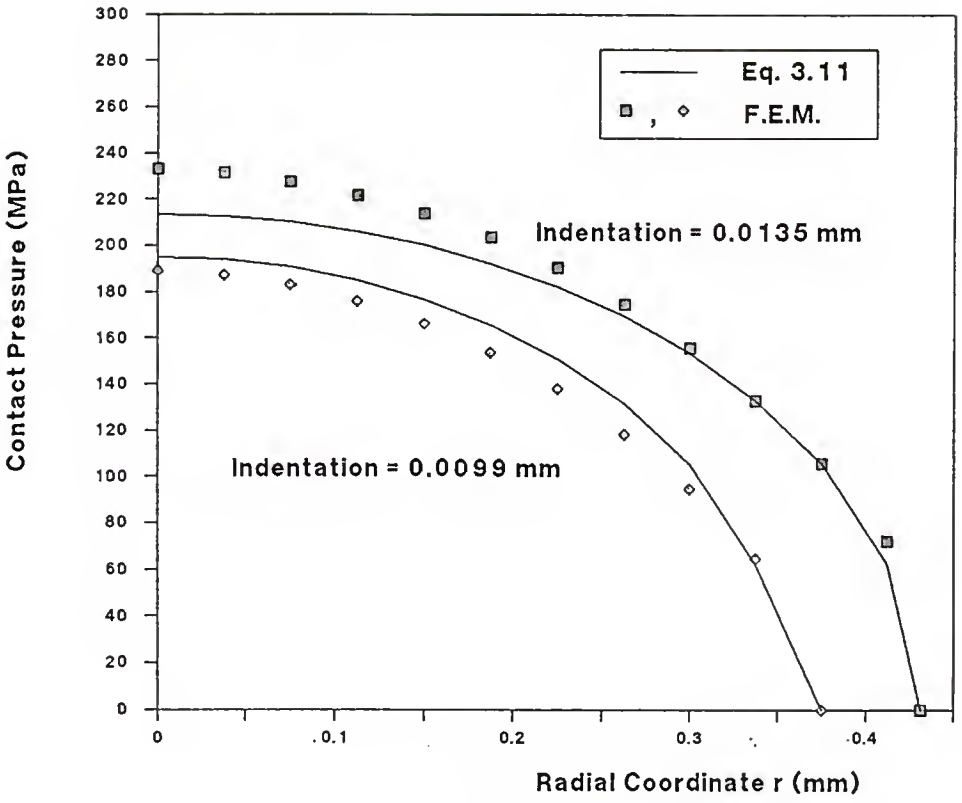

Figure 3.13. Contact pressure distribution

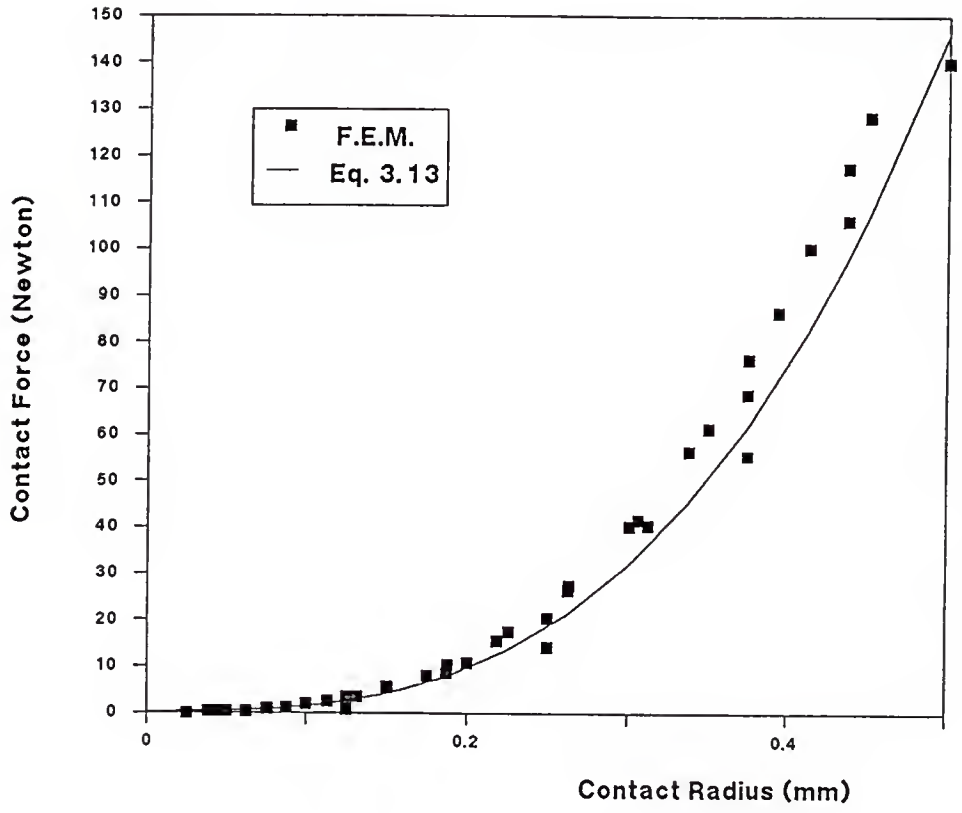

Figure 3.14. Contact force vs. contact radius

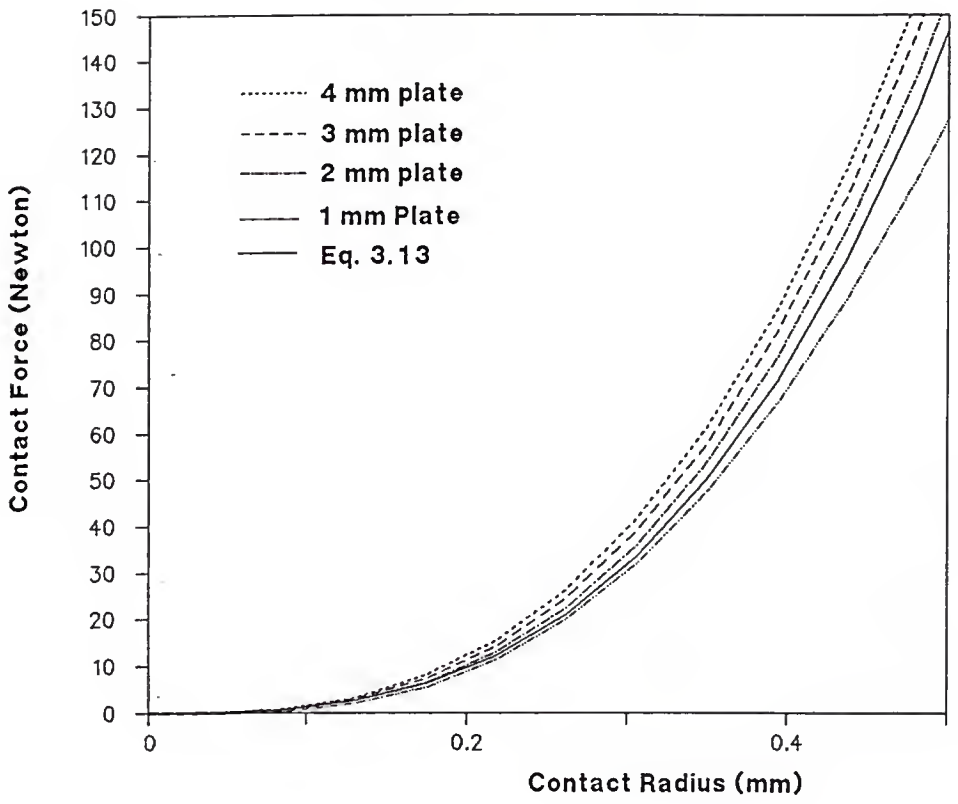

Figure 3.15. Contact force vs. contact radius, comparison

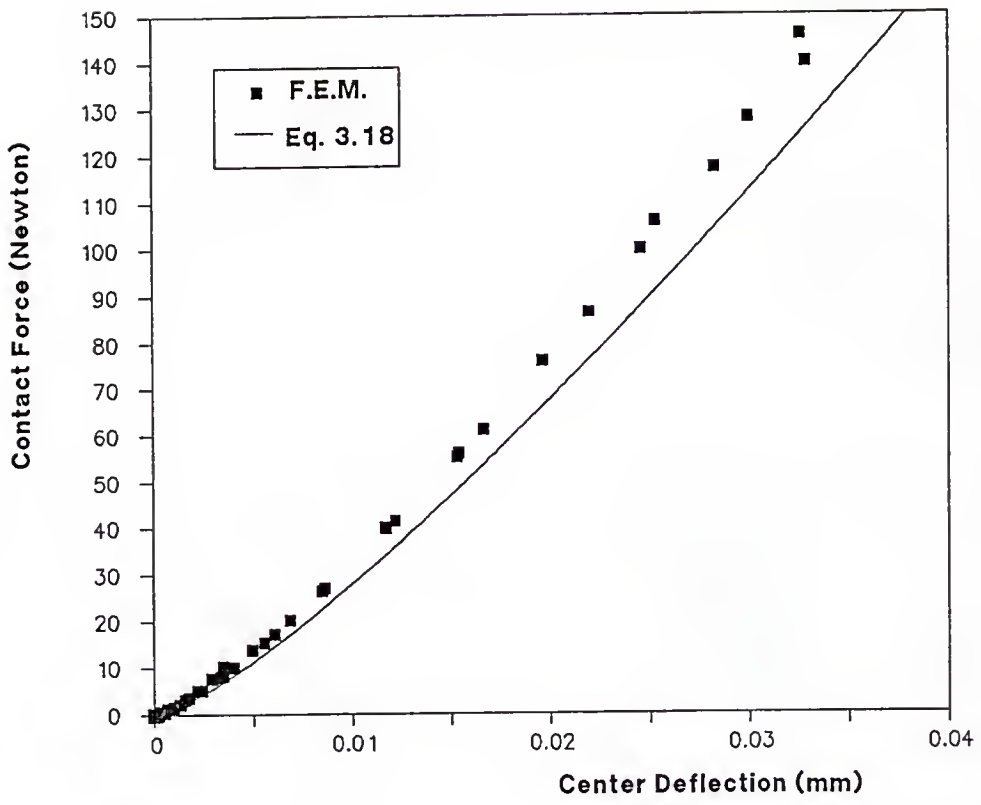

Figure 3.16. Contact force vs. center deflection

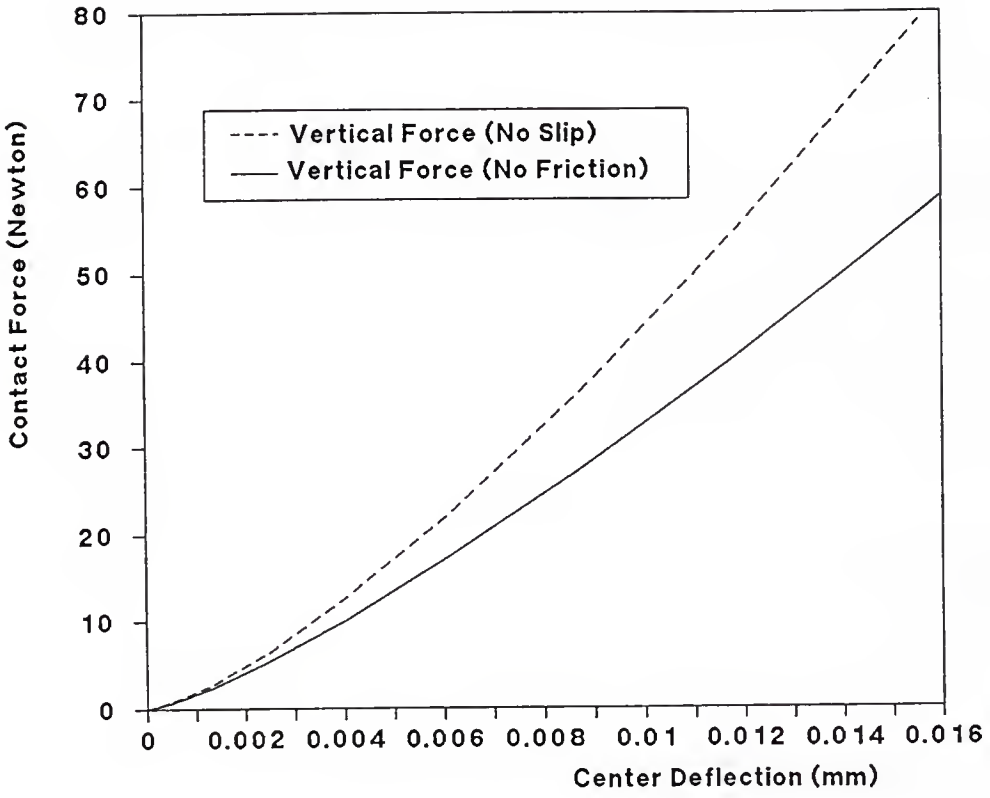

Figure 3.17. Friction effect

CHAPTER 4

DAMAGE ANALYSIS

4.1 Failure Criteria

The calculated stresses and strains from the axisymmetric elements are based on the assumption that the plate is transversely isotropic. However, the plate consists of multiple plies where each ply is orthotropic and has different fiber orientation. Hence, direct application of any existing failure criteria which are based on stresses in the material coordinates is not possible. An estimate of stresses in the material coordinates has to be obtained from the axisymmetric results.

The existing failure criteria for composite materials can be divided into two types. One is a interactive failure criterion and the other is a set of independent failure criteria for different failure modes. The interactive failure criterion is basically an empirical technique, and determination of the components in the polynomials of the criterion requires difficult and expensive biaxial tests. The most important criterion in this category is the Tsai-Wu theory, which uses a general quadratic polynomial including

linear terms. This theory says that a failure surface in the stress space exists in the form as

$$F_i\sigma_i + F_{ij}\sigma_i\sigma_j = 1 \quad , \quad i,j = 1,\ldots,6 \qquad (4.1)$$

where F_i and F_{ij} are second and fourth order strength tensors. This criterion can not be widely used because of difficulties in obtaining F_{ij}. These criterion only predicts the onset of failure and not the failure modes. However, if F_i and F_{ij} can be obtained correctly, this criterion may be satisfactory, and it is simple to use [13,14].

Independent failure criteria, typically maximum stress theory or maximum strain theory, can predict the onset of failure and also failure modes. Distinguishing failure modes is very important for the design of composite materials and also for the progressive finite element program which must modify its total stiffness matrix depending on the failure modes. However, it lacks accounting for the interaction of various components of stresses or strains in the failure process.

Good failure criteria must predict the principal failure modes separately, such as fiber breakages, matrix cracking and delamination, and each failure mode criterion should be interactive such as the quadratic formula while they do not require biaxial tests to determine the coefficients. The quadratic failure criteria must take into account of the

compressive or tensile stresses. The work of Hashin, which deals with the three-dimensional stresses fits this category and is given in Ref. [13]. It leads to six independent criteria, given in Equations (4.2) to (4.7). As input to the failure criteria, the following material strength parameters are needed.

X_T ; fiber direction tensile strength

X_C ; fiber direction compressive strength

Y_T ; transverse tensile strength

Y_C ; transverse compressive strength

S_{12} ; shear strength in the 1-2 plane

S_{13} ; shear strength in the 1-3 plane

S_{23} ; shear strength in the 2-3 plane

X_I ; interlaminar (through-the-thickness) tensile stress

S_I ; interlaminar shear strength

Fiber failure criteria have two modes; compressive fiber buckling mode and tensile fiber breakage mode.
For tensile fiber direction stress, $\sigma_1 > 0$, Hashin's fiber failure criterion is

$$\left(\frac{\sigma_1}{X_T} \right)^2 + \left(\frac{\tau_{12}}{S_{12}} \right)^2 + \left(\frac{\tau_{13}}{S_{13}} \right)^2 = 1 \qquad (4.2)$$

For the fiber buckling mode, $\sigma_1 < 0$, the criterion is

$$\left(\frac{\sigma_1}{X_c} \right)^2 = 1 \tag{4.3}$$

There are also two types of failure modes for the matrix cracking, depending upon $\sigma_2 + \sigma_3$, such that when $(\sigma_2 + \sigma_3) > 0$, the matrix cracking criterion is

$$\left(\frac{\sigma_2 + \sigma_3}{Y_T} \right)^2 + \frac{1}{S_{23}^2}\left(\tau_{23}^2 - \sigma_2 \sigma_3 \right) + \left(\frac{\tau_{12}}{S_{12}} \right)^2 + \left(\frac{\tau_{13}}{S_{13}} \right)^2 = 1 \tag{4.4}$$

and when $(\sigma_2 + \sigma_3) < 0$, the matrix cracking criterion is

$$\begin{aligned} &\frac{1}{Y_C}\left[\left(\frac{Y_C}{2 S_{23}} \right)^2 - 1\right](\sigma_2 + \sigma_3) + \frac{1}{4 S_{23}^2}(\sigma_2 + \sigma_3)^2 \\ &\left(\frac{\tau_{23}^2 - \sigma_2 \sigma_3}{S_{13}^2} \right) + \left(\frac{\tau_{12}}{S_{23}} \right)^2 + \left(\frac{\tau_{13}}{S_{13}} \right)^2 = 1 \end{aligned} \tag{4.5}$$

There are two basic approaches to predict delamination initiation [32]. One is the mechanics of materials approach, which essentially compares the local state of stress in the interply matrix layer where delamination occurs with relevant strength parameters. The other approach is based on the application of fracture mechanics principles and will not be

discussed here. However, once the delamination initiates, the concept of a critical strain energy release rate, G_c, will be applied to predict delamination growth.

In this study, delamination was predicted by the mechanics of materials with a simple quadratic interactive formula which depends upon σ_3, such that when $\sigma_3 < 0$, only shear stresses induce delamination such as Mode II type, and the criterion is

$$\frac{\tau_{13}^2 + \tau_{23}^2}{S_I^2} = 1 \qquad (4.6)$$

when $\sigma_3 > 0$, it behaves like a combination of Mode I and Mode II type crack initiation, and the criterion is

$$\left(\frac{\sigma_3}{X_I} \right)^2 + \frac{\tau_{13}^2 + \tau_{23}^2}{S_I^2} = 1 \qquad (4.7)$$

Here X_I and S_I can be assumed as the tensile strength and pure shear strength of the matrix. This assumption is justified by the experimental observations that toughened matrix materials apparently reduce the onset of delaminations.

Assume damage of a particular nature occurs at a location given by α in the 0^0 layer. Then the same type and extent of damage will occur in the 45^0 layer at $(45^0 + \alpha)$ and in the -45^0

layer at $(-45^0 + \alpha)$ and so on. That means in a quasi-isotropic laminate the damage pattern will look like a stair-case in the form of a helix. This phenomenon has been observed in impact experiments also [15,33].

At a particular segment where the fiber direction is at angle θ to the x axis, the stress components in material coordinates can be obtained as follows

$$\begin{Bmatrix} \sigma_1 \\ \sigma_2 \\ \tau_{12} \\ \sigma_3 \\ \tau_{13} \\ \tau_{23} \end{Bmatrix} = \begin{bmatrix} \cos^2\theta & \sin^2\theta & 2\cos\theta\sin\theta & 0 & 0 & 0 \\ \sin^2\theta & \cos^2\theta & -2\cos\theta\sin\theta & 0 & 0 & 0 \\ -\cos\theta\sin\theta & \cos\theta\sin\theta & \cos^2\theta-\sin^2\theta & 0 & 0 & 0 \\ 0 & 0 & 0 & 1 & 0 & 0 \\ 0 & 0 & 0 & 0 & \cos\theta & \sin\theta \\ 0 & 0 & 0 & 0 & -\sin\theta & \cos\theta \end{bmatrix} \begin{Bmatrix} \sigma_r \\ \sigma_\theta \\ \sigma_{r\theta} \\ \sigma_{zz} \\ \sigma_{rz} \\ \sigma_{\theta z} \end{Bmatrix} \tag{4.8}$$

because $\sigma_{r\theta}$ and $\sigma_{\theta z}$ are zero for the axisymmetric analysis, stresses can be easily obtained as in Equation (4.9).

$$\begin{aligned} \sigma_1 &= \cos^2\theta\ \sigma_r + \sin^2\theta\ \sigma_\theta \\ \sigma_2 &= \sin^2\theta\ \sigma_r + \cos^2\theta\ \sigma_\theta \\ \tau_{12} &= -\cos\theta\sin\theta\ (\sigma_r - \sigma_\theta) \\ \sigma_3 &= \sigma_{zz} \\ \tau_{13} &= \cos\theta\ \sigma_{rz} \\ \tau_{23} &= -\sin\theta\ \sigma_{rz} \end{aligned} \tag{4.9}$$

By combining Equations (4.2) through (4.7) and Equation (4.9), the failure criteria for implementation into the finite element program are obtained as follows.

Fiber failure

(i) $\cos^2\theta\ \sigma_r + \sin^2\theta\ \sigma_\theta > 0$

$$\left(\frac{\cos^2\theta\,\sigma_r + \sin^2\theta\,\sigma_\theta}{X_T}\right)^2 + \left(\frac{\cos\theta\sin\theta\,(\sigma_\theta - \sigma_r)}{S_{12}}\right)^2 + \left(\frac{\cos\theta\,\sigma_{rz}}{S_{13}}\right)^2 = 1$$

(ii) $\cos^2\theta\ \sigma_r + \sin^2\theta\ \sigma_\theta < 0$

$$\left(\frac{\cos^2\theta\,\sigma_r + \sin^2\theta\,\sigma_\theta}{X_C}\right)^2 = 1$$

Matrix failure

(i) $\sin^2\theta\ \sigma_r + \cos^2\theta\ \sigma_\theta + \sigma_{zz} > 0$

$$\frac{1}{S_{23}^2}\left(\sin^2\theta\,\sigma_{rz}^2 - \sin^2\theta\,\sigma_r\,\sigma_{zz} - \cos^2\theta\,\sigma_\theta\,\sigma_{zz}\right) + \left(\frac{\cos\theta\sin\theta\,(\sigma_\theta - \sigma_r)}{S_{12}}\right)^2 + \left(\frac{\cos\theta\,\sigma_{rz}}{S_{13}}\right)^2 + \left(\frac{\sin^2\theta\,\sigma_r + \cos^2\theta\,\sigma_\theta + \sigma_{zz}}{Y_T}\right)^2 = 1$$

(ii) $\sin^2\theta\ \sigma_r + \cos^2\theta\ \sigma_\theta + \sigma_{zz} < 0$

$$\frac{1}{S_{23}^2}\left(\sin^2\theta\,\sigma_{rz}^2 - \sin^2\theta\,\sigma_r\,\sigma_{zz} - \cos^2\theta\,\sigma_\theta\,\sigma_{zz}\right)$$
$$+ \left(\frac{\cos\theta\sin\theta\,(\sigma_\theta - \sigma_r)}{S_{12}}\right)^2 + \left(\frac{\cos\theta\,\sigma_{rz}}{S_{13}}\right)^2$$
$$+ \frac{1}{Y_C}\left[\left(\frac{Y_C}{2\,S_{23}}\right)^2 - 1\right]\left(\sin^2\theta\,\sigma_r + \cos^2\theta\,\sigma_\theta + \sigma_{zz}\right)$$
$$+ \frac{1}{4\,S_{23}^2}\left(\sin^2\theta\,\sigma_r + \cos^2\theta\,\sigma_\theta + \sigma_{zz}\right)^2 = 1$$

Delamination

(i) $\sigma_{zz} < 0$

$$\left(\frac{\sigma_{rz}}{S_I}\right)^2 = 1$$

(ii) $\sigma_{zz} > 0$

$$\left(\frac{\sigma_{rz}}{S_I}\right)^2 + \left(\frac{\sigma_{zz}}{X_I}\right)^2 = 1$$

Note that the delamination failure criteria are not functions of θ. This fact can also be verified from the C-scan results shown in Figure 1.5.

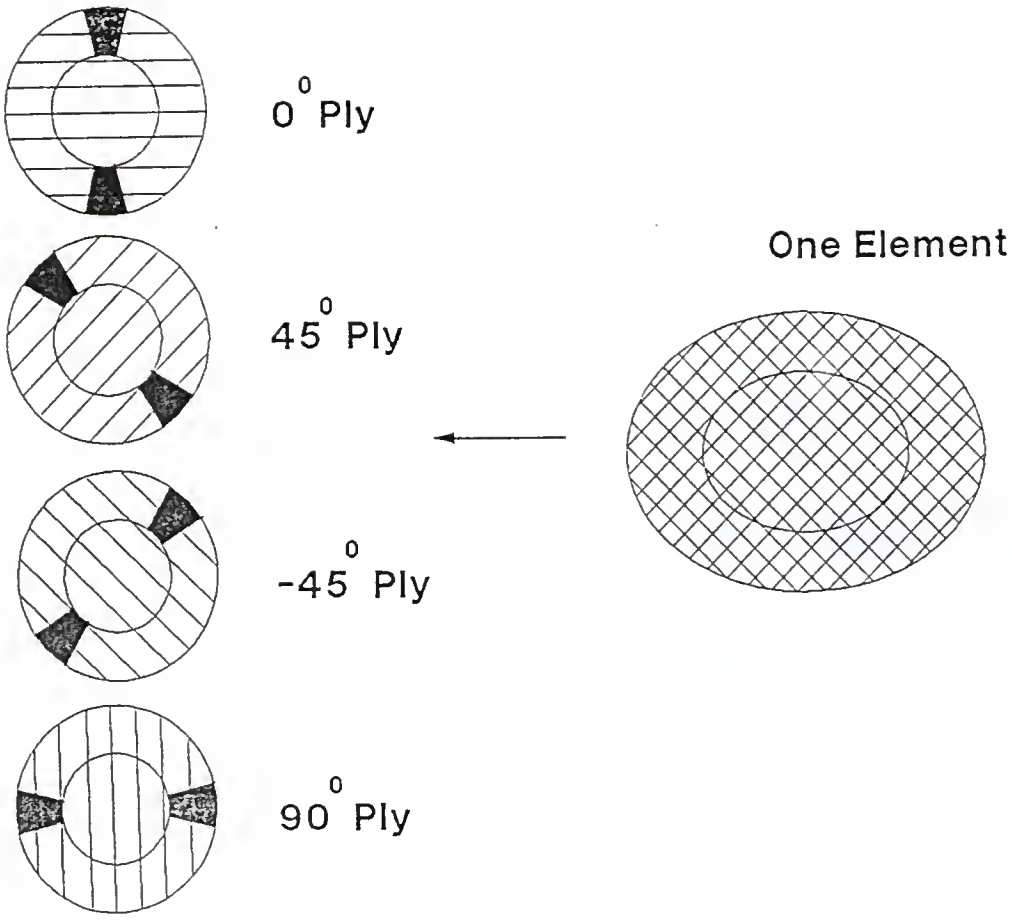

Figure 4.1 Partial failure patterns

Table 4.1. Ultimate strength of AS4/3501-6 lamina

unit (MPa)

X_T ; 2172	X_C ; 1724
Y_T ; 53.8	Y_C ; 205.5
S_{12} ; 120.7	S_{13} ; 120.7
S_{23} ; 89.3	X_I ; 56.5
S_I ; 89.3	

* Courtesy of Hercules Aerospace Company

4.2 Implementing Delamination into the Finite Element Program

4.2.1 Introduction

Delamination initiates from where the shear stress is high, such as above the mid-surface of the plate close to the contact surface. Then delaminations start to expand radially, and more delaminations appear in the bottom plies. Delaminations can be simulated in the finite element program by creating slip surfaces between elements as seen in Figure 4.2. New nodes are created, and rigid elements (spring elements with very large spring constants K) are added between two nodes across slip surfaces when the normal force is compressive to prevent interpenetration of the nodes. Adding new surfaces and consequently adding new nodes makes a cumbersome procedure, which is a weakness of the finite element method. The total stiffness matrix of the plate must be recalculated after delaminations occur or grow. Also the dimension of the total matrix is increased due to the introduction of new nodes. If tensile stress exists at the tip of delaminations, the spring element must be eliminated to allow Mode I type (Opening Mode) delamination propagation. Then, iteration of the program is necessary to assure that the rigid elements are placed only where compressive stresses exist. However, unless the contact force is high, delaminations seemed to appear only at the upper portion of the plate where through-the-thickness stresses σ_z are compressive. The present finite element program monitors the

signs of all σ_z across the delamination surfaces while implementing Hashin's failure criteria, and it was found that all σ_z's are compressive in the present study. It is safe to assume that in this study the delamination growth is Mode II type (Shear Mode) and to put rigid elements at all the nodes across delamination surfaces. When delaminations become extensive, especially beyond the mid-surface of the plate, then the tip of the delaminations could have high tensile stresses. This Mode I crack growth combined with Mode II type will accelerate delamination growth faster than by Mode II delamination alone.

4.2.2 Numerical Experiment

A simple numerical experiment was done to check the effect of delaminations on the contact force vs. center deflection curve and also to see the frictional effect across the delamination surface. Assume that the experimental test configuration shown in Figure 1.2 has pre-existing delaminations of 12.7 mm diameter uniformly distributed through the thickness. As 16 elements were employed through the thickness, 15 delaminations were assumed in the finite element program. An incremental point force was applied at the center of the plate. Rigid elements were placed across all the delamination surface nodes as shown in Figure 4.3.

Figure 4.4 shows contact force vs. center deflection curve of the plate with pre-existing delaminations compared

with experimental test results. Delaminations reduced the slope of the contact force vs. center deflection curve. It is apparent that this numerical experiment has exaggerated the extent of delaminations. However, it justifies the conclusion that delamination failures can change the contact force vs. center deflection curve. Combined with matrix failures, delamination failures will change the slope of the contact vs. center deflection curve shown in Figure 3.5 which was obtained for the elastic range by the finite element program.

4.3 Implementing Fiber and Matrix Failure into the Finite Element Program

When the matrix fails, the elastic modulus of the matrix, E_m, can be replaced by zero, so that, from elementary composite material theory,

$$E_1 = E_f v_f + E_m v_m = E_f v_f$$

Because the value of $E_m v_m$ is very small compared with $E_f v_f$, the original E_1 can be used after matrix failure. However, the other elastic moduli, E_2 and E_3, and Poisson's ratios become zero. With these new values input, $[\ C\ ]_{av}$ computed by the method described in Section 2.3 becomes singular with zeros for C_{22} and C_{33}. Also the total stiffness matrix assembled with these singular element stiffness matrices can also be singular. It is found that the singularity can better be

avoided by assigning very small values to the zero diagonal terms in the $[\ C\ ]_{av}$ matrix rather than to the diagonal terms of the total stiffness matrix.

Matrix failures were initiated first and then expanded extensively. There were no fiber failures for the range of calculations in the present study.

The finite element program could easily handle matrix failures by assigning reduced $[\ C\ ]_{av}$ values corresponding to damaged elements which were detected by Hashin's failure criteria. When partial failures are detected, $[\ C\ ]_{av}$ must be reduced proportionally depending upon the degree of the failure. However, in this research, partial failures were detected only at a small portion of the fringes of totally failed elements. So partial failures could be either ignored or considered as total failure depending upon the degree of partiality without losing much accuracy. The total stiffness matrix is reassembled and the contact algorithm is applied again according to the method discussed in the next section.

4.4 Incremental Finite Element Method for Damage Analysis

Hashin's failure criteria discussed in Section 4.1 have been implemented in the finite element program. After all the displacements are calculated as in Equation (2.18), stresses in each element can be calculated according to Equation (2.35). The finite element program checks Hashin's failure

criteria with the element stresses and prints damage information.

When damages are detected, the total stiffness matrix is reassembled to take account of delaminations and matrix failures as discussed in Sections 4.2 and 4.3. When failures occur inside the plate, the displacements of all nodes except the contacted nodes beneath the indenter are changed. Among the accumulated displacements, only the vertical displacements of the contacted nodes of the plate, d_c, remain unchanged and become the input to Equation (4.10) which solves the mixed boundary value problem. Here, d_c becomes the prescribed displacement boundary condition, and zero traction forces at the uncontacted nodes become zero force boundary conditions. Other displacements d_r and new contact forces F_c can be obtained from Equations (4.11) and (4.12) respectively.

$$\begin{bmatrix} K_{cc} & K_{cr} \\ K_{rc} & K_{rr} \end{bmatrix} \begin{Bmatrix} d_c \\ d_r \end{Bmatrix} = \begin{Bmatrix} F_c \\ 0 \end{Bmatrix} \tag{4.10}$$

$$d_r = - K_{rr}^{-1} K_{rc} d_c \tag{4.11}$$

$$F_c = (K_{cc} - K_{cr} K_{rr}^{-1} K_{rc}) d_c \tag{4.12}$$

The incremental contact algorithm is then applied to close the gap at the next candidate contact node as discussed in Section

2.4 until new damages are developed or until the assigned contact radius is reached.

Sometimes, stiffness reduction due to damage causes a node just outside the contact region to penetrate into the indenter. Since this is not physically possible, the program imposes a displacement boundary condition on such nodes so that they just touch the indenter, and the problem is solved again using the new stiffness matrix. Equation (2.25) must be modified as

$$\delta_i = \frac{w_j - w_i + g_i}{(1 - d_i)} \tag{4.13}$$

to maintain smooth contact as seen in Figure 4.5. When δ_i is negative, the indenter must touch that node automatically and proceed to the next contact node to maintain smooth contact. Here, Gap g_i is the z-distance of the indenter from the corresponding two contact candidate nodes, as shown in Figure 4.5.

Usually, matrix failure occurs beneath the indenter because of compression. At almost the same time, the matrix at the bottom of the plate starts to fail because of the bending of the plate. Delamination occurs near the top surface of the plate beneath the indenter because of high shear stresses, as seen in Figures 3.3 and 3.4, and in Figure 4.8.

When matrix cracking and delamination failure occur, the slope of the contact force vs. center deflection curve changes smoothly, as seen in experimental data (Figure 3.5). It is speculated that the load cell attached at the indenter may not catch the slight load drop due to matrix failure, which behaves like plastic deformation [9]. The finite element program recalculates the new contact force and center deflection with updated damage information and continuously interpolates with the point of the previous damage status. Although contact force drops with increased internal damages, as shown by the vertical dotted lines in Figure 4.6, it is reasonable to draw the contact force curve continuously with respect to center deflection as a solid line, as in Figure 3.5. Contact force was assumed to proceed ignoring the effects of small growth of internal damage in Figure 4.6. This does not explain the sudden drop of contact force shown in Figure 1.3. In Ref. [9], this sudden drop was assumed to be largely due to fiber failure. However, examination of specimens of the impacted or indented plates at the University of Florida did not reveal fiber failures [11]. Damage patterns of the composite plate obtained from the finite element program are shown in Figures 4.8-4.10, where dotted area represents matrix failed elements and delaminations are shown as solid lines. Judging from the failure growth map (Figures 4.8-4.10), it can be assumed that extensive matrix failures, which drastically reduce the transverse stiffness, combined with delamination

growth, induce this sudden drop of contact force. Delaminations are expected to initiate from matrix cracks, and including this initiation phenomenon in the finite element program requires further research.

By changing element mesh sizes, three contact force vs. center deflection curves were obtained, as shown in Figure 4.7, where they are compared with the experimental curves reproduced from Figure 3.5. In Figure 4.7, the curve C has the coarsest mesh size, and the curve A which is the reproduction from Figure 4.6 has the finest mesh size.

Although the finite element program appeared to be an upper bound of the test results in the elastic range, it was no longer an upper bound when the damage analysis was included. Also, the damage analysis was highly path dependent. Change of mesh size may alter output, and results can vary as much as the experimental data. The finite element program was stopped at near 2000 N contact force or 0.7 mm center deflection because of two reasons. First, some of the top layer elements of the plate which the indenter had not contacted yet were damaged. Recalculated contact force became near zero because the damaged top surface did not give resistance to indentation. Damage on the top surface was very sensitive to the contact force. Second, the stiffness matrix of the system became singular numerically. Assumption of $[\ C\ ]_{av}$ matrix for the element in which matrix has failed as discussed in Section 4.3 must be too conservative. By

increasing values of C_{22} and C_{33}, the numerical singularity can be avoided. By numerical experiments, good values, which can make finite element results match well with experimental data, might possibly be found.

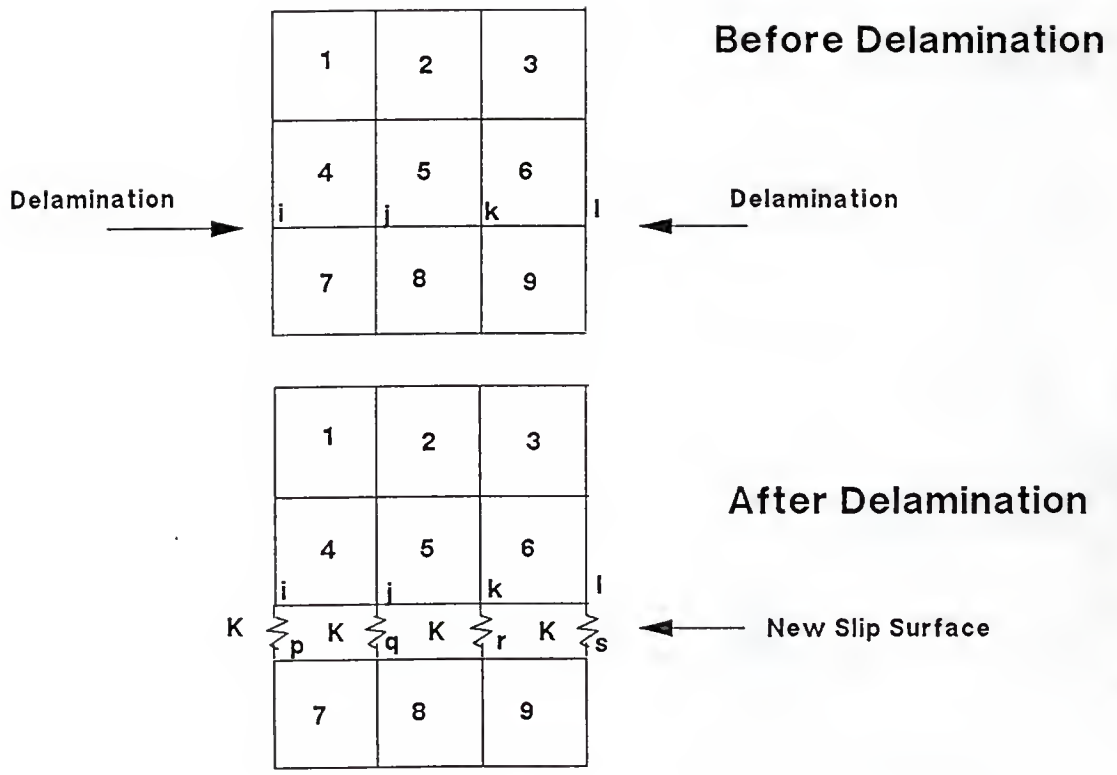

Figure 4.2 Delamination simulation

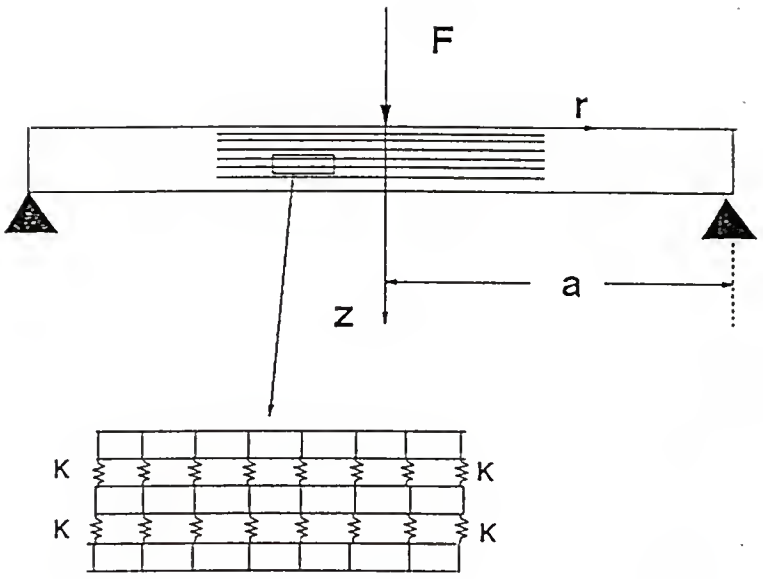

Figure 4.3 Numerical application of delamination effect

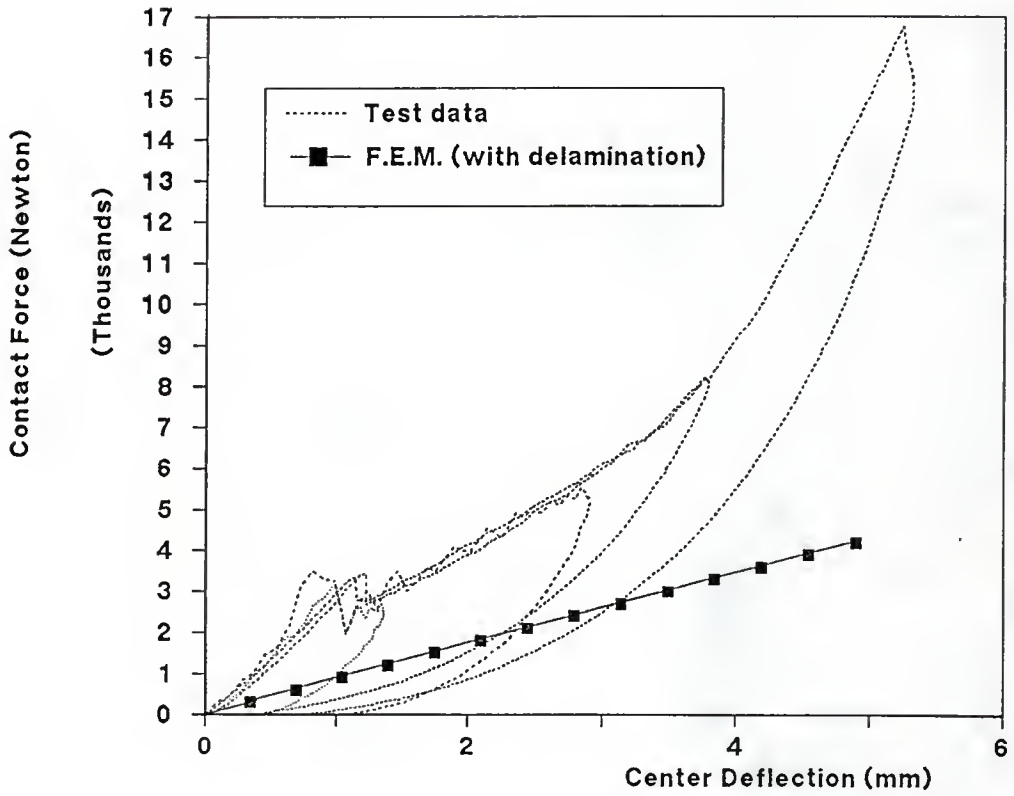

Figure 4.4 Delamination effect on Contact force vs. center deflection curve

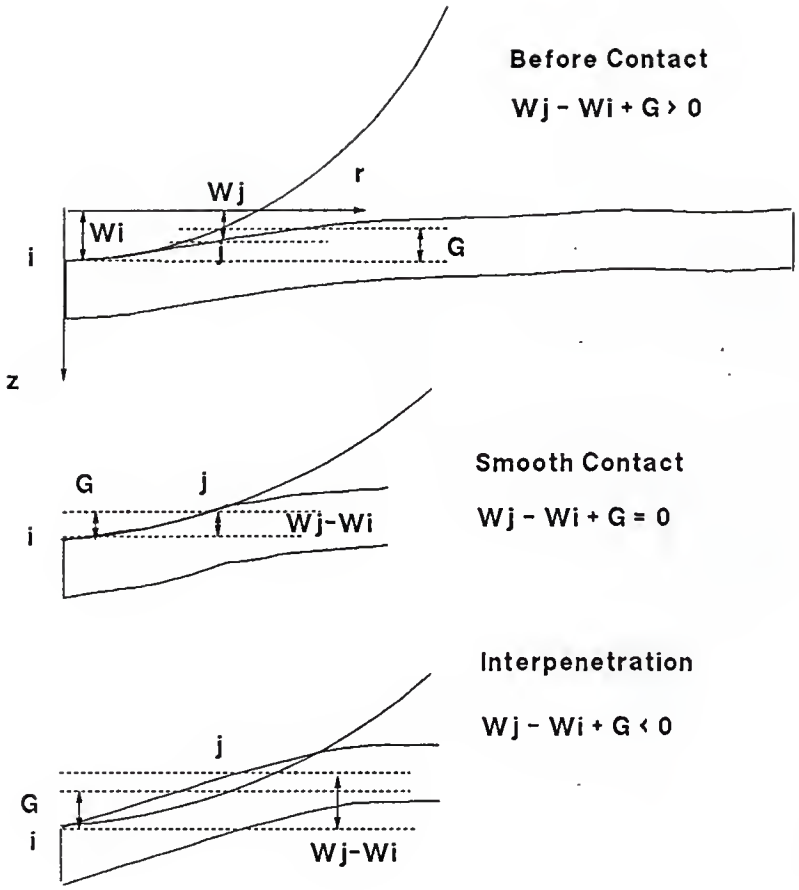

Figure 4.5 Geometry of contact surface

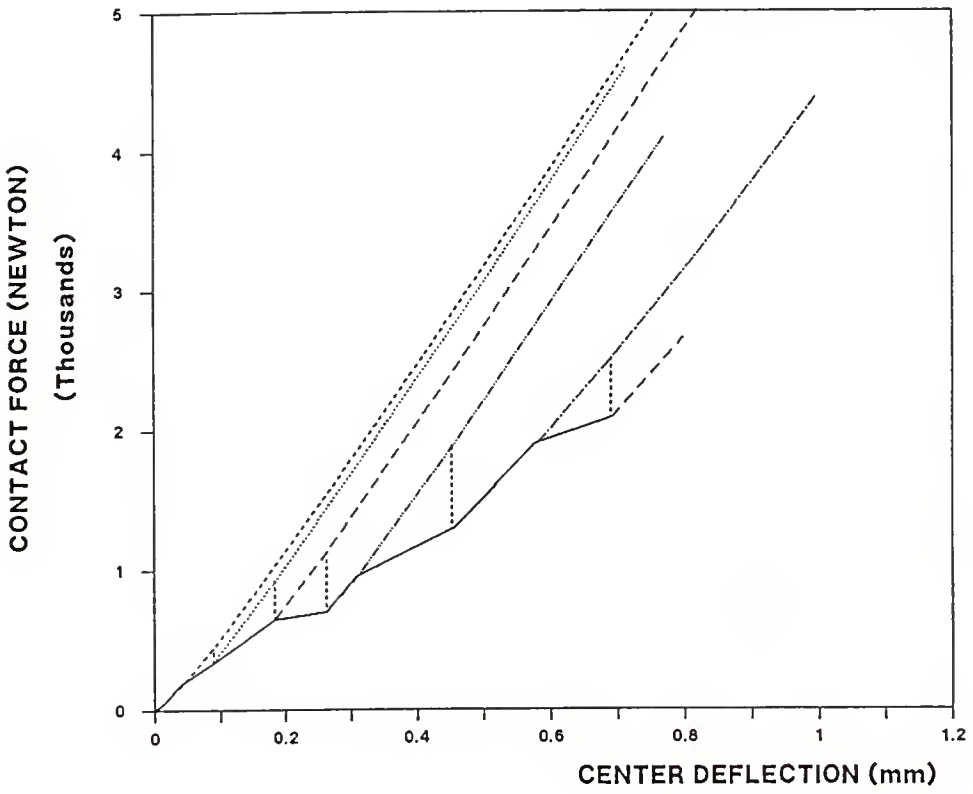

Figure 4.6 Contact force vs. center deflection curve

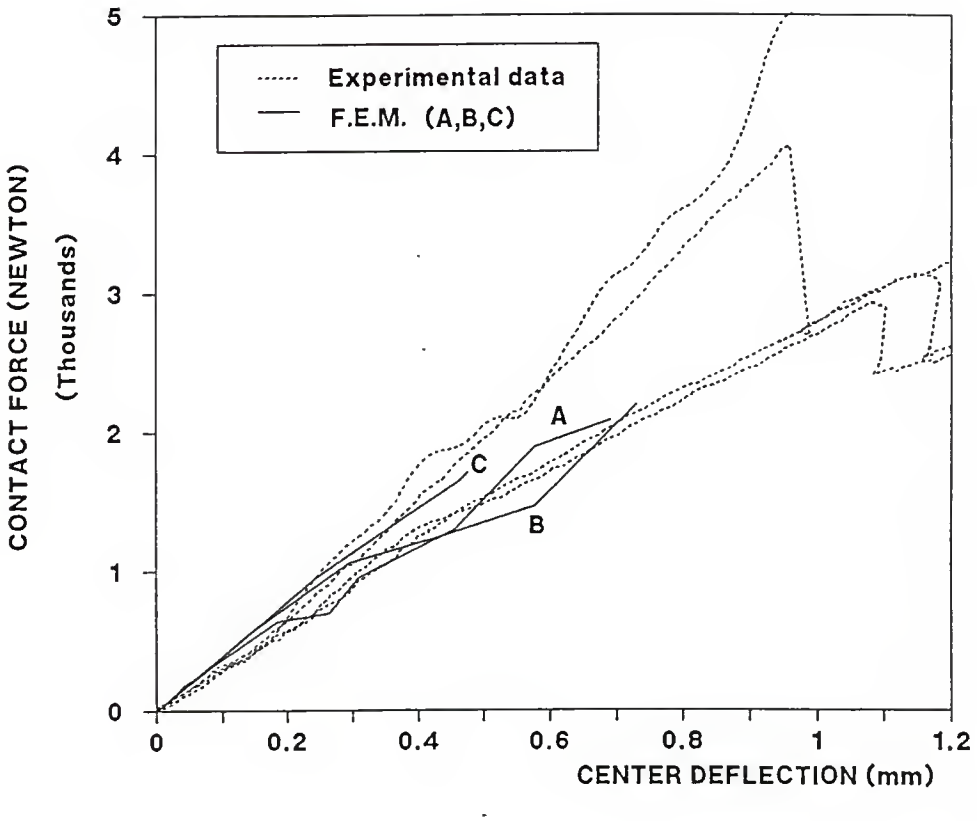

Figure 4.7 Contact force vs. center deflection curve

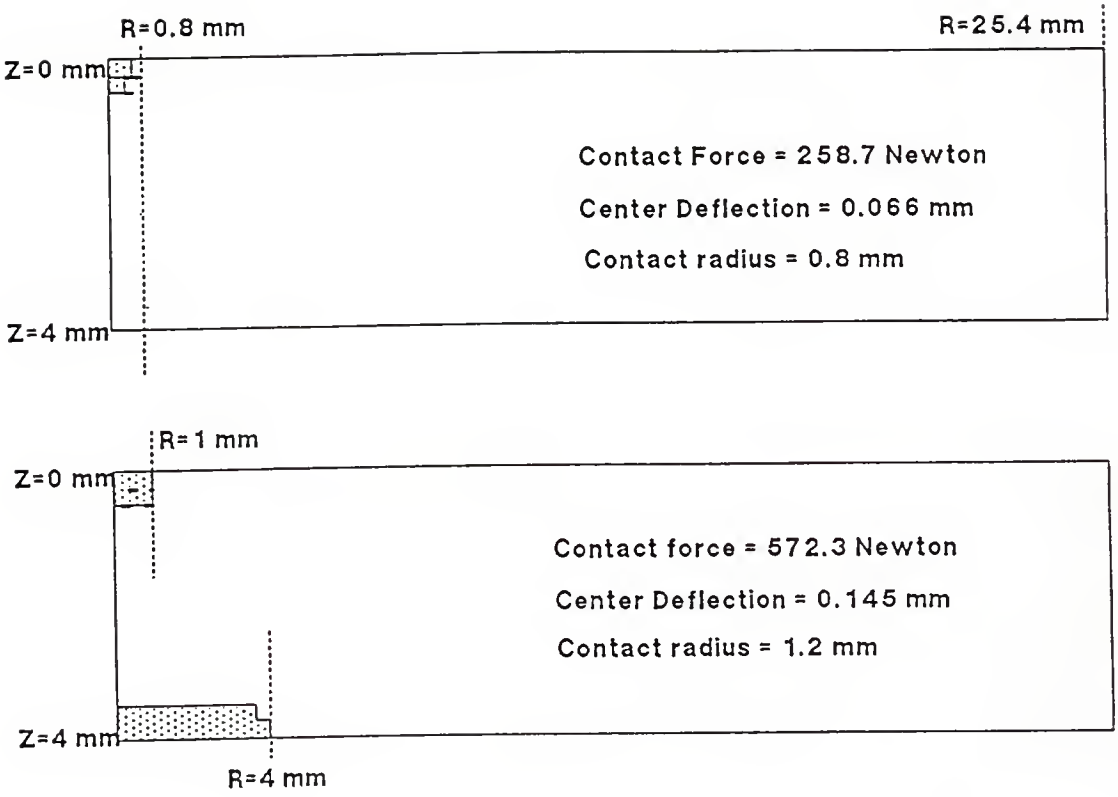

Figure 4.8 Damage pattern of the composite plate

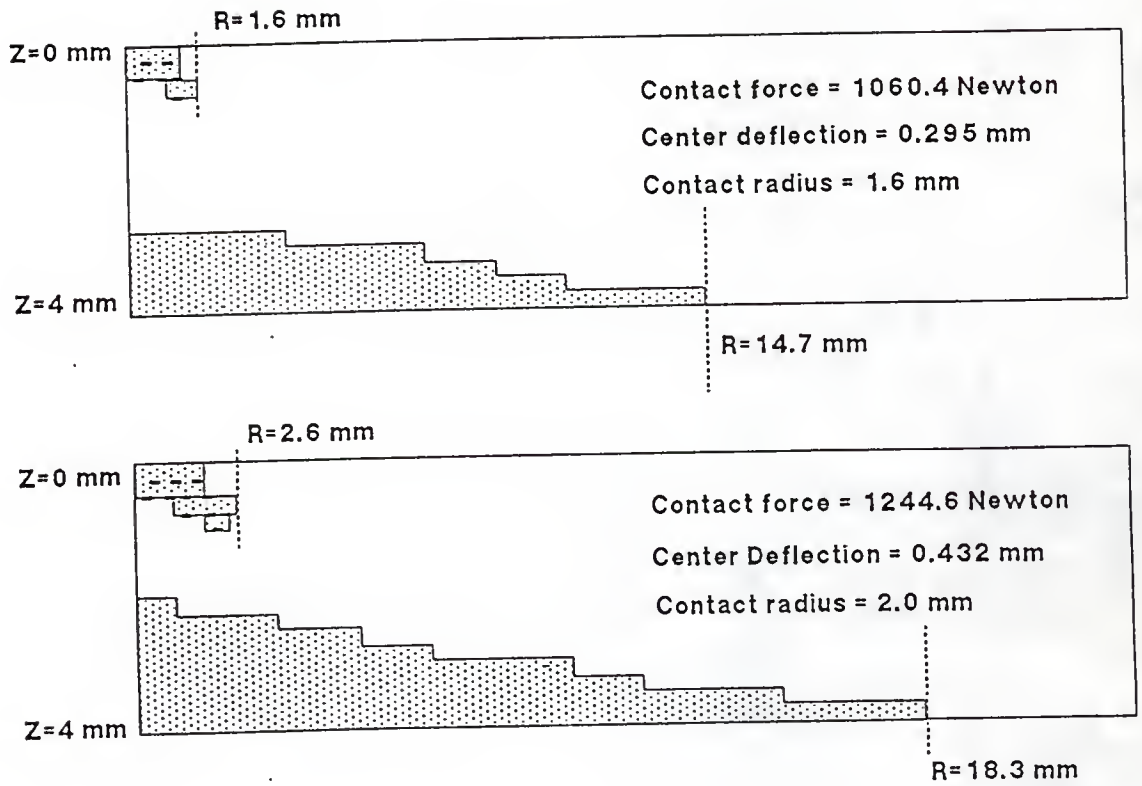

Figure 4.9 Damage pattern of the composite plate

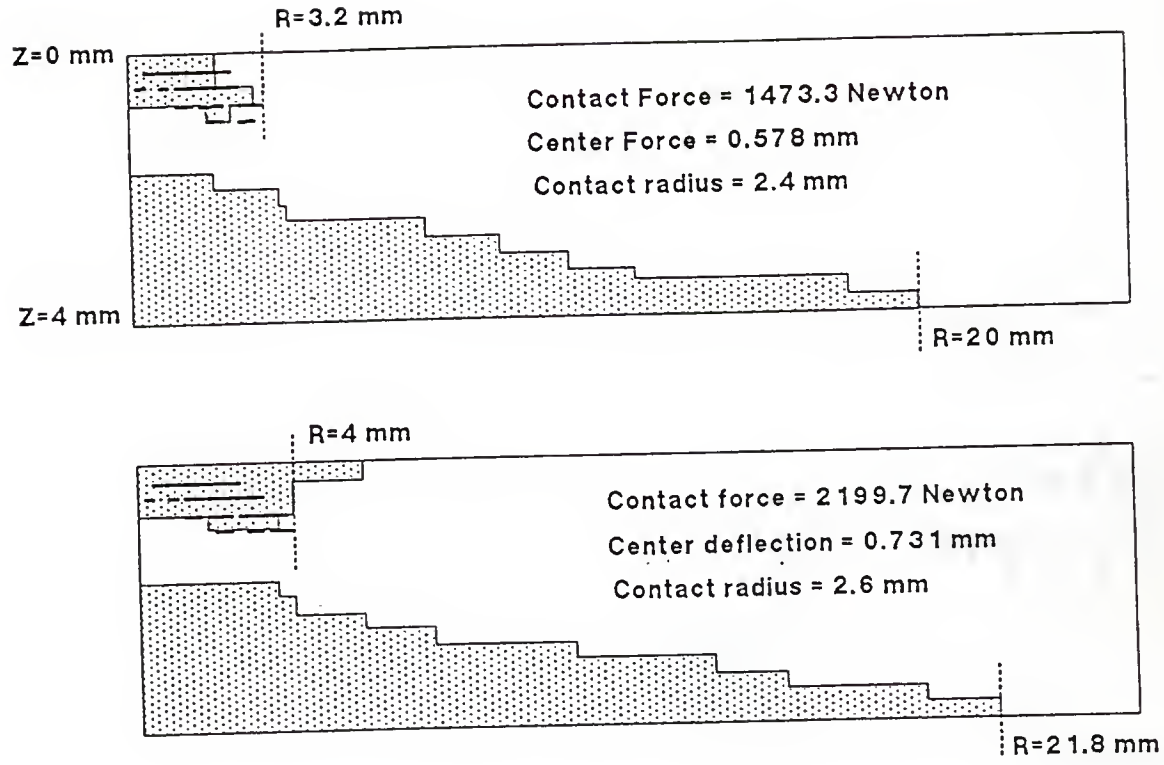

Figure 4.10 Damage pattern of the composite plate

CHAPTER 5

CONCLUSIONS

5.1 Conclusion

The contact problem of a circular composite plate by a spherical indenter was analyzed by a finite element program which employed quadrilateral, isoparametric, axisymmetric elements. After averaging the orthotropic laminar material properties, axisymmetric element properties of cross-ply or quasi-isotropic laminate turned out to be transversely isotropic. Hashin's failure criteria, which were written in material coordinates, were transformed to be applicable to the axisymmetric element. Delamination criteria turned out to be independent of angle transformation. A circular pattern of delamination was also shown from the C-scan picture of experimental data. For the AS4/3501-6 graphite/epoxy plate (25.4 mm radius), the elastic region is only up to 140 Newton contact force or 0.33 mm center deflection for a spherical indenter of radius 12.7 mm. In this elastic region, results of the finite element program matched well with the experimental data in most cases, and were an upper bound of the test data for the remaining. The finite element analysis showed that matrix failure was initiated both from top and bottom -

beneath the indenter because of compression and in the bottom surface of the plate due to bending. Matrix failure expanded radially and also toward the mid-surface of the plate from both the top and bottom. Delamination initiated at almost the same time as matrix failure near the top surface beneath the indenter. Delamination expanded radially and also downward. When the delamination and matrix failures were accounted for, the finite element results matched well with experimental data in predicting the force-deflection relationship, as shown in Figure 4.7. Combined extensive matrix failure and delamination, which make it very compliant at the center of the plate, is believed to be the cause of the sudden drop of the contact force at the contact force vs. center deflection curve. Widely used contact laws and equations are compared with finite element results.

5.2 Comments for Future Research

The sudden drop of the contact force could not be explained without modeling the delamination propagation, which is very complex. Connecting nodes with vertical and horizontal springs and iterating schemes to account for the growth of delamination are needed. Also, as matrix cracks will lead to delaminations, understanding of this growth is needed. When the matrix fails, a better model of the constitutive equations of the finite element is required for accurate prediction of further damage propagation.

REFERENCES

[1] Agarwal, B. D. and Browtman, L. T., 'Analysis and Performance of Fiber Composites', John Wiley & Sons, New York, NY, 1980

[2] Hoskin, B. C., Baker, A. A., 'Composite Materials for Aircraft Structures', AIAA Education Series, Published by American Institute of Aeronautics and Astronuatics, Inc., New York, NY, 1986

[3] Kelkar, A., Elber, W. and Raju, I. S., 'Large Deflection Behaviour of Circular Quasi-Isotropic Laminates under Point Loading', 85-0723 at the AIAA/ASME/ASCE/AHS 26th Structures, Structural Dynamics and Materials Conference, Orlando, FL, April 15-17, 1985

[4] Bostaph, G. M. and Elber, W., 'A Fracture Mechanics Analysis for Delamination Growth During Impact on Composite plates ', Presentation at the Army Symposium on Solid Mechanics, Cape Cod, MA, 1982

[5] Chen, P. C. and Ramkumar, R. L., 'Static and Dynamic Analysis of Clamped Orthotropic Plates using Lagrangian Multiplier Technique', AIAA Journal, Vol. 23, No. 2, Feb., 1987, pp. 316-323

[6] Yang, S. H. and Sun, C. T., 'Indentation Law for Composite Laminates', Composite Materials: Testing and Design (Sixth Conference). ASTM STP 787.I, 1982. pp. 425-449

[7] Wu, Hsi-Yung Tom, 'Impact Damage of Composites', Ph.D. Thesis, Stanford University, 1987

[8] Shivakumar, K. N., Elber, W. and Illg, W., 'Analysis of Progressive Damage in Thin Circular Laminates Due to Static-Equivalent Impact Loads', Presentation at the 24th AIAA/ASME/ASCE/AHS Structures, Structural Dynamics, and Materials Conference, Lake Tahoe, NV, May 2-4, 1983

[9] Sjoblom, P. O., Hartness, J. T. and Cordell, T. M., 'On Low Velocity Impact Testing of Composite Materials', Journal of Composite Materials Vol. 22, January, 1988, pp. 30-52

[10] Sankar, B. V., 'Interlaminar Shear Stresses in Composite Laminates Due To Static Indentation', Journal of Reinforced Plastics and Composites, Vol. 8, September, 1989, pp. 458-471

[11] Kwon, Y. S., 'Indentation-Flexure Damage in Graphite/Epoxy Laminates', Master's Thesis, University of Florida, 1991

[12] Production Data Number 843-3, Hercules Carbon Prepreg Tape AS4/3501-6, Hercules Advanced Materials and Systems Company, Magna, UT

[13] Hwang, W. C., 'Three-Dimensional Finite Element Based, Iterative Approach for Analysis of Laminated Composites', Ph.D Thesis, University of Florida, 1986

[14] Nahas, M. N., 'Survey of Failure and Post-Failure Theories of Laminated Fiber-Reinforced Composites', Journal of Composites Technology & Research, Vol. 8, No. 4, Winter 1986, pp. 138-153

[15] Dost, E. F., Ilcewicz, L. B. and Gosse, J. H., 'Sublaminate Stability Based Modeling of Impact-Damaged Composite Laminates', Proceedings of the American Society for Composites 3rd technical conference, Sept. 25-29, Seattle, WA, pp. 354-363

[16] Chang, S. H., 'A Finite Element Simulation of Elasto-Plastic Contact Problems ', Ph.D. Thesis, West Virginia University, 1985

[17] Conry, T. F. and Seireg, A., 'A Mathematical Programming Method for Design of Elastic Bodies in Contact', Journal of Applied Mechanics, June, 1971, pp. 387-392

[18] Kalker, J. J. and Van Randen, Y., 'A Minimum Principle for Frictionless Elastic Contact with Application to Non-Hertzian Half-Space Contact Problems', Journal of Engineering Mathematics, Vol. 6, 1972, pp. 193-206

[19] Marks, W. R. and Salamon, N. J., 'A Modified Conjugate Gradient Method for Frictionless Contact Problems ', Presentation at the ASME International Conference on Reliability, Stress Analysis and Failure Prevention, San Francisco, CA, Aug. 18-21, 1980

[20] Chandrasekaran, N., Haisler, W. E. and Goforth, R. E., 'A Finite Element Solution Method for Contact Problems with Friction', International Journal for Numerical Methods in Engineering, Vol. 24, 1987, pp. 477-495

[21] Chand, R., Haug, E. H. and Rim, K., 'Analysis of Unbounded Contact Problems by Means of Quadratic Programming', Journal of Optimization Theory and Application, Vol. 20, No. 2, October, 1976, pp. 171-189

[22] Hughes, Thomas J. R., 'The Finite Element Method', Prentice Hall, Englewood Cliffs, NJ, 1987

[23] Wu, Hsi-Yung T. and Springer, G. S., 'Impact Induced Stresses, Strains and Delaminations in Composite Plates', Journal of Composite Materials, Vol. 22, June, 1988, pp. 519-560

[24] Bathe, K. J. and Wilson, E. L., 'Numerical Methods in Finite Element Analysis', Prentice Hall, Englewood Cliffs, NJ, 1976

[25] Zienkiewicz, O. C., 'The Finite Element Method', 3rd Edition, McGraw Hill,New York, NY, 1977

[26] Wang, C. Y., 'A Study of Impact Damage in Composite Laminates', Ph.D. Thesis, University of Texas at Austin, 1989

[27] Sankar, B. V., 'Contact Law for Transversely Isotropic Materials', AIAA-85-0745,AIAA/ASME/ASCE/AHS 26th Structures, Structural Dynamics and Materials Conference, Orlando, FL, April 15-17, 1985, pp. 516-521

[28] Abrate, Serge, 'Impact on Laminated Composite Materials', Applied Mechanics Reviews, Vol. 44, No. 4, April, 1991, pp. 155-190

[29] Timoshenko, S. and Woinowsky-Krieger, S., 'Theory of Plates and Shells', McGraw-Hill Book Company, Second Edition, New York, NY, 1959

[30] Rahman, M. U., Rowlands, R. E., Cook, R. D. and Wilkinson, T. L., 'An Iterative Procedure for Finite Element Stress Analysis of Frictional Contact problems', Computer & Structures, Vol. 18, No. 6, 1984, pp. 947-954

[31] Haber, R. B. and Hariandja, B. H., 'An Eulerian-Lagrangian Finite Element Approach to Large-Deformation Frictional Contact', Computers & Structures, Vol. 20, No. 1-3, 1985, pp. 153-201

[32] Brewer, J. C. and Lagace, P. A., 'Quadratic Stress Criterion for Initiation of Delamination', Journal of Composite Materials, Vol. 22, December, 1988, pp. 1141-1155

[33] Clark, G., 'Modelling of Impact Damage in Composite Laminates', Composites, Vol. 20, No. 3, May, 1989, pp. 209-214

[34] Cairns, D. C., 'Impact and Post-Impact Response of Graphite/Epoxy and Kevlar/Epoxy Structures', Ph.D. Thesis, M.I.T., 1987

[35] Chang, T. Y., Saleeb, A. F. and Shyu, S. C., 'Finite Element Solutions of Two-Dimensional Contact Problems Based on a Consistent Mixed Formulation', Computers and Structures, Vol. 27, No. 4, 1987, pp. 455-466

[36] Sun, C. T. and Grady, J. E., 'Dynamic Delamination Fracture Toughness of a Graphite/Epoxy Laminate Under Impact', Composite Science and Technology, Vol. 31, 1988, pp. 55-72

[37] Kuncis, J. A., 'Estimation of Damage in Conventional and Hybrid Fiber Reinforced Composites Due to Static Indentation', Master's Thesis, University of Florida, 1989

[38] Garg, Amar, 'Delamination - A Damage Mode in Composite Structures', Engineering Fracture Mechanics, Vol. 29, No. 5, 1988, pp. 557-584

[39] Battancharya, A. K. and Nix, W. D., 'Finite Element Simulation of Indentation Experiments', International Journal of Solids and Structures, Vol. 24, No. 9, 1988, pp. 881-891

[40] Ross, C. A., Malvern, L. E., Sierakowski, R. L. and Takeda, N., 'Finite Element Analysis of Interlaminar Shear Stress Due to Local Impact', Recent Advances in Composites in the United States and Japan, ASTM STP 864, Philadelphia, 1985, pp. 355-367

[41] Jones, R. M., 'Mechanics of Composite Materials', McGraw Hill, New York, NY, 1975

[42] Liu, Dashin and Malvern, L. E., 'Matrix Cracking in Impacted Glass/Epoxy Plates', Journal of Composite Materials, Vol. 21, July, 1987, pp. 594-609

APPENDIX

Description of the Program

Because of a computing time limitation, this program assembles and condenses the total stiffness matrix one time only. A totally automatic program for a damage analysis can be developed by modifying inputs and outputs of this program.

1. Read input data

   A. Total contact candidate node number (NCAND)
   B. Total number of nodes (NODES)
      Total number of elements (NELMS)
      Number of different materials (MPTOTAL); reduced modulus matrices due to matrix and fiber failure can be applied here
   C. Number of total radial elements (NA)
      Number of radial fine mesh elements (NAFINE)
      Number of elements through the thickness (NH)
      Radius of the plate (AR)
      Thickness of the plate (HT)
      Radius of total fine mesh elements (ARFINE)
   D. Boundary conditions (see program list)
   E. Material identification number (MP)
   F. Material properties (C11, C12, C13, C33, C44)
   G. Ultimate strength of the materials (XT, XC, XI, YT, YC, S1, S12, S13, S23)
   H. Indenter radius (RB)
   I. Maximum node identification number to calculate Contact process (NTRY); when indenter contacts node NCONT(NTRY), program stops.
   J. Restarting identification number (NREST)- last contacted node identification number to recalculate contact force due to change of internal damage; zero for elastic analysis
   K. Total number of delamination layers (NTCR)
   L. Identification of each delamination layer (NCRACK(I)); number of delaminated elements (MECR(J,I); first element identification
   M. Total number of matrix-failed layers (NRMF)

NRMF1; number of elements at each layer
NRMF2; first node identification

N. Total number of fiber-failed layers (NRFF)
NRFF1; number of elements at each layer
NRFF2; first node identification

O. Vertical displacements of contacted nodes, input for the damage analysis; (DISP(I),I=1,NREST))

2. Automatically generate elements, nodes, element material properties information.

3. If restart identification number is not zero (step 1, J), then

   A. Create new delamination surface by generating new nodes, solid element across free surface to prevent interpenetration of the nodes.
   B. Assign new reduced stiffness matrix to the failed (matrix, fiber) elements.

4. Construct global stiffness matrix

5. Create condensed stiffness matrix as in Equation (2.18)

6. If restart, solve Equation (4.10), then proceed to next node contact

7. Create sub-condensed stiffness matrix as Equation (2.22)

8. Apply contact algorithm as in Equation (2.25) or Equation (4.13)

9. Obtain displacements and forces

10. Obtain strains and stresses

11. Apply modified Hashin's failure criteria

12. Print failure information

13. Repeat step 7 - step 12 until assigned node (step 1, I) is contacted.

List of the Finite Element Program

```
      PROGRAM CONTACT
      IMPLICIT REAL*8(A-H,O-Z)
C     INPUT INFORMATION
C     1)  NCAND / I5
C     2)  NA, NAFINE, NH, AR, ARFINE, HT / 3I4, 3F6.3
```

```
C    3)  NELMS, NODES, MPTOTAL / 3I5
C    4)  BOUNDARY CONDITIONS / N1,N2,N3 /3I5
C         N1; FIRST NODE IDENTIFICATION OF FIXED D.O.F.
C         N2; DIRECTION, R=1, Z=2
C         N3; INCREMENTAL NUMBER
C              POSITIVE : THICKNESSWISE
C              NEGATIVE : FIX ALONG THE RADIUSWISE
C         END OF INPUT; PUT 0 IN N1
C    5)  ASSIGNING MATERIAL PROPERTY / N1,N2,N3 / 3I5
C         N1, FIRST ELEMENT IDENTIFICATION OF THE LAMINAR
C         N2, MATERIAL PROPERTY IDENTIFICATION OF THE LAYER
C         N3, NUMBER OF STACKS OF SAME MATERIAL LAMINATES
C         END OF INPUT; PUT 0 IN N1
C    6)  MP, C11, C12, C13, C33, C44 / I5, 5(F12.4)
C          {S_rr, S_θθ, S_zz, S_rz}^T = [ C_ij ] { E_j }
C    7)  READ ULTIMATE STRENGTH OF THE MATERIAL / 3F10.3
C             XT, XC, XI
C             YT, YC, SI
C             S12, S13, S23
C    8)  RB / F10.5
C    9)  NTRY / I5
C    10) NREST / I5
C    11) NTCR / I5
C    12) NCRACK(I), MECR(J,I) / I5, I5
C    13) NRMF /I5
C    14) NRMF1, NRMF2 / I5, I5
C    15) NRFF / I5
C    16) NRFF1, NRFF2 / I5, I5
C    17) DISP(I) / F20.12; (I=1,NREST)
C    OUTPUT (DELETED IN THIS LIST)
C      MATRIX AND FIBER FAILURE (KFAIL(I))
C        1 ; TOTAL MATRIX FAILURE
C        2 ; PARTIAL MATRIX FAILURE
C        3 ; TOTAL FIBER FAILURE
C        4 ; PARTIAL FIBER FAILURE
C      DELAMINATION (KDELA(I))
C        1 ; MODE II FAILURE
C        2 ; MODE I AND MODE II, TENSILE STRESS (Sz) EXITS
       DIMENSION RC(650),ZC(650),NBC(650,2),MNODE(550,4)
       DIMENSION S(8,8),CORD(2,4),D(4,4),B(4,8),DB(4),H(4)
       DIMENSION GAUSS(4),WEIGHT(4),P(2,4),XJI(2,2),XJ(2,2)
       DIMENSION MPROP(550),C11(5),C12(5),C13(5),C33(5)
       DIMENSION C44(5),NCONT(20),AC(20,20),STREC(4,2)
       DIMENSION AX(20,20),BX(20,1250),CX(1250,1250)
       DIMENSION AA(20,20),AB(20,20),ZM(20),FXX(20)
       DIMENSION WKAR(5500),RF(20),ZR(1250),ZU(20),ZZ(1,1)
       DIMENSION DISP(1250),F(20),X(1250,20),MECR(30,15)
       DIMENSION QUE(8),NSOLID(150,2),ST(4),NCRACK(15)
       DIMENSION STRESS(550,4),STRAIN(550,4),SA(4),SN(4)
       DIMENSION KFAIL(550), KDELA(550),ASN(4)
       DATA GAUSS/0.5773502692D0,-0.5773502692D0,0.,0./
       OPEN(UNIT=1,FILE='ZI.DAT',STATUS='OLD')
```

```
      OPEN(UNIT=2,FILE='ZO.DAT',STATUS='NEW')
C  **** READ NODE AND ELEMENT DATA
      READ(1,2000) NCAND
 2000 FORMAT(I5)
      WRITE(2,1000) NCAND
 1000 FORMAT(10X,'NUMBER OF CONTACT CANDIDATES',5X,I4)
      READ(1,2010) NA,NAFINE,NH,AR,ARFINE,Ht
 2010 FORMAT(3I4,3F6.3)
      WRITE(2,1010) NA,NAFINE,NH,AR,ARFINE,HT
 1010 FORMAT(/,3X,'NUMBER OF DIVISION OF TOTAL RADIUS',I4,/,
     +3X,'NUMBER OF FINE DIVISION',I4,/,3X,'DIVISION OF
     +THICKNESS',I4,/,3X,'TOTAL RADIUS',F10.5,/,3X,'FINE
     +MESHED RADIUS',F10.5,/,3X,'THICKNESS',F10.5,//)
      IC=0
      READ(1,2020) NELMS,NODES,MPTOTAL
 2020 FORMAT(3I5)
C **** AUTOMATIC NODE GENERATION
      DO 1 N=1,NODES
      DO 1 I=1,2
      NBC(N,I)=1
   1  CONTINUE
C
      YH=NH
      YFINE=NAFINE
      XAFINE=ARFINE/YFINE
      YAC=NA-NAFINE
      XAC=(AR-ARFINE)/YAC
      XH=HT/YH
      DO 2 N=1,NAFINE+1
      I=N-1
      XI=I
      NI=(NH+1)*I+1
      RC(NI)=XAFINE*XI
      ZC(NI)=0.0
      IAUTO=1
  100 RC(NI+IAUTO)=RC(NI)
      ZC(NI+IAUTO)=ZC(NI+IAUTO-1)+XH
      IAUTO=IAUTO+1
      IF(IAUTO.NE.NH+1) GO TO 100
    2 CONTINUE
C
      DO 4 N=1,NA-NAFINE
      I=N-1
      XI=I
      NI=(NH+1)*I+1
      NQX=(NH+1)*(NAFINE+1)
      RC(NI+NQX)=XAC*(XI+1.)+ARFINE
      ZC(NI+NQX)=0.0
      IAUTO=1
  104 RC(NI+NQX+IAUTO)=RC(NI+NQX)
      ZC(NI+NQX+IAUTO)=ZC(NI+NQX+IAUTO-1)+XH
      IAUTO=IAUTO+1
```

```
      IF(IAUTO.NE.NH+1) GO TO 104
    4 CONTINUE
C **** READ FIXED DEGREE OF FREEDOM
C       N;FIRST NODE NUMBER TO BE FIXED
C       I; DEGREE OF FREEDOM TO BE FIXED ( R=1,Z=2 )
C       L; INCREMENTAL NUMBER. 0 FOR SINGLE NODE INPUT
C       PUT N=0 AT THE END OF THE DATA
 2030 FORMAT(3I5)
  101 READ(1,2030) N,I,L
      IF(N.EQ.0) GO TO 102
      NBC(N,I)=0
      IF(L.EQ.0) GO TO 101
      IF(L.LT.0) GO TO 103
      DO 3 J=1,L
    3 NBC(N+J,I)=0
      GO TO 101
  103 DO J=1,NA
      NI=(NH+1)*J+N
      NBC(NI,I)=0
      END DO
      GO TO 101
  102 WRITE(2,1020)
 1020 FORMAT(/,3X,'AUTOMATIC GRID AND ELEMENT GENERATION',/)
C **** AUTOMATIC ELEMENT GENERATION
      MNODE(1,1)=NH+3
      MNODE(1,2)=2
      MNODE(1,3)=1
      MNODE(1,4)=NH+2
      DO 5 N=1,NA
      I=N-1
      XI=I
      NI=NH*I+1
      DO 6 J=1,4
      MNODE(NI,J)=MNODE(1,J)+(NH+1)*I
    6 CONTINUE
      IAUTO=1
  110 DO 7 L=1,4
      MNODE(NI+IAUTO,L)=MNODE(NI+IAUTO-1,L)+1
    7 CONTINUE
      IAUTO=IAUTO+1
      IF(IAUTO.NE.NH) GO TO 110
    5 CONTINUE
C **** AUTOMATIC MATERIAL PROPERTY GENERATION
C         GIVE INPUT OF FIRST ELEMENT NUMBER OF THE LAYER,
C        PROPERTY ID NUMBER, THEN INCREMENTAL LAYER NUMBER
 120 READ(1,2030) NN,M,L
      N=NN
      IF(N.EQ.0) GO TO 140
      DO 9 J=1,NA
      I=J-1
      MPROP(N+NH*I)=M
    9 CONTINUE
```

```
      IF(L.EQ.0) GO TO 120
      IAUTO=1
  130 N=N+IAUTO
      DO 10 K=1,NA
      II=K-1
   10 MPROP(N+NH*II)=M
      IF(N.NE.L) GO TO 130
      GO TO 120
  140 WRITE(2,1040)
 1040 FORMAT(/,3X,'MATERIAL PROPERTIES ARE ASSIGNED',/)
C **** STRESS-STRAIN RELATION INFORMATION
  150 READ(1,2040) MP,C11(MP),C12(MP),C13(MP),C33(MP),C44(MP)
      IF(MP.LT.MPTOTAL) GO TO 150
      DO 13 I=1,MPTOTAL
      MP=I
      CALL DD(MP,C11,C12,C13,C33,C44,D)
      WRITE(2,1071) MP
      WRITE(2,1070) ((D(K,J),J=1,4),K=1,4)
   13 CONTINUE
 1071 FORMAT(3X,'STRESS-STRAIN RELATIONS; MATERIAL ID= ',I5/)
 1070 FORMAT(4(F15.2,3X))
 2040 FORMAT(I5,5F12.4)
C **** READ DATA OF ULTIMATE STRENGTH OF COMPOSITES
      READ(1,2045) XT,XC,XI,YT,YC,SI,S12,S13,S23
 2045 FORMAT(3F10.3)
      WRITE(2,2046) XT,XC,XI,YT,YC,SI,S12,S13,S23
 2046 FORMAT(3X,'ULTIMATE STRENGTH OF THE COMPOSITES',/,3X,
     +'XT=',F11.3,3X,'XC=',F11.3,3X,'XI=',F11.3,/,3X,'YT=',
     +F11.3,3X,'YC=',F11.3,3X,'SI=',F11.3,/,3X,'S12=',F10.3,
     +3X,'S13=',F10.3,3X,'S23=',F10.3,/)
C **** CONTACT INFORMATION
      READ(1,2050) RB
 2050 FORMAT(F10.5)
      WRITE(2,1080) RB
 1080 FORMAT(3X,'RADIUS',F8.3,'BALL INDENTING THE PLATE',/)
      DO I=1,NCAND
      NCONT(I)=(NH+1)*(I-1)+1
      END DO
      READ(1,2060) NTRY
 2060 FORMAT(I5)
      WRITE(2,1091) NTRY
 1091 FORMAT(3X,'MAXIMUM CONTACT PROGRESSION NODE ID.',I5,)
      READ(1,2060) NREST
C **** INPUT OF DELAMINATION
      READ(1,2065) NTCR
      IF(NTCR.EQ.0) THEN
      WRITE(2,1044)
 1044 FORMAT(3X,'NO DELAMINATION PRESENT FOR THIS RESTART',/)
      GO TO 172
      END IF
 2065 FORMAT(I5)
      WRITE(2,1043) NTCR
```

```
 1043 FORMAT(3X,'NUMBER OF DELAMINATIONS',I5,/,3X,
     +'DELAMINATION I.D.',3X,'LENGTH(ELEMENT NO.)',3X,
     +'STARTING POINT(ELEMENT I.D.)',/)
      DO 16 I=1,NTCR
      READ(1,2070) NCRACK(I), MECR(1,I)
 2070 FORMAT(I5,I5)
      WRITE(2,1041) I, NCRACK(I), MECR(1,I)
 1041 FORMAT(10X,I5,10X,I5,10X,I5)
   16 CONTINUE
      KSOLID=0
      DO 21 J=1,NTCR
      DO 12 I=2,NCRACK(J)
      MECR(I,J)=MECR(1,J)+NH*(I-1)
   12 CONTINUE
      DO 14 I=1,NCRACK(J)
      MNODE(MECR(I,J),2)=NODES+I
      IF(I+1.LE.NCRACK(J)) THEN
         MNODE(MECR(I,J),1)=NODES+I+1
      END IF
      RC(NODES+I)=RC(MNODE(MECR(I,J)+1,3))
      ZC(NODES+I)=ZC(MNODE(MECR(I,J)+1,3))
      NBC(NODES+I,1)=1
      NBC(NODES+I,2)=1
      NSOLID(I+KSOLID,1)=MNODE(MECR(I,J),2)
      NSOLID(I+KSOLID,2)=MNODE(MECR(I,J)+1,3)
   14 CONTINUE
      NODES=NODES+NCRACK(J)
      KSOLID=KSOLID+NCRACK(J)
      DO 15 I=1,NCRACK(J)-1
      MNODE(MECR(I,J),4)=MNODE(MECR(I,J)+NH,3)
   15 CONTINUE
      IF(RC(MNODE(MECR(1,J),2)).EQ.0.0) THEN
      NBC(MNODE(MECR(1,J),2),1)=0
      END IF
   21 CONTINUE
      DO J=1,NTCR
      DO I=1,NCRACK(J)
      KDELA(MECR(I,J))=1
      END DO
      END DO
      WRITE(2,1042) ((NSOLID(I,J),J=1,2),I=1,KSOLID)
 1042 FORMAT(2(I5,2X))
  172 CONTINUE
C **** INPUT OF FAILED MATRIX ELEMENTS
      READ(1,2066) NRMF
 2066 FORMAT(I5)
      IF(NRMF.EQ.0) THEN
      WRITE(2,1045)
 1045 FORMAT(/,3X,'NO MATRIX FAILURE IN THIS RESTART',/)
          GO TO 170
      END IF
      WRITE(2,1046) NRMF
```

```
 1046 FORMAT(3X,'TOTAL NO. OF STACKS OF FAILED MATRIX',I5,
     +/,3X,'NO. OF ELEMENTS IN EACH STACK',3X,'FIRST ELEMENT
     +ID.',/)
       DO 33 I=1,NRMF
       READ(1,2077) NRMF1,NRMF2
       WRITE(2,1047) NRMF1,NRMF2
 2077 FORMAT(2I5)
 1047 FORMAT(25X,I5,10X,I5)
       DO 33 J=1,NRMF1
       DUM=NRMF2+(J-1)*NH
       MPROP(DUM)=2
       KFAIL(DUM)=1
   33 CONTINUE
  170 CONTINUE
C **** INPUT OF FIBER-FAILED ELEMENTS
       READ(1,2066) NRFF
       IF(NRFF.EQ.0) THEN
       WRITE(2,1051)
 1051 FORMAT(/,3X,'NO FIBER FAILURE IN THIS RESTART',/)
           GO TO 171
       END IF
       WRITE(2,1048) NRFF
 1048 FORMAT(3X,'TOTAL NO. OF STACKS OF FAILED FIBER',I5,/,3X,
     +'NO. OF ELEMENTS IN EACH STACK',3X,'FIRST ELEMENT
     +ID.',/)
       DO 34 I=1,NRFF
       READ(1,2077) NRFF1,NRFF2
       WRITE(2,1049) NRFF1,NRFF2
 1049 FORMAT(25X,I5,10X,I5)
       DO 34 J=1,NRFF1
       DUM=NRFF2+(J-1)*NH
       MPROP(DUM)=3
       KFAIL(DUM)=3
   34 CONTINUE
  171 CONTINUE
C **** NBC(N,I) GIVES GLOBAL EQUATION NUMBER OF
C      N; NODE NUMBER
C      I; D.O.F. ID. NUMBER (R=1, Z=2)
       DO 22 I=1,NCAND
       NBC(NCONT(I),2)=0
   22 CONTINUE
       NEQ=NCAND
       DO 25 N=1,NODES
       DO 25 I=1,2
       IF(NBC(N,I).EQ.0) GO TO 25
       NEQ=NEQ+1
       NBC(N,I)=NEQ
   25 CONTINUE
       DO 28 I=1,NCAND
       NBC(NCONT(I),2)=I
   28 CONTINUE
C **** PRINTING GENERAL INPUT INFORMATION
```

```
      WRITE(2,1030)
 1030 FORMAT(//,3X,'ELEMENT DATA',//)
      DO 11 I=1,NELMS
      WRITE(2,1050) I,(MNODE(I,J),J=1,4),MPROP(I)
   11 CONTINUE
 1050 FORMAT(3X,'ELEMENT ID',I4,3X,'NODES',4(3X,I3),3X,
     +' MATERIAL PROPERTY ID',I4)
      DO 29 I=1,NODES
      WRITE(2,1100) I,RC(I),ZC(I),NBC(I,1),NBC(I,2)
   29 CONTINUE
 1100 FORMAT(3X,'NODE ID=',I4,3X,'R-CORD',3X,F7.3,3X,'Z-CORD'
     +,3X,4F7.3,3X,'R-GLOBAL EQUATION NUMBER ',I4,3X,'Z-G.E.N
     +',I4)
C **** CALL GLOBAL STIFFNESS CONSTRUCTION AND CONDENSATION
      CALL GLOBS(AX,BX,CX,CORD,RC,ZC,MPROP,NCAND,NBC,MNODE,
     +NEQ,NELMS,C11,C12,C13,C33,C44,NSOLID,KSOLID,NTCR)
C **** START CONTACT PROGRESSION
      KCONT=1
      IF(NREST.NE.0) THEN
      WRITE(2,1201) NREST
 1201 FORMAT(3X,'RESTART PROGRAM AT KCONT=',I5,/,3X,
     +'RESTARTING CONTACTED NODE DISPLACEMENTS',/)
      KCONT=NREST+1
      DO K=1,KCONT
      READ(1,2080) DISP(K)
 2080 FORMAT(F20.12)
      WRITE(2,2080) DISP(K)
      END DO
      END IF
      WRITE(2,1900)
  999 CONTINUE
      IF(NREST.EQ.0) THEN
      WRITE(2,1200) KCONT,NCONT(KCONT)
      WRITE(2,1900)
      WRITE(2,1900)
      END IF
  888 NCR=NCAND-KCONT
      IF(NREST.EQ.0) THEN
 1200 FORMAT(/,3X,'PROGRESS OF THE CONTACT',I4,/,3X,'CONTACTED
     +AT ',I3,'NODE AND NEXT NODE WILL BE CONTACTED')
      END IF
C **** CONDENSING [AX] INTO [AA],[AB],[AC]
      CALL CONCEN(AX,AA,AB,AC,KCONT,NCAND)
C **** [ AC ]{ Zm }= - [AB]T {1, 1,...1}T
      IF(NREST.NE.0) THEN
      DO I=1,NCR
      DUM=0.0
      DO K=1,KCONT
      DUM=DUM-AB(K,I)*DISP(K)
      END DO
      ZM(I)=DUM
      END DO
```

```
      ELSE
      DO 30 I=1,NCR
      DUM=0.0
      DO 31 K=1,KCONT
      DUM=DUM-AB(K,I)
   31 CONTINUE
      ZM(I)=DUM
   30 CONTINUE
      END IF
      WRITE(2,1210) (ZM(I),I=1,NCR)
 1210 FORMAT(3X,'INPUT TO SOLVE ZM',/,5(2X,F20.4))
C **** SOLVE LINEAR EQUATION
C       ZM IS TREATED LIKE INPUT FORCE
C       IMSL PACKAGE EMPLOYED
      IA=20
      IDGT=0
      MM=1
      CALL LEQT1F(AC,MM,NCR,IA,ZM,IDGT,WKAR,IER)
      IF (NREST.EQ.0) THEN
      WRITE(2,1220) (ZM(I),I=1,NCR)
 1220 FORMAT(3X,'ZM: DISP. TO THE UNIT INPUT',/,5(2X,F15.8))
      ELSE
      WRITE(2,1221) (ZM(I),I=1,NCR)
 1221 FORMAT(3X,'RESTARTED DISPLACEMENTS OF NODES NOT
     +CONTACTED YET',/,3X,6(F12.6,2X))
      DELTA=ZM(1)-DISP(KCONT)
      GAP=DSQRT(RB**2-RC(NCONT(KCONT))**2)-DSQRT(RB**2-
     +RC(NCONT(KCONT+1))**2)
        IF((DELTA+GAP).LE.0.0) THEN
        KCONT=KCONT+1
        DISP(KCONT)=ZM(1)
        WRITE(2,1211) DELTA, GAP,DISP(KCONT),NCONT(KCONT)
 1211 FORMAT(2X,'AUTOMATIC NEW CONTACT BETWEEN INDENTER
     +AND PLATE',/,3X,'Dj-Di',F10.5,'GAP',F10.5,/,3X,
     +'DISP(KCONT)=',F12.6,3X, 'NEW CONTACTED NODE',I5)
        GO TO 888
        END IF
      END IF
C         NOW, Zm IS OUTPUT DISPLACEMENTS
C         [AC] IS (NCR x NCR) DIMENSION
C         {Zm}  IS (NCR x 1) DIMENSION
      NR=NEQ-NCAND
      IF(NREST.NE.0) THEN
      DO I=1,KCONT
      DUM1=0.0
      DUM2=0.0
      DO J=1,KCONT
      DUM1=DUM1+AA(I,J)*DISP(J)
      END DO
      DO K=1,NCR
      DUM2=DUM2+AB(I,K)*ZM(K)
      END DO
```

```
      F(I)=DUM1+DUM2
      END DO
      DO JJ=1,NCR
      DISP(KCONT+JJ)=ZM(JJ)
      END DO
      DUM=0.0
      DO J=1,KCONT
      DUM=DUM+F(J)
      END DO
      WRITE(2,1900)
      WRITE(2,1231) DUM
      WRITE(2,1232) (F(I),I=1,KCONT)
 1231 FORMAT(3X,'RECALCULATED TOTAL FORCE AFTER FAILURE',
     +F10.3,/, 3X,'NODAL FORCES',/)
 1232 FORMAT(3X,F20.8)
      DO I=1,NR
      DUM=0.0
      DO K=1,NCAND
      DUM=DUM+BX(K,I)*DISP(K)
      END DO
      DISP(I+NCAND)=DUM
      END DO
C **** PRINTING RECALCULATED DISPLACEMENTS
      DO IJ=2,NH+1
      DUM=DISP(NBC(IJ,2))-DISP(1)
      WRITE(2,1234) ZC(IJ),DISP(NBC(IJ,2)),DUM
      END DO
      WRITE(2,1235) RC(NCONT(KCONT+1))
      WRITE(2,1900)
 1234 FORMAT(3X,'Z-CORD',F8.4,2X,'DISP',F12.8,2X,'RELATIVE
     +INDENTATION',F12.8)
 1235 FORMAT(/,3X,'RECALCULATED RADIUS',F8.5,/)
C **** CHECK DAMAGES(CALCULATE ELEMENT STRESSES AND APPLY
C       MODIFIED HASHIN'S CRITERIA)
      CALL RECOVER(CORD,RC,ZC,MNODE,MPROP,C11,C12,C13,C33,C44,
     +D,NBC,DISP,STRESS,STRAIN,NA,NH,GAUSS,XT,YT,XC,YC,S12,
     +S13,S23,XI,SI,SA,NELMS,KDELA,KFAIL)
      NREST=0
      GO TO 999
      END IF
C **** CLOSE GAP AT THE NEXT CONTACT CANDIDATE NODE
      GAP=DSQRT(RB**2-RC(NCONT(KCONT))**2)-DSQRT(RB**2-
     +RC(NCONT(KCONT+1))**2)
      CM=(DISP(KCONT+1)-DISP(KCONT)+GAP)/(1.-ZM(1))
      WRITE(2,1230) CM
 1230 FORMAT(/,3X,' ADJUSTMENT FACTOR TO CLOSE GAP',F20.8)
      IF(CM.LE.0.0) THEN
      WRITE(2,1233)
 1233 FORMAT(3X,'WARNING; CONTACT PROCEEDS WITHOUT
     +EXERTING ANY FORCE')
      END IF
C **** CALCULATE DISPLACEMENTS AND FORCES
```

```
      DO 35 I=1,KCONT
      ZU(I)=CM
   35 CONTINUE
      DO 36 J=1,NCR
      ZU(KCONT+J)=ZM(J)*CM
   36 CONTINUE
      WRITE(2,1240) (ZU(I),I=1,NCAND)
 1240 FORMAT(/,3X,'UPPER SURFACE INCREMENTAL DISPLACEMENT',/,
     +5(F12.8,2X))
C **** {RF} = CM*([AA]{1,1,...1}T + [AB]{Zm})
      DO 40 I=1,KCONT
      DUM=0.0
      DO 41 K=1,KCONT
      DUM=DUM+AA(I,K)
   41 CONTINUE
      DUM1=0.0
      DO 42 J=1,NCR
      DUM1=AB(I,J)*ZM(J)+DUM1
   42 CONTINUE
      RF(I)=(DUM+DUM1)*CM
   40 CONTINUE
      WRITE(2,1250) (RF(I),I=1,NCAND)
 1250 FORMAT(/,3X,'INCREMENTAL NODAL FORCE',/,5(1X,F20.4))
C ****  { Zr }  =  [ X ] { Zu }, SEE SUBROUTINE GLOB
      DO 45 I=1,NR
      DUM=0.0
      DO 46 K=1,NCAND
      DUM=DUM+BX(K,I)*ZU(K)
   46 CONTINUE
      ZR(I)=DUM
   45 CONTINUE
C ****  TOTAL DISPLACEMENTS AND NODAL FORCES
      DO 55 I=1,NCAND
      DISP(I)=DISP(I)+ZU(I)
      F(I)=F(I)+RF(I)
   55 CONTINUE
      DO 60 I=1,NR
      J=I+NCAND
      DISP(J)=DISP(J)+ZR(I)
   60 CONTINUE
      WRITE(2,1280) (F(I),I=1,NCAND)
 1280 FORMAT(/,3X,'UPDATED CONTACT NODAL FORCE',/,5(1X,F15.4))
      WRITE(2,1290) (DISP(I),I=1,NCAND)
 1290 FORMAT(/,3X,'UPDATED DISPLACEMENTS',/,5(1X,F15.8))
C **** CALCULATE ELEMENT STRAINS AND STRESSES
      CALL RECOVER(CORD,RC,ZC,MNODE,MPROP,C11,C12,C13,C33,
     +C44,D,NBC,DISP,STRESS,STRAIN,NA,NH,GAUSS,XT,YT,XC,YC,
     +S12,S13,S23,XI,SI,SA,NELMS,KDELA,KFAIL)
C **** NOTATION OF STRESS DATA, STRESS(N,L)
C        N; NODE IDENTIFICATION
C           STRESS(N,1) ; σr
C           STRESS(N,2) ; σz
```

```
C            STRESS(N,3) ; τ_rz
C            STRESS(N,4) ; σ_θ
C **** GENERAL CONTACT INFORMATION
      DUM=0.0
      DO 80 I=1,KCONT
      DUM=F(I)+DUM
   80 CONTINUE
      FXX(KCONT)=DUM
      WRITE(2,1902)
 1902 FORMAT(3X,'**** CONTACT INFORMATION ')
      WRITE(2,1400) NCONT(KCONT+1),RC(NCONT(KCONT+1)),DISP(1),
     +FXX(KCONT)
 1400 FORMAT(4X,'NODE',5X,'CONTACT RADIUS',10X,'TOP DEFLECT',
     +3X,'CONTACT FORCE',/,4X,I4,2X,F20.5,1X,F20.8,3X,F30.4)
      DUM=DISP(1)-DISP(NBC(1+NH,2))
      WRITE(2,1901) DISP(NBC(1+NH,2)),DUM
 1901 FORMAT(3X,'BOTTOM DEFLECTION=',F20.12,3X,'INDENTATION='
     +,F20.12)
      WRITE(2,1900)
      DO IJ=2,NH+1
      DUM=DISP(NBC(IJ,2))-DISP(1)
      WRITE(2,1234) ZC(IJ),DISP(NBC(IJ,2)),DUM
      END DO
      WRITE(2,1900)
 1900 FORMAT(3X,'************************************')
      WRITE(2,1500)
 1500 FORMAT(/,3X,' RADIUS ',5X,'AREA',10X,'Szz',10X,'THEORY')
      WRITE(2,1900)
      PI=3.141592625D0
      DO 85 I=1,KCONT
      J=(I-1)*NH+1
      IF(I.EQ.1) THEN
         AREA=RC(NCONT(2))**2*PI/4.
      ELSE
         AREA=RC(NCONT(I))*PI*2.*XAC
      END IF
      PRESS=STRESS(J,2)
      DUM=RC(NCONT(KCONT+1))**2
      THEO=-1.5*FXX(KCONT)/PI/DUM*SQRT(1.-RC(NCONT(I))**2/DUM)
      WRITE(2,1550) RC(NCONT(I)),AREA,PRESS,THEO
 1550 FORMAT(3X,F8.4,F9.4,F20.4,F20.4)
   85 CONTINUE
C **** ITERATE TO NEXT CONTACT NODE UNTIL INDENTER CONTACTS
C       NCONT(NTRY) NODE
      WRITE(2,1900)
      KCONT=KCONT+1
      IF(KCONT.LE.NTRY) GO TO 999
      STOP
      END
C
      SUBROUTINE AXISYM(CORD,S,D)
C
```

```
      IMPLICIT REAL*8(A-H,O-Z)
      DIMENSION S(8,8),CORD(2,4),D(4,4),B(4,8),DB(4)
      DIMENSION GAUSS(4),WEIGHT(4)
C **** GAUSS -LEGENDRE INTEGRATION COEFFICIENTS
      DATA WEIGHT/ 1.0D0,1.0D0,0.,0./
      DATA GAUSS/ 0.5773502692D0,-0.5773502692D0,0.,0./
C **** INITIATE STIFFNESS MATRIX
      DO 10 I=1,8
      DO 10 J=1,8
      S(I,J)=0.0
   10 CONTINUE
C **** EVALUATE  MATRIX B
      PI=3.141592625D0
      DO 20 I=1,2
      R=GAUSS(I)
      DO 20 J=1,2
      Z=GAUSS(J)
      CALL BJ(CORD,B,DET,R,Z,RADIUS,D)
      WT=WEIGHT(I)*WEIGHT(J)*RADIUS*DET*2.0*PI
      DO 30 JJ=1,8
      DO 40 K=1,4
      DB(K)=0.0
      DO 40 L=1,4
   40 DB(K)=DB(K)+D(K,L)*B(L,JJ)
      DO 50 M=JJ,8
      STIFF=0.0
      DO 60 LL=1,4
   60 STIFF=STIFF+B(LL,M)*DB(LL)
   50 S(M,JJ)=S(M,JJ)+STIFF*WT
   30 CONTINUE
   20 CONTINUE
      DO 90 J=1,8
      DO 90 I=J,8
      S(J,I)=S(I,J)
   90 CONTINUE
      RETURN
      END
C
      SUBROUTINE BJ(CORD,B,DET,R,Z,RADIUS,D)
      IMPLICIT REAL*8(A-H,O-Z)
      DIMENSIONCORD(2,4),B(4,8),H(4),P(2,4),XJI(2,2),XJ(2,2)
      RP=1.0+R
      SP=1.0+Z
      RM=1.0-R
      SM=1.0-Z

C **** INTERPOLATION FUNCTION
      H(1)=0.25*RP*SP
      H(2)=0.25*RM*SP
      H(3)=0.25*RM*SM
      H(4)=0.25*RP*SM
      P(1,1)=0.25*SP
```

```
      P(1,2)=-P(1,1)
      P(1,3)=-0.25*SM
      P(1,4)=-P(1,3)
      P(2,1)=0.25*RP
      P(2,2)=0.25*RM
      P(2,3)=-P(2,2)
      P(2,4)=-P(2,1)
      DO 30 I=1,2
      DO 30 J=1,2
      DUM=0.0
      DO 20 K=1,4
   20 DUM=DUM+P(I,K)*CORD(J,K)
   30 XJ(I,J)=DUM
      DET=XJ(1,1)*XJ(2,2)-XJ(2,1)*XJ(1,2)
      IF(DET.GT.0.0000001) GO TO 40
      WRITE(2,1000) ((CORD(I,J),J=1,4),I=1,2)
 1000 FORMAT(3X,'JACOBIAN FAILED AT ',/,3X,8(F9.4,1X))
      STOP
   40 DUM=1./DET
      XJI(1,1)=XJ(2,2)*DUM
      XJI(1,2)=-XJ(1,2)*DUM
      XJI(2,1)=-XJ(2,1)*DUM
      XJI(2,2)=XJ(1,1)*DUM
C **** EVALUATE GLOBAL DERIVATIVE OPERATOR
      KK=0
      DO 60 K=1,4
      KK=KK+2
      B(1,KK-1)=0.
      B(1,KK)=0.
      B(2,KK-1)=0.
      B(2,KK)=0.
      DO 50 I=1,2
      B(1,KK-1)=B(1,KK-1)+XJI(1,I)*P(I,K)
   50 B(2,KK)=B(2,KK)+XJI(2,I)*P(I,K)
      B(3,KK)=B(1,KK-1)
   60 B(3,KK-1)=B(2,KK)
      RADIUS=0.0
      DO 70 K=1,4
   70 RADIUS=RADIUS+H(K)*CORD(1,K)
      DUM=1./RADIUS
      KK=0
      DO 90 K=1,4
      KK=KK+2
      B(4,KK)=0.
   90 B(4,KK-1)=H(K)*DUM
      RETURN
      END
C
      SUBROUTINE DD(MP,C11,C12,C13,C33,C44,D)
      IMPLICIT REAL*8(A-H,O-Z)
C **** STRESS-STRAIN RELATIONS
      DIMENSION D(4,4)
```

```
      DIMENSION C11(1),C12(1),C13(1),C33(1),C44(1)
      DO 10 I=1,4
      DO 10 J=1,4
      D(I,J)=0.0
   10 CONTINUE
      D(1,1)=C11(MP)
      D(1,2)=C13(MP)
      D(1,4)=C12(MP)
      D(2,2)=C33(MP)
      D(2,4)=C13(MP)
      D(3,3)=C44(MP)
      D(4,4)=C11(MP)
      DO 20 I=1,4
      DO 20 J=I,4
      D(J,I)=D(I,J)
   20 CONTINUE
      RETURN
      END
C
      SUBROUTINE CLEAR(ZZ,N,M)
      IMPLICIT REAL*8(A-H,O-Z)
      DIMENSION ZZ(1,1)
      DO 1 I=1,N
      DO 1 J=1,M
      ZZ(I,J)=0.0
    1 CONTINUE
      RETURN
      END
C
      SUBROUTINE GLOBS(AX,BX,CX,CORD,RC,ZC,MPROP,NCAND,NBC,
     +MNODE,NEQ,NELMS,C11,C12,C13,C33,C44,NSOLID,KSOLID,NTCR)
      IMPLICIT REAL*8(A-H,O-Z)
      DIMENSION AX(20,20),BX(20,1250),CX(1250,1250),D(4,4)
      DIMENSION CORD(2,4),RC(650),ZC(650),MPROP(550)
      DIMENSIONNBC(650,2),MNODE(550,4),X(1250,20),WKAR(5500)
      DIMENSION C11(1),C12(1),C13(1),C33(1),C44(1),S(8,8)
      DIMENSION NSOLID(150,2)
C **** CONSTRUCTING  GLOBAL STIFFNESS
      NR=NEQ-NCAND
      WRITE(2,1000) NR
 1000 FORMAT(/,3X,'SUBROUTINE GLOBS IS CALLED IN ,NR=',I5)
      CALL CLEAR(AX,NCAND,NCAND)
      CALL CLEAR(BX,NCAND,NR)
      CALL CLEAR(CX,NR,NR)
      IC=0
      DO 10 N=1,NELMS
      DO 20 JJ=1,4
      CORD(1,JJ)=RC(MNODE(N,JJ))
      CORD(2,JJ)=ZC(MNODE(N,JJ))
   20 CONTINUE
C **** CALL SUBROUTINE DD WHEN MATERIAL PROPERTY OF A ELEMENT
C          HAS CHANGED
```

```
      MP=MPROP(N)
      IF(IC.EQ.MP) GO TO 100
      CALL DD(MP,C11,C12,C13,C33,C44,D)
  100 IC=MP
      CALL AXISYM(CORD,S,D)
      DO 10 I=1,8
      K=(I+1)/2
      L=I-2*K+2
      NROW=NBC(MNODE(N,K),L)
      IF(NROW.EQ.0) GO TO 10
      DO 10 J=1,8
      K=(J+1)/2
      L=J-2*K+2
      NCOL=NBC(MNODE(N,K),L)
      IF(NCOL.EQ.0) GO TO 10
      IR=NROW-NCAND
      IC=NCOL-NCAND
      IF(IR.GT.0.AND.IC.GT.0)THEN
        CX(IR,IC)=CX(IR,IC)+S(I,J)
      ELSE IF(IR.LE.0.AND.IC.GT.0)THEN
        BX(NROW,IC)=BX(NROW,IC)+S(I,J)
      ELSE IF(IR.LE.0.AND.IC.LE.0)THEN
        AX(NROW,NCOL)=AX(NROW,NCOL)+S(I,J)
      ELSE
        GO TO 10
      END IF
   10 CONTINUE
C **** IMPLEMENT DELAMINATIONS
      IF(NTCR.EQ.0) THEN
        GO TO 200
      END IF
      XK=9000000000.0
      DO 15 I=1,KSOLID
      IR=NBC(NSOLID(I,1),2)-NCAND
      IC=NBC(NSOLID(I,2),2)-NCAND
      CX(IR,IR)=CX(IR,IR)+XK
      CX(IC,IC)=CX(IC,IC)+XK
      CX(IR,IC)=CX(IR,IC)-XK
      CX(IC,IR)=CX(IC,IR)-XK
   15 CONTINUE
  200 CONTINUE
C **** CONDENSE; [K]*{Zu} ={RF}
C        [X] = - [CX]^-1 [BX]^T
C        [X] HAS DIMENSION OF (NR x NCAND)
C             {Zr}=[X]{Zu}
C             [AA]{Zu}={RF}, WHERE
C         [AA]=[AX]-[BX][CX]^-1[BX]^T
C **** FIRST, DEFINE [X] AS -[BX]^T
      DO 30 I=1,NR
      DO 30 J=1,NCAND
      X(I,J)=-BX(J,I)
   30 CONTINUE
```

```
C **** NOW, MAKE [X]=-[CX]^-1[BX]^T
      IDGT=0
      IA=1250
      CALL LEQT1F(CX,NCAND,NR,IA,X,IDGT,WKAR,IER)
C **** MAKE AA MATRIX (CONDENSED FORM )
      DO 40 I=1,NCAND
      DO 40 J=1,NCAND
      DUM=0.0
      DO 50 K=1,NR
      DUM=DUM-BX(I,K)*X(K,J)
   50 CONTINUE
      AX(I,J)=AX(I,J)-DUM
   40 CONTINUE
      DO 60 I=1,NCAND
      DO 60 J=1,NR
      BX(I,J)=X(J,I)
   60 CONTINUE
C **** END OF CONDENSATION
      RETURN
      END
C
      SUBROUTINE CONCEN(AX,AA,AB,AC,KCONT,NCAND)
      IMPLICIT REAL*8(A-H,O-Z)
      DIMENSION AX(20,20),AA(20,20)
      DIMENSION AB(20,20),AC(20,20)
      NCR=NCAND-KCONT
      CALL CLEAR (AA,KCONT,KCONT)
      CALL CLEAR(AB,KCONT,NCR)
      CALL CLEAR(AC,NCR,NCR)
      DO 10 I=1,NCAND
      DO 10 J=1,NCAND
      IF(I.LE.KCONT.AND.J.LE.KCONT)THEN
        AA(I,J)=AX(I,J)
      ELSE IF(I.LE.KCONT.AND.J.GT.KCONT)THEN
        AB(I,J-KCONT)=AX(I,J)
      ELSE IF(I.GT.KCONT.AND.J.GT.KCONT) THEN
        AC(I-KCONT,J-KCONT)=AX(I,J)
      ELSE
        GO TO 10
      END IF
   10 CONTINUE
      RETURN
      END
C
      SUBROUTINE RECOVER(CORD,RC,ZC,MNODE,MPROP,C11,C12,
     +C13,C33,C44,D,NBC,DISP,STRESS,STRAIN,NA,NH,GAUSS,
     +XT,YT,XC,YC,S12,S13,S23,XI,SI,SA,NELMS,KDELA,KFAIL)
      IMPLICIT REAL*8(A-H,O-Z)
      DIMENSION CORD(2,4),RC(650),ZC(650),MNODE(550,4),
      DIMENSION C11(5),C12(5),C13(5),C33(5),C44(5),D(4,4)
      DIMENSIONDISP(1250),STRESS(550,4),STRAIN(550,4),QUE(8)
      DIMENSION ST(4),SA(4),SN(4),ASN(4),GAUSS(4),B(4,8)
```

```
      DIMENSION NBC(650,2),KFAIL(550),KDELA(550),MPROP(550)
      IC=0
      DO 10 K=1,NA
      DO 20 I=1,NH
      II=(K-1)*NH+I
      DO 30 J=1,4
      CORD(1,J)=RC(MNODE(II,J))
      CORD(2,J)=ZC(MNODE(II,J))
   30 CONTINUE
      MP=MPROP(II)
      IF(IC.EQ.MP) GO TO 1000
      CALL DD(MP,C11,C12,C13,C33,C44,D)
 1000 IC=MP
C **** CALCULATE ELEMENT NODAL DISPLACEMENT
      DO 40 L=1,8
      MM=(L+1)/2
      NN=L-2*MM+2
      IF(NBC(MNODE(II,MM),NN).EQ.0) THEN
      QUE(L)=0.0
      ELSE
      QUE(L)=DISP(NBC(MNODE(II,MM),NN))
      END IF
   40 CONTINUE
      DO 45 J=1,4
      SA(J)=0.0
   45 CONTINUE
      DO 50 M=1,2
      DO 50 N=1,2
      R=GAUSS(M)
      Z=GAUSS(N)
      CALL BJ(CORD,B,DET,R,Z,RADIUS,D)
C **** CALCULATE ELEMENT STRAIN
      DO 60 IN=1,4
      DUM=0.0
      DO 65 IM=1,8
      DUM=DUM+B(IN,IM)*QUE(IM)
   65 CONTINUE
      SN(IN)=DUM
   60 CONTINUE
C **** CALCULATE STRESS
      DO 70 LL=1,4
      DUM=0.0
      DO 75 JJ=1,4
      DUM=DUM+D(LL,JJ)*SN(JJ)
   75 CONTINUE
      ST(LL)=DUM
   70 CONTINUE
      DO 80 J=1,4
      SA(J)=SA(J)+ST(J)
      ASN(J)=ASN(J)+SN(J)
   80 CONTINUE
   50 CONTINUE
```

```
      DO 85 J=1,4
      SA(J)=SA(J)*0.25
      ASN(J)=ASN(J)*0.25
      STRESS(II,J)=SA(J)
      STRAIN(II,J)=ASN(J)
   85 CONTINUE
      CALL CRIT(II,XT,YT,XC,YC,S12,S13,S23,XI,SI,SA,
     +KFAIL,KDELA,NELMS)
   20 CONTINUE
   10 CONTINUE
      DO K=1,NA
      WRITE(2,1200) (K-1)*NH+1,(KFAIL(I+(K-1)*NH),I=1,NH),
     +(KDELA(I+(K-1)*NH),I=1,NH)
      END DO
 1200 FORMAT(1X,I3,3X,16(1X,I1),4X,16(1X,I1))
      RETURN
      END
C
      SUBROUTINE CRIT(II,XT,YT,XC,YC,S12,S13,S23,XI,SI,SA,
     +KFAIL,KDELA,NELMS)
      IMPLICIT REAL*8(A-H,O-Z)
      DIMENSION SA(4),IFFAIL(72),IMFAIL(72),KFAIL(550),
     +KDELA(550)
      PI=3.141592625D0
      DO 5 I=1,72
      IFFAIL(I)=0
      IMFAIL(I)=0
    5 CONTINUE
      DO 10 I=1,72
      XI=I
      X=PI/36.0*XI
C
      C=COS(X)**2*SA(1)+SIN(X)**2*SA(4)
      D=(SIN(X)*COS(X)*(SA(4)-SA(1))/S12)**2
      E=(COS(X)*SA(3)/S13)**2
      F=C+SA(2)
      G=(SIN(X)*SA(3))**2-SIN(X)**2*SA(1)*SA(2)-
     +COS(X)**2*SA(4)*SA(2)
C **** CHECKING FIBER FAILURE
      IF(C.LT.0.0)THEN
        IF(((C/XC)**2-1.0).GE.0.0) THEN
            IFFAIL(I)=1
         END IF
      ELSE
         IF(((C/XT)**2+D+E).GE.1.0)THEN
            IFFAIL(I)=1
         END IF
      END IF
C **** CHECKING MATRIX FAILURE
      IF(F.GE.0.0)THEN
      H=(F/YT)**2+G/(S23**2)+D+E
        IF(H.GE.1.0)THEN
```

```
            IMFAIL(I)=1
          END IF
        ELSE
        A=F*(YC/(2.*S23)**2-1./YC)+(F/(2.*S23))**2+G/S23**2+D+E
           IF(A.GE.1.0)THEN
              IMFAIL(I)=1
           END IF
        END IF
   10 CONTINUE
C **** MATRIX FAILURE PRINTOUT. PARTIAL FAILURES ARE PRINTED
C      HERE. FOR OTHER INFORMATION, PRINT KFAIL(I)
        DO 50 I=1,72
           IF(IMFAIL(I).EQ.1) THEN
             MI=I
           GO TO 110
           END IF
   50 CONTINUE
        GO TO 998
  110 CONTINUE
        IF(MI.EQ.1) THEN
        DO 55 J=2,72
        IF(IMFAIL(J).EQ.0) THEN
        WRITE(2,1500) II,J*5
 1500 FORMAT(3X,'** MATRIX FAILURE AT',I5,3X,'ELEMENT',3X,
     +'ZERO THROUGH',I5,3X,'DEGREE , SYMMETRIC')
        KFAIL(II)=2
        GO TO 998
        END IF
   55 CONTINUE
        KFAIL(II)=1
        ELSE
        DO 60 J=MI+1,72
        IF(IMFAIL(J).EQ.0) THEN
        WRITE(2,1700) II ,MI*5,J*5
 1700 FORMAT(3X,'** MATRIX FAILURE AT ',I5,3X,'ELEMENT',3X,
     +'FROM',I5,' DEGREE TO',I5,' DEGREE ,SYMMETRIC ')
        KFAIL(II)=2
        GO TO 998
        END IF
   60 CONTINUE
        END IF
  998 CONTINUE
C **** FIBER FAILURE PRINTOUT. PARTIAL FAILURES ARE PRINTED
C      HERE. FOR OTHER INFORMATION, PRINT KFAIL(I)
        DO 30 I=1,72
           IF(IFFAIL(I).EQ.1) THEN
             MI=I
           GO TO 100
           END IF
   30 CONTINUE
        GO TO 999
  100 CONTINUE
```

```
      IF(MI.EQ.1) THEN
      DO 35 J=2,72
      IF(IFFAIL(J).EQ.0) THEN
      WRITE(2,1000) II,J*5
 1000 FORMAT(3X,'$$$ FIBER FAILURE AT',I5,3X,'ELEMENT',3X,
     +'ZERO THROUGH',I5,3X,'DEGREE , SYMMETRIC')
      KFAIL(II)=4
      GO TO 999
      END IF
   35 CONTINUE
      KFAIL(II)=3
      ELSE
      DO 40 J=MI+1,72
      IF(IFFAIL(J).EQ.0) THEN
      WRITE(2,1200) II ,MI*5,J*5
 1200 FORMAT(3X,'$$$ FIBER FAILURE AT',I5,3X,'ELEMENT',3X,
     +'FROM',I5,' DEGREE TO',I5,' DEGREE ,SYMMETRIC ')
      KFAIL(II)=4
      GO TO 999
      END IF
   40 CONTINUE
      END IF
  999 CONTINUE
C ****  DELAMINATION PRINTOUT. FOR THE INFORMATION, PRINT
C       KDELA(I), I = ELEMENT IDENTIFICATION
      IF(SA(2).GT.0.0) THEN
      B=(SA(2)/XI)**2+(SA(3)/SI)**2
         IF(B.GE.1.0) THEN
         KDELA(II)=2
         END IF
      ELSE
      B=(SA(3)/SI)**2
          IF(B.GE.1.0) THEN
          KDELA(II)=1
          END IF
      END IF
      RETURN
      END
```

BIOGRAPHICAL SKETCH

Han Soo Jung was born on January 6, 1952, as the first son of Young Whee and Rae Won Jung in Korea. He has one brother, Yoon Soo, and one sister, Jae Hee. He married Ki Young Kim, the daughter of Dong Seung Kim and Sun Hee Son, on April 25, 1978. She has four brothers, Yun Sup, Jun Sup, Ja Sup, and Kwang Sup.

He graduated from Seoul National University with a B.S. degree in aeronautical engineering in 1974. After graduation, he joined the Agency for Defense Development as a research engineer. He became a senior research engineer in 1980. Before he came to University of Florida in 1988, he has served fourteen years in A.D.D. conducting various research projects. He also worked at the Flight Dynamics Laboratory, Wright-Patterson AFB, OH, from 1975 to 1976 and at the Armament Laboratory, Eglin AFB, FL, from 1982 to 1984 as an exchange engineer.

He received M.S. degree in aerospace engineering from the University of Florida in August, 1984 and the Ph.D. degree in August, 1991. After graduation, he is going to be the chairman of the Department of Mechanical Engineering, Saint Martin's College, Lacey, Washington 98503.

I certify that I have read this study and that in my opinion it conforms to acceptable standards of scholarly presentation and is fully adequate, in scope and quality, as a dissertation for the degree of Doctor of Philosophy.

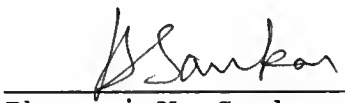

Bhavani V. Sankar, Chairman
Associate Professor of Aerospace Engineering, Mechanics, and Engineering Science

I certify that I have read this study and that in my opinion it conforms to acceptable standards of scholarly presentation and is fully adequate, in scope and quality, as a dissertation for the degree of Doctor of Philosophy.

Chang-Tsan Sun
Professor of Aerospace Engineering, Mechanics, and Engineering Science

I certify that I have read this study and that in my opinion it conforms to acceptable standards of scholarly presentation and is fully adequate, in scope and quality, as a dissertation for the degree of Doctor of Philosophy.

Lawrence E. Malvern
Professor of Aerospace Engineering, Mechanics, and Engineering Science

I certify that I have read this study and that in my opinion it conforms to acceptable standards of scholarly presentation and is fully adequate, in scope and quality, as a dissertation for the degree of Doctor of Philosophy.

Ibrahim K. Ebcioglu
Professor of Aerospace Engineering, Mechanics, and Engineering Science

I certify that I have read this study and that in my opinion it conforms to acceptable standards of scholarly presentation and is fully adequate, in scope and quality, as a dissertation for the degree of Doctor of Philosophy.

John J. Mecholsky, Jr.
Professor of Materials Science and Engineering

This dissertation was submitted to the Graduate Faculty of the College of Engineering and to the Graduate School and was accepted as partial fulfillment of the requirements for the degree of Doctor of Philosophy.

August 1991

for Winfred M. Phillips
Dean, College of Engineering

Madelyn M. Lockhart
Dean, Graduate School